BEWARE of C-60

Start your research on embryo toxicity of C-60. C-60 binds and deforms nucleotides. A large scale association for nanoparticle C-60 uncovers mechanism of nanotoxicity disrupting the native conformations of DNA and RNA - start there and go forth. And remember this is a form of graphene as well which is 3 times harder than diamond and 100 times harder then steel. ~ It does not come out like they said either. ~ If anyone even looks at the research on nano then you can see that nano and pico metallics or particulates does not release, and translocates throughout the whole body. He who has eyes to see let them see and he who has ears to hear let them. The rest ~ C-60 and AI await you. - Tony

C_{60}, otherwise known as “bucky balls” or “Buckminster fullerenes”, have been proposed for use in fuel cells, groundwater remediation, cosmetics and drug delivery. The lack of solubility of C_{60} in water has limited its research in biological systems

In our studies, embryo exposure to fullerenes elicited increased mortality, sublethal malformations and increased cellular death. Studies in an embryonic mammalian model (mouse) also report severe morphological malformations and increased mortality when exposed to C_{60} *in utero*. All carbon fullerenes tested in our system produced deleterious effects to the developing fin regions indicative

of signaling perturbation during early development. C_{60} and C_{70} elicited similar responses, indicating the small difference in size does not significantly affect the toxic potential of these materials.

When you see what DAARPA wants --it is an update version of Elon Musk's neural thread, but instead of a surgical implant now you just guzzle this carbon 60. And it goes into the head and activates the network --the scientist here talks about your brain interfacing with data now you have a better connection to get to the cloud which is AI (artificial intelligence). Chemtrails above you are the cloud they collect and store data. Study this and make it abundantly clear to your congregation and to the christian (believers) that this is going to take them over if they are (not so nice of a word) remain ignorant of this.
Tony

I am going to cover this thoroughly in the Targeting message that is coming. But for now I have included research links here as well as the research Tony shared on it too.

Remember:

Matt.10:16 - Behold, I send you forth as sheep in the midst of wolves: be ye therefore wise as serpents, and harmless as doves.

The wolves are bearing their teeth and we need to be aware of what they are up to.

https://www.youtube.com/watch?v=cPgPz6NbtdA

https://www.researchgate.net/publication/23140919_In_vivo_evaluation_of_carbon_fullerene_toxicity_using_embryonic_zebrafish

http://europepmc.org/articles/PMC2186061

https://en.wikipedia.org/wiki/Fullerene

TONY'S RESEARCH BELOW:


C60 nanotoxicity of dna and rna.pdf


C60 Binds to and Deforms Nucleotides


The Painful Truth About Omega 3 Fatty


Fullerenes shown to penetrate healthy sk


Carbon nanotubes introduced into the a


Toxicity Studies of c60 Fullerene and Ca


evaluation of carbon fullerene toxicity usin

Tony's website:

http://augmentinforce.50webs.com/

7622–7632 Nucleic Acids Research, 2012, Vol. 40, No. 16 Published online 1 June 2012
doi:10.1093/nar/gks517

A large-scale association study for nanoparticle C60 uncovers mechanisms of nanotoxicity disrupting the native conformations of DNA/RNA

Xue Xu[1], Xia Wang[1], Yan Li[2], Yonghua Wang[1,*] and Ling Yang[3]

[1]Center of Bioinformatics, College of Life Science, Northwest A&F University, Yangling, Shaanxi 712100, China, [2]School of Chemical Engineering, Dalian University of Technology, Dalian 116024, Liaoning and [3]Laboratory of Pharmaceutical Resource Discovery, Dalian Institute of Chemical Physics, Chinese Academy of Sciences, Dalian 116023, China

Received April 3, 2012; Revised May 5, 2012; Accepted May 9, 2012

ABSTRACT

Nano-scale particles have attracted a lot of attention for its potential use in medical studies, in particular for the diagnostic and therapeutic purposes. However, the toxicity and other side effects caused by the undesired interaction between nanoparticles and DNA/RNA are not clear. To address this problem, a model to evaluate the general rules governing how nanoparticles interact with DNA/RNA is demanded. Here by, use of an examination of 2254 native nucleotides with molecular dynamics simulation and thermodynamic analysis, we demonstrate how the DNA/RNA native structures are disrupted by the fullerene (C60) in a physiological condition. The nanoparticle was found to bind with the minor grooves of double-stranded DNA and trigger unwinding and disrupting of the DNA helix, which indicates C60 can potentially inhibit the DNA replication and induce potential side effects. In contrast to that of DNA, C60 only binds to the major grooves of RNA helix, which stabilizes the RNA structure or transforms the configuration from stretch to curl. This finding sheds new light on how C60 inhibits reverse transcription as HIV replicates. In addition, the binding of C60 stabilizes the structures of RNA riboswitch, indicating that C60 might regulate the gene expression. The binding energies of C60 with different genomic fragments varies in the range of -56 to $-10\,\mathrm{kcal\,mol^{-1}}$, which further verifies the role of nanoparticle in DNA/RNA damage. Our findings reveal a general mode by which C60 causes DNA/RNA damage or other toxic effects at a systematic level, suggesting it should be cautious to handle these nanomaterials in various medical applications.

INTRODUCTION

Without a doubt, nanotoxicology has to mature as a scientific discipline to enable the widespread application of nanoparticles (1). Despite the early acceptance and rapid progress of nanoparticle toxicity assessments, the potential toxic mechanisms of interactions between the nanoparticles and the biological systems have not yet been fully elucidated. Studies on the interactions of the nanoparticles and proteins/nucleic acids may provide guidance for understanding the basic questions in nanotoxicology.

Most of the studies have so far focused on changes in the protein structure or local or global changes in protein dynamics upon binding to nanoparticles. Single-walled carbon nanotubes (SWNTs) are found to plug into the hydrophobic core of protein WW domains to disrupt and block the active sites, which finally leads to the loss of the original function of protein (2). Similar effects have also been observed with the irreversible gold nanoparticles (AuNP)-induced conformational changes of human ubiquitin (hUbq) protein (3). Separately, it is also shown in our recent work that fullerene C60 adsorbs onto the cell-membrane P-glycoprotein through hydrophobic interactions, but the stability and secondary structure of the protein are barely affected (4). Also, we note the strong association of C60 molecules with ion channels, enzyme and antibodies where the binding depends on the particle size and native protein structures (5).

Despite the extensive studies in the nanoparticle–protein hybrids, to date, the 'substantive nature' of the

*To whom correspondence should be addressed. Tel: +86 029 87092262; Fax: +86 029 7091175; Email: yh_wang@nwsuaf.edu.cn

The authors wish it to be known that, in their opinion, the first two authors should be regarded as joint First Authors.

effects of nanoparticles on nucleic acids has only been partially clarified. The nano studies are limited by the fact that researchers mainly focus on the hybrids of carbon nanotubes with DNA sequences in most cases. For example, poly(GT) DNA sequences are shown to be rolled up onto SWNTs to form stable barrels, which results in structures analogous to the well-known protein β-sheet motifs (6). Through molecular simulation (MD) studies, single-stranded DNA (ssDNA) has been found to form right-handed helical wraps around the outside of SWNTs, dependent on both the DNA sequence and the SWNT chirality (7). In our previous work, we also found the unique wrapping behaviors of chiral and armchair SWNTs by DNA dinucleotides that display base flipping, local dynamic stability of structure and conformational shifting (8). The resulting structural destabilization and deformation of the DNA sequences imply that the nanomolecules probably exert certain toxic effects in organisms, which is very different from the traditional large-scale materials.

The molecular recognition features of carbon nanotubes with DNA are somewhat clarified at the moment; while for another carbon nanomaterial C60, one of the most important nano-drug carriers, its interaction mechanism with DNA/RNA are still illusive. Indeed, a pioneering study has found that C60 binds tightly to DNA and speculated that this association may negatively impact the self-repairing process of the double-stranded DNA (dsDNA) (9). Nonetheless, several fundamental questions still remain unclear due to the restrictions associated with the earlier disadvanced computing facilities. For example, whether RNA hybridizes to C60? What is the structural basis for the DNA/RNA recognition of C60 particle? Could the native structures of DNA/RNA be disrupted by C60 binding? Do the hybrids of DNA/RNA with C60 bear any biological relevance that leads to the potential nanotoxicity?

In this study, we report the static and dynamic bindings of DNA/RNA to C60 by using geometry-based algorithm and molecular dynamics (MDs) simulations, and find that the nanomolecule enables to disrupt the native conformations of these fragments. Further thermodynamic analysis verifies our results, and explains the specific hybrids between C60 and nucleotide fragments from the energy aspect.

MATERIALS AND METHODS

Preparation of structure-based test set

To investigate the binding properties of C60 with nucleotides, a total of 2254 animal and bacteria nucleotide samples were selected from the Nucleic Acid Database (NDB) to achieve the most extensive sampling (http://ndbserver.rutgers.edu/index.html, accession time: February 23, 2012), which consisted of four sets of crystal structures, including ligand–DNA/RNA complexes and free DNA/RNA structures. A nucleic acid fragment was selected according to the following criteria: (i) selecting the structure without artificial mutations (e.g. PDB codes 1CS7, 1PUY and 265D) or cleavages (e.g. PDB codes 1F6C, 1P24 and 2FII) around the binding site where C60 binds based on the geometry-based algorithm and (ii) deleting the ssDNA (e.g. PDB codes 1G6D, 1QYK and 382D). Finally, 589 ligand–DNA complexes yielded a total number of 313 cases, while 432 ligand–RNA complexes formed a set of 230 cases. For the 767 free-DNA fragments and 466 free-RNA fragments, 193 and 166 cases were generated according to the above selection criteria, respectively (the PDB codes for the selected structures can be seen in Supplementary Data). All these structures were manually inspected using VMD 1.9.1 (10) and PyMOL v1.4 (http://www.pymol.org/).

Binding modes and dynamics of nucleotides

Geometry-based algorithm (11) was applied to identify the binding modes of C60 with the nucleic acid strands that were treated as rigid bodies. This method employed three-dimensional transformations driven by local feature matching, and spatial pattern detection techniques, such as the geometric hashing and pose clustering, to yield good molecular shape complementarity with high efficiency. After the fast transformational search, the best geometric fit obtained the highest scores (~5000), while the low scores (~500) exhibited poor matches. For the complexes in our work, the clustering root mean square deviation (RMSD) was 4 Å. The 5 lowest binding energy matches for each complex were selected and analyzed visually.

To analyze the dynamics of nucleotides under physiological conditions, each complex was further simulated with MD using the GROMACS 4.5.1 MD package (12) on a simulation time scale of 70 ns. These structures were solvated in triclinic boxes with box vectors of ~10 Å length. The systems were energy minimized, followed by a relaxation for 400 ps, with positional restraints on the DNA/RNA atoms by using a force constant of $k = 1000\,\mathrm{kJ\,mol^{-1}\,nm^{-2}}$. The CHARMM27 force field (13) with CMAP corrections (14) was used for the nucleic acid and SPC/E for the water model (15). All simulations were performed in the NPT ensemble. The temperature was kept constant by Nose–Hoover temperature coupling at $T = 300\,\mathrm{K}$, with a coupling time of $T_p = 0.5$ ps (16). The pressure was coupled to a Parrinello–Rahman with $T_p = 4$ ps and an isotropic compressibility of $4.5 \times 10^{-5}\,\mathrm{bar^{-1}}$ in the x, y and z directions (17). All bonds were constrained with the LINCS algorithm (18). Electrostatic interactions were calculated explicitly at a distance smaller than 10 Å; long-range electrostatic interactions were calculated by particle mesh Ewald method, with a grid spacing of 0.12 nm and fourth order B-spline interpolation (19). Structures were written out every 10 ps for subsequent analysis.

Calculation of binding affinity

The calculation of binding free energies for the C60–DNA and C60–RNA complexes was evaluated using MM-GBSA (molecular mechanics general Borned surface area) method (20,21). This approach employed molecular mechanics, generalized Born model and solvent accessibility method to elicit the free energy from the structural information circumventing the computational complexity of the free-energy simulations. It was parametrized within

the additivity approximation (22) wherein the net free-energy change was treated as a sum of a comprehensive set of individual energy components, each with a physical basis. Briefly, in the MM-GBSA approach, the C60–DNA/RNA binding free energy ($\Delta G_{binding}$) for each snapshot was estimated as

$$\Delta G_{binding} = \left[G_{complex}\right] - \left[G_{DNA/RNA}\right] - \left[G_{C60}\right] \quad (1)$$

The free energy of each of the above terms was calculated from

$$\Delta G_{tot} = \Delta E_{MM} + \Delta G_{solv} - T\Delta S \quad (2)$$

where E_{MM} is the molecular mechanics energy of the molecule expressed as the sum of the internal energy (bonds, angles and dihedrals) (E_{int}), the electrostatic energy (E_{ele}) and van der Waals (E_{vdW}) terms. For the unique nanoparticle C60, its E_{int} and E_{ele} equal to 0 kcal mol^{-1}. G_{solv} accounts for the solvation energy, which can be divided into the polar and nonpolar parts. Obtaining the solvation free energy (G_{solv}) from an implicit description of the solvent as a continuum is advantageous because it affords a solvation potential that is only a function of the solute's geometry, as discussed and implemented by Srinivasan *et al.* (23). As reported by our previous studies (8), the contribution of the entropy ($T\Delta S$) was negligible because the difference of $T\Delta S$ was very small considering the similarity of the systems.

RESULTS AND DISCUSSION

It is known that DNA/RNA fragments possess complex structural features such as high density charge and helix chiral geometry, and do not present a single and well-defined binding site. For the nanoparticle C60, this unique molecule shapes like a hollow sphere and behaves chemically and physically as electron-deficient alkenes, thus probably eliminating more interferences from the nucleic acid specificity and identifying their potential targets. In addition, for most of the successful drugs targeting the nucleic acids, they are organic molecules such as the aromatic and heterocyclic compounds, which enable to form noncovalent or covalent interactions in the grooves with different sequence selectivity. This is overwhelmingly favorable for C60 to interact with the nucleic acids due to its benzene-derived ring structure. Indeed, previous studies have already shown the unique carbon nanotube–DNA hybridization modes with an emphasis on the structural deformation of nucleotides (6–8). However, it is still unclear whether and how C60 binds to DNA/RNA, and do the hybrids produce serious toxic effects on nucleotides?

Static hybridization of C60 with DNA

To address this, we begin our study by simulating the binding of C60 with the dsDNAs derived from the ligand–DNA crystal structures that show the representative properties of nucleotide segments. Figure 1A shows 205 interactions of C60 with the base pair guanine and cytosine (C60-guanine–cytosine; C60GC), in which 118 (48.0%) involve three consecutive GC base pairs ($C60GC_3$). Of the 129 complexes, where the binding sites of C60 contain the base pair adenine and thymine (AT), there are only 42 structures (17.1%) encompassing three consecutive AT base pairs ($C60AT_3$) (Figure 1A). These results indicate that C60 selectively binds to the GC base pair compared with the AT base pair.

Further analysis shows that C60 has varying degrees of groove preference for different sequences (Figure 1A), i.e. the $C60GC_3$ binding mode occurs far more often in the minor grooves (41.1%), while the $C60AT_3$ mode display a higher preference for the major grooves (13.4%). More strikingly, for those binding modes where the base pairs GC and AT coexist, i.e. C60GC-GC-AT, C60GC-AT-GC, C60AT-GC-AT and C60AT-AT-GC, the C60 molecule is found to bind to the DNA segments with the same preference for the major grooves as the $C60AT_3$ mode, which indicates a significant role of the base pair AT in determining the groove binding specificity of C60.

The binding of ligand probably alters the native conformations of free nucleotide fragments, thus leading to certain changes in C60 binding modes. In order to eliminate this, we further collected 193 crystal structures of free-dsDNA segments from NDB to analyze their interactions with C60 and to compare the binding modes with those of ligand-bound complexes. As shown in Figure 1B, C60 shows the same preference for the $C60GC_3$ binding mode (>36%), whereas the proportions of $C60AT_3$ binding mode are still found to be very low (<18%), supporting our idea that C60 has a strong tendency to bind to the GC-rich regions of nucleotides. Also, the hybrids of C60 molecule with the three consecutive GC or AT base pairs of free-dsDNA segments are found to display the same preference for the minor or major grooves (77.1 and 66.7%, respectively). Screening of the free-DNA segments obviously vouches for the accuracy of our modes, and meanwhile, reveals the potential C60 binding targets of interest for biological and pharmacological activity.

Consequently, the above observations raise a question of why C60 prefers to hybrid with the GC_3 sequences in the minor grooves. In fact, it has been reported that the GC-rich regions of nucleotides have a strong tendency to be minor groove wide (width >5 Å), while the AT-rich DNA tend to be minor groove narrowing (width <5 Å) (24), which suggests the sequence dependence of minor groove width. As C60 molecule shapes like a hollow sphere with a diameter of 7.0 Å, larger than the minor groove width of AT-rich regions, it is thus reasonable to believe that this nanoparticle tends to bind to the wider minor grooves along the GC sequences.

To further investigate the binding preference of C60, we select four representative systems from the C60GC3 and C60AT3 binding modes to estimate their binding free energies, respectively (Table 1). It is worth to note that since the C60 in our systems carries no charge, the contribution of the electrostatic energy is neglected. The results show that the systems in the C60GC3 mode have much lower G_{total} (nearly 6 kcal mol^{-1}) than those in the C60AT3 binding modes, indicating the more favorable interactions of the C60 molecule with the GC-rich

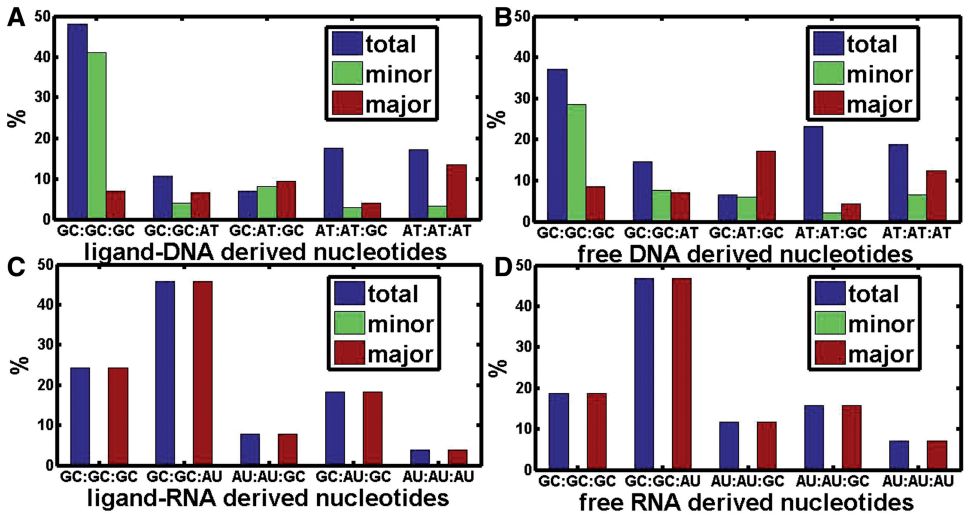

Figure 1. Static hybridization characteristics of C60–DNA/RNA complexes. (**A** and **B**) show percentages of nucleotide sequences derived from the ligand–DNA and free-DNA crystal structures that hybrid with C60 in the GC:GC:GC, GC:GC:AT, GC:AT:GC, AT:AT:GC and AT:AT:AT regions, respectively. (**C** and **D**) show those from ligand–RNA and free-RNA structures that hybrid with C60 in the GC:GC:GC, GC:GC:AU, AU:AU:GC, GC:AU:GC and AU:AU:AU regions, respectively. Blue color represents the total percentages of C60–DNA/RNA recognition; cyan the percentages of minor groove recognition; red the percentages of major groove recognition, respectively.

Table 1. Calculation of binding free energy for static hybridization of C60 with DNA/RNA

Nucleic acid	Binding sites	System	E_{vdW}		G_{solv}		G_{tot}	
			Mean (kcal mol^{-1})	Standard deviation	Mean (kcal mol^{-1})	Standard deviation	Mean (kcal mol^{-1})	Standard deviation
DNA	GC:GC:GC	1IH1	−33.51	5.07	7.89	0.96	−25.62	2.57
		461D	−32.90	2.01	7.43	0.87	−25.47	1.86
	AT:AT:AT	2V3L	−14.80	1.79	5.04	0.94	−9.76	1.33
		432D	−32.49	2.59	8.99	0.81	−23.50	2.12
RNA	GC:GC:GC	1F79	−33.39	6.37	15.87	2.02	−17.52	5.04
		1KD4	−10.73	1.33	4.16	0.85	−6.56	1.01
	GC:GC:AU	1F7I	−36.43	3.86	15.32	1.59	−21.10	2.90
		1Y99	−48.60	2.77	21.28	2.18	−27.33	2.47
	GC:AU:GC	3NJT	−11.61	1.84	4.88	0.78	−6.73	1.34
		2NOK	−33.53	6.56	14.89	2.44	−18.63	4.51
	AU:AU:GC	1LNT	−34.22	3.45	18.40	2.94	−15.82	2.25
		2KU0	−26.45	2.52	10.69	1.09	−15.76	1.90
	AU:AU:AU	1YY0	−36.55	5.95	15.54	2.55	−21.01	3.88
		3S49	−33.85	2.44	12.17	0.88	−21.68	1.95

regions of DNA. This thus further explains why C60 prefers for the minor grooves of the GC sequences to some extent.

Static hybridization of C60 with RNA

Next, we have investigated the molecular recognition features of RNA after the hybridization. As shown in Figure 1C, C60 prefers for the GC-rich regions of RNA, especially the GC-GC-AU sequences that contain ~2.6–9.8 times the number of AT-rich sequences. Most strikingly, the nano molecule C60 binds only to the major groove sites of RNA, and no association has been observed at the minor groove sites in our simulations, as shown by the blank cyan plots in Figure 1C. Since the major groove of RNA (12.9 Å) is much deeper compared to its minor groove (3.3 Å) (25), we expect that the depth of the RNA grooves greatly impacts the accommodation of C60, and finally leads to the extremely high tendency of C60 hybrids for the major grooves.

To further evaluate the binding tendency of RNA, we choose two representative C60–RNA complexes from each of the modes to calculate their binding energies. The data in Table 1 show that the binding energies vary considerably with different base sequences. The systems in the C60GC-GC-AU mode have binding energies of ~ -24 kcal mol^{-1}. While for the systems containing two or three AU base pairs, the changes in sequences give relatively larger increases in the G_{total}, 3–9 kcal mol^{-1}. For systems in the C60GC-GC-GC and C60GC-AU-GC modes, the binding energies become more positive than

those of the systems in the C60GC-GC-AU mode (12 kcal mol^{-1}). Since lower binding affinities imply more stable binding of the ligands, the analysis of binding affinity of the C60–RNA complexes provides strong evidence for the preference of the nanoparticle for the GC-GC-AU sequences of the nucleotides.

Finally, we select 166 free-RNA structures from the NDB to enable the unbiased statistics. The results show similar preferences for C60 to hybrid with RNA (46.8% for the GC-GC-AU sequences) (Figure 1D). Moreover, the nanomolecule is still found to only hybrid with the major groove regions of RNA. These results confirm the accuracy of our modes, and imply that the hybridization features of C60 depend on the nature of the nucleotides.

Hybridization-induced structural changes in DNA/RNA

The above observations provide new insight into the recognition of DNA/RNA by C60. These models, however, also reveal a lack of realistic circumstance for the C60 hybridization, and little consideration to the issue of the dynamics of DNA/RNA. Toward the next level of understanding, we thus investigated the hybridization-induced structural changes of DNA/RNA using MD simulations.

DNA

dsDNA twist. The C60-induced twist on dsDNA is firstly observed, which accounts for 17% of the total C60–DNA dynamic interaction systems (e.g. PDB codes 1XRW, 1CYZ, 1QSX, 378D and 245D). As shown in Figure 2A (PDB code 1XRW), the C60 molecule is initially located at the GC:GC binding site where the minor groove of the DNA faces the nanomolecule surface. After 1–2 ns, the C60 slides along a linear path, parallel to the DNA axis, with distance of ~8 Å to the neighboring AT:GC site, and sticks to the site for the rest of the simulation time (50–60 ns) (Figure 2B). During the process, significant conformational changes of the DNA sequence occur, showing an anti-clockwise twist of the nucleotide along its helix-parallel axis (~40°) with respect to its initial position.

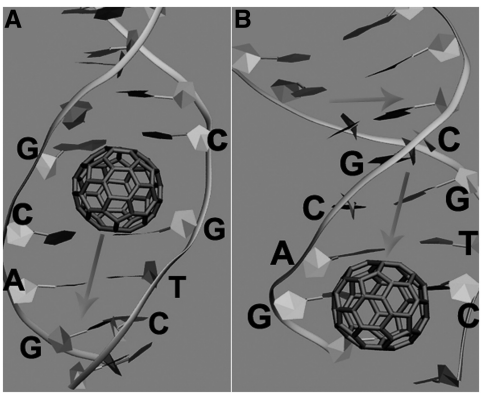

Figure 2. Interactions of C60 with dsDNA in the 1XRW system. (**A**) The binding of C60 to the DNA at GC:GC binding site, and (**B**) shows the sliding of the nanoparticle to the GC:AT site. The arrows show the sliding directions of the C60 molecule and the rotation direction of the DNA fragment.

Comparison of the MD trajectory with the static C60–DNA hybridization mode reveals a difference between the initial identified site of C60 (the GC:GC:AT binding region obtained from the geometry-based algorithm) and its final stabilized site (the AT:GC binding region obtained from the MD simulation). This interesting change might be similar to the process of food intake by mouth (initial) and then digestion in stomach (final). Detailed analysis of the final stabilized sites for all the C60–DNA systems is given in Section ''Statistical analysis of dynamic hybridization''.

Evidently, these sequences in the sliding-induced twist mode share a unique binding region that is composed of two successive GC:GC or AT:AT base pairs and the following AT:GC base pairs. In fact, the above analysis of static hybridization has described the direct binding of C60 with the GC:GC or AT:AT sites on the basis of the geometric fit. Such hybrid, however, exhibits an unstable state in the MD simulations due to the asymmetry of the GC or AT repeats, and thus causes the sliding of the C60 molecule and the subsequent conformational changes of the dsDNA fragments.

dsDNA unwinding. Another intriguing finding is that the binding of C60 has high probability for triggering the initiation of DNA unwinding, accounting for 32.1% of the total systems. For example, C60 interacts with the GC:AT site of DNA through hydrophobic interactions in the initial 4 ns (Figure 3A). Then, the nanomolecule slides along the DNA helix to the neighboring base pairs GC:GC with a distance of 6 Å, and stays in the location for ~45 ns (Figure 3B). Due to the dynamic instability induced by the C60 binding, the nanomolecule slides rapidly back to the AT:GC site again. Almost immediately, the AT:AT sequence in the 3′-terminal undergoes a torsion deformation involving the outward tilting of T1 and T2 (~100°) and the rotation of A7 and A8 (~30°), which finally leads to the partial unwinding of the DNA fragment (Figure 3C).

Two types of DNA sequence properties that correlate with the unwinding mode are identified in this section: (i) For the AT:AT:$(GC)_3$ sequences, such as the structures with the PDB codes of 1CP8, 1QCH and 2D55, C60 initially binds to the AT:GC site, and then slides to the third GC base pair. After return to the AT:GC site, the binding site is forced to unwind. (ii) For the GC:GC:AT:AT(GC) sequences, such as the structures with the PDB codes of 1I5V and 1MPT, C60 interacts with the GC:GC region in the first 3 ns and subsequently slides along the DNA helix to the neighboring AT:AT or AT:GC sites. After a transient pause (~5–15 ns), the small molecule relocates at the GC:GC region, and finally induces the partial unwinding of this site.

It is known that Okazaki fragments are newly synthesized DNA fragments that are formed on the lagging template strand during the DNA replication, and are short molecules of ssDNA between 100 and 200 nt long in eukaryotes (26). Since our results show the unwinding mode of DNA fragments when hybridized with C60, it is reasonable to speculate that the binding of C60 molecule could inhibit the DNA discontinuous

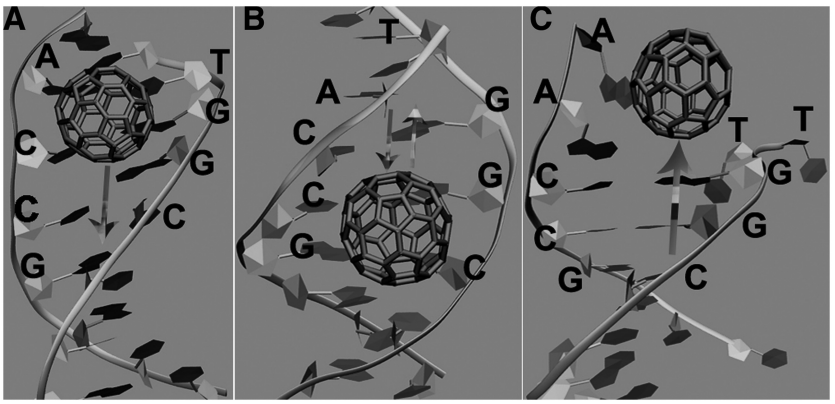

Figure 3. Interactions of C60 with dsDNA in the 1CP8 system. (**A** and **B**) show the binding of C60 to the DNA at AT:GC binding site, and the subsequent sliding to the GC:GC site, respectively. (**C**) The unwinding of the dsDNA fragment. The arrows show the sliding directions of the C60 molecule.

replication by disrupting the structures of Okazaki fragments and lagging the strand template. This thus should raise great concerns about the introduction of nanoparticles in the therapeutic fields.

dsDNA stability. Evidence from MD simulations (e.g. PDB codes 108D, 1AMD, 1MTG, 1N37, 1RQY, 2ADW, 2GWA and 3GSK) shows that the binding of C60 has little or no effects on the conformations of DNA fragments involving the AT:GC:GC(AT) sequences, which accounts for 32% of the total C60–DNA complexes. Figure 4 shows that the C60 molecule intercalates into the AT:GC base pairs with the plane of the aromatic nucleotide bases oriented parallel to the surface of the nanotube, and maintains such binding mode through the entire 70 ns simulation. Since the π–π stacking interactions of C60 with the DNA fragment contribute most to the complex stability, and this type of directional force is comparable in strength to hydrogen bonding and can, in some case, be a decisive intermolecular force, we believe that the strong stacking is the key to this phenomenon, in which the nucleic acid fragment maintains its rigidity upon the binding of C60.

Indeed, among the main DNA binding modes, intercalation is proposed to be the most common way through which small and rigid aromatic molecules recognize the DNA (27). However, since the binding of intercalators to DNA depends basically on π-stacking and electrostatic interactions, most of the ligands possess less sequence specificity, which is a major obstacle to the target recognition. In this section, we have found the DNA–C60 interactions and the resulting intercalation structure is dependent on both the DNA sequence and the C60 structure. This points to the possibility of selecting C60 for specific DNA sequence recognition.

G-quadruplex disruption. DNA is polymorphic, and can adopt diverse structures other than the Watson–Crick duplex when actively participating in the replication, transcription, recombination and damage repair (28). Of particular interest are guanine-rich regions, which present a non-canonical four-stranded topology, called the G-quadruplex. Such architecture involved in the 3′-overhang of telomeres of human chromosomes enables to block the catalytic reaction of the telomerase, a relevant target in oncology.

Figure 5A shows an example of the hybrid of C60 with the G-quadruplex DNA fragment in the wide groove (PDB code: 2JT7). The nanomolecule remains stable with no significant changes in orientation during the entire simulation (Figure 5D). In contrast, the bases T6 and T1 of the DNA fragment exhibit large tilts (∼90°) due to the attraction of C60-induced π–π stacking (Figure 5B), and finally form a 'sandwich' state with the nanomolecule, i.e. the C60 is clipped between T1 and T6 (Figure 5C). Scanning of all the trajectories in the G-quadruplex disruption mode confirms our results, and suggests that C60 enables to bind into the hydrophobic grooves of the G-quadruplex in a sidewise approach, but also stacks on the surface of the terminal quartet in an external mode. Despite the target disparity of C60, all the structures of G-quadruplex DNA fragments display great deformation after hybridization, which accounts for 9.2% of the total systems.

It is known that in normal somatic cells, telomere length decreases at each round of division and consequently these cells have a finite lifetime. While in human tumor cells, the reverse transcriptase enzyme telomerase is activated to maintain the telomere length so that tumor cells are effectively immortalized (29). Since the formation of a G-quadruplex structure at the 3′-end of telomeric DNA effectively hinders the telomerase from adding further repeats, we speculate that C60 that disrupts the G-quadruplex could activate the telomerase by facilitating its access to the telomeres and could therefore induce potential side effects of therapeutic treatments when C60 was used as anticancer drug carriers.

RNA

RNA curling. After being perceived for a long time merely as an intermediate between DNA (the depository of the genetic information) and proteins (the macromolecules that work inside a cell), RNA now is the center of attention in biomedical research. RNA's boost in fame is

partially attributable to the discovery of its role in being an integral part of many biological processes.

In this section, we find a structural transition of RNA between two states, the RNA stretch state and the RNA curling state, and such transition only exists in the HIV trans-activating region (TAR) RNA fragments (e.g. PDB codes: 1AKX, 1ARJ, 1LVJ, 1QD3 and 1UTS, accounting for 9.5% of the total). The dynamics of the stretch→curling transition, monitored using time-dependent changes in RMSD of the RNA, shows that the molecules undergo specific transitions at ~10 ns, and spend a substantial fraction of time (~60 ns) in the curling state (Figure 6D). Since the transition involves the formation of intersubunit contacts, we take the TAR RNA in the 1AKX system as an example to dissect the transition.

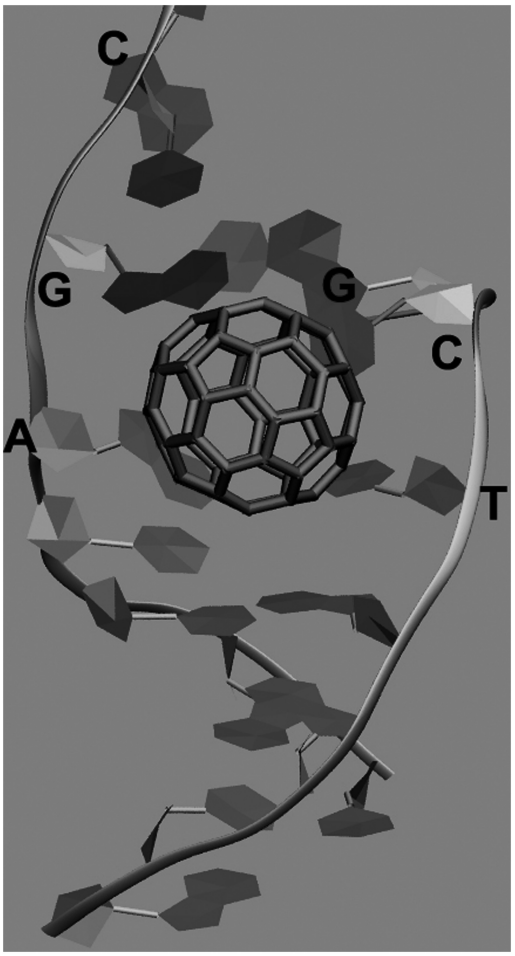

Figure 4. Binding of C60 to the dsDNA at GC:AT binding site in the 108D system.

Upon the binding of C60, the two bases A22 and U23 capture the nanomolecule via π–π stacking interactions and remain constant during the entire simulation (Figure 6A). This event accompanies the significant fluctuation of A35 as evidenced by its large rotation of angle (CB-CG-CD-CE) from −180° to ~180° (Figure 6B and E). Subsequently, the G33 in the middle of the stem region has tilted by ~50° (CD-ND-CA-CB) to form π-stacking with the C60 molecule (Figure 6C). Coupled with the significant conformational change of G33, the loop region is forced to undergo the upward curling and maintain the state for ~30 ns as evidenced by the torsional rigidity of G33 and A35 (from ~40 ns to ~60 ns) (Figure 6E).

Indeed, the interaction between positive transcription elongation factor complex b (P-TEFb), Tat protein and TAR is a key step in the transactivation process of HIV-1, and TAR RNA is shown to exhibit specificity to P-TEFb–Tat-TAR complex formation (30,31), which implies the major role of TAR RNA molecule in assembling a regulatory switch in HIV replication. Thus, we speculate that the structural changes of the TAR RNA induced by C60 could disrupt the structural association of the RNA molecule with its protein partners, resulting in inhibiting the HIV reverse transcription and repressing the expression of HIV.

Riboswitch stabilization. Riboswitches have been reported to be capable of binding cellular metabolites using a diverse array of secondary and tertiary structures to modulate the gene expression (32). Results of the MD simulations (e.g. PDB codes: 2HOK, 2H0M, 3NPB, 2YDH and 2GIS, accounting for 19.5% of the total) show that the C60 molecule presents a similar binding mode as those of riboswitch substrates, and enables to stabilize the conformations of riboswitches.

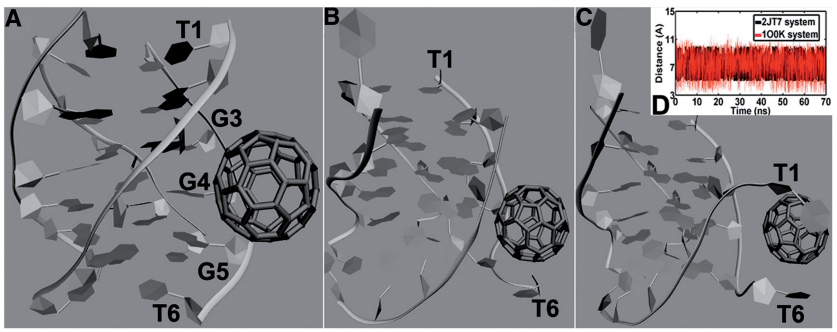

Figure 5. Interactions of C60 with G-quadruplex DNA in the 2JT7 system. (**A–C**) show the conformational changes of G-quadruplex with the binding of C60. (**D**) shows the time evolutions of the distance between the G-quadruplex DNA fragment and C60.

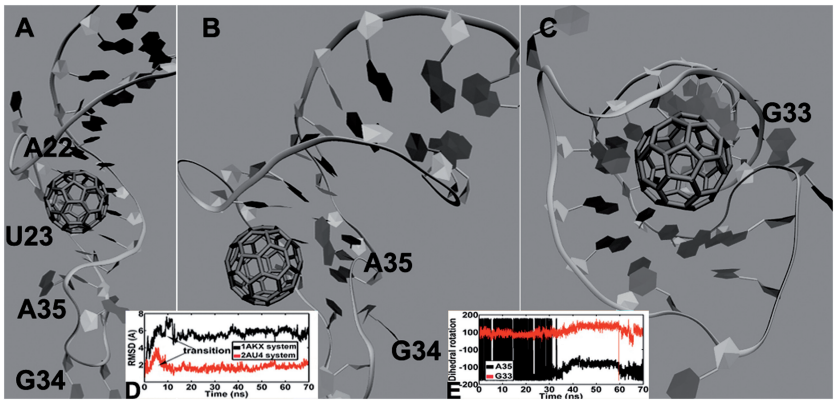

Figure 6. Interactions of C60 with double-stranded RNA in the 1AKX system. (**A–C**) show the conformational changes of dsRNA with the binding of C60. (**D**) The RMSD of dsRNA versus simulation time in the 1AKX and 2AU4 systems. (**E**) reveals the time-dependent rotation of G33 and A35 about the (CD-ND-CA-CB) and (CB-CG-CD-CE) dihedral angles, respectively.

For example, the SAM-I riboswitch is based around an elaborated four way helical junction (PDB code: 3NPB). Several nucleic acids (notably C48, G79 and A111) in the P1 and P3 helices, and the intervening J1/2 and J3/J4 joining regions of the junction interact with the C60 molecule thus creating a ligand binding pocket (Figure 7A). This nanomolecule constantly sticks to this binding site during the entire simulation (Figure 7B). More interestingly, in the presence of C60, the riboswitch is found to engage in the same conformation as the binding of substrate *S*-adenosylmethionine, thereby probably maintaining the folding of the expression platform (33). Since the conformations of the expression platform direct the transcriptional or translational controls, the C60 has great potential to be a new type of riboswitch substrate to regulate the gene expression.

dsRNA stabilization. It is commonly accepted that molecular recognition and formation of the noncovalent complex are driven by non-specific interactions and sequence-specific structural features along the major groove of RNA (28). Figure 8A shows that the C60 molecule locates at the major grooves of RNA and displays a modest selectivity for G-rich regions involving at least four G bases (e.g. PDB codes: 1BYJ, 1EI2, 2JUK, 2FCX and 1FYD), which accounts for 35.6% of the total systems. Once the binding sites have been identified, the C60 molecule rapidly slides along the major groove (Figure 8C). At ~25 ns, this molecule turns out of the groove to form a relatively stable complex through hydrophobic interactions via its hydrophobic surface and the end of the RNA strand (Figure 8B). Interestingly, during the whole MD simulations, we do not observe evident conformational changes of the RNA fragments.

Since DNA with high GC content is more stable than DNA with low GC content (34), it is possible that the G-rich RNA sequences also adopt stable conformations in spite of the interferences induced by the C60 hybridization. This indicates that the structural stability of dsRNA relies on sequence specificity of nucleotides.

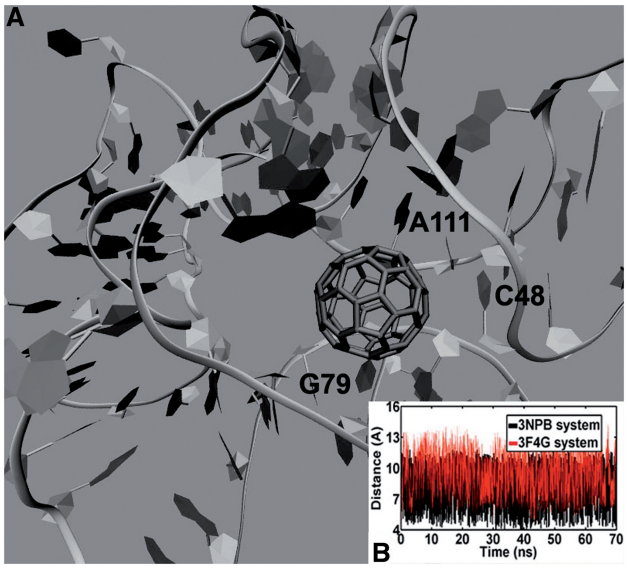

Figure 7. (**A**) Interactions of C60 with riboswitch RNA in the 3NPB system. (**B**) Time evolution of the distance between C60 and the riboswitch RNA fragment in the 3NPB and 3F4G systems.

Statistical analysis of dynamic hybridization

In this section, we have statistically analyzed the final stabilized sites of C60 in all the C60-dsDNA/dsRNA dynamic interaction systems, and compared these sites with the initial identified sites (Figure 1). Figure 9 shows the four or three types of the hybridization modes of C60 with DNA/RNA. For the C60-DNA hybrids, the nanomolecule is significantly preferred over the GC:AT sites (40.8%). Although the specific recognition of minor/major groove and the intercalation by C60 are found in almost all DNA hybridization modes (GC:AT, AT:AT and GC:GC), their preference in each can vary dramatically. The GC:AT regions have a relatively high percentage of 28.6% to form stronger hydrophobic interactions with C60 in the minor grooves. Contrary to this, the AT:AT and GC:GC regions have comparatively low

minor groove-recognition percentages of 7%, but high percentages of 13% to hybrid with C60 by intercalating. In the case of the C60-RNA hybrids, GC:AU sites are highly favored over GC:GC regions (56.2% versus 18.7%), and show a strong preference for the major grooves.

These results show the substantial differences between the final stabilized sites of C60 and its initial identified sites, which suggest the sequence-specific changes in realistic physiological circumstances.

Binding energy analysis

The above sections have revealed the dynamic interactions of DNA/RNA with C60, and indicated seven unique types of nucleotide conformations. Such observations strongly indicate that the different interaction interfaces and binding specificity of nucleotides may be coupled to binding energies with enormous disparities. To examine the hypothesis, we have thus selected two representative systems from each binding mode, and estimated their binding free energies with C60, respectively.

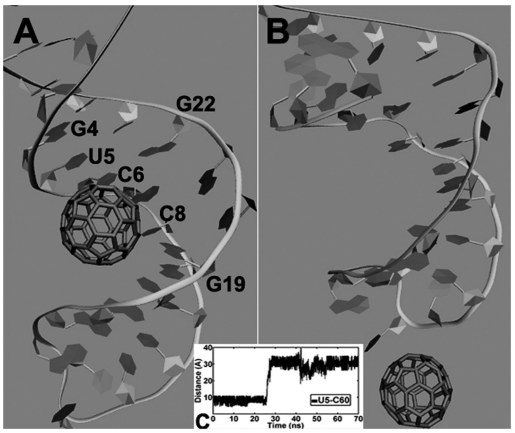

Figure 8. (**A**) Interactions of C60 with double-stranded RNA in the 1BYJ system. (**B**) Time evolution of the distance between C60 and U5. (**C**) The time evolution of the distance between the base U5 and the C60 molecule.

The data in Table 2 show the much higher binding affinities (~10 kcal mol^{-1}) of nucleotides in the dsDNA/riboswitch stabilization and G-quadruplex disruption modes compared with those in the other hybridization models. Indeed, the C60 is found to constantly stick to the nucleotides and remain in the stable state through the whole simulation time in the above three modes. Under such condition, the surface of nanomolecule provides more spaces for the hybrids of DNA/RNA, therefore aggrandizing the vdW interaction (~43 kcal mol^{-1}). In contrast, the nucleotides in the dsDNA twist, dsDNA unwinding, dsRNA curling and dsRNA stability modes display much weaker vdW energies (~30 kcal mol^{-1}). This is quite reasonable since the large and flexible movement of these nucleotides enables to induce their less favorable interactions with C60.

In addition, we notice that the C60 hybridization in all cases is accompanied by the reduction of solvent accessible surface area (SASA) due to the burial of large portions of C60 surface through the stacking of DNA bases, thus leading to a comparatively large, negative contribution of the solvation free energies (G_{solv}) to the binding free energy. Closer inspection reveals that the systems in the dsDNA twist, dsDNA unwinding, dsRNA curling and dsRNA stability modes have relatively smaller G_{solv} (3–5 kcal mol^{-1}) than those in the other binding modes. Indeed, the C60 molecule has displayed different sliding movements along the DNA/RNA axis in the above four modes. Such unique motions probably significantly decrease the SASA during the simulations, and thereby lead to the smaller G_{solv}.

Surprisingly, further comparison of the C60-nucleotides binding affinities in the initial identified sites with those in the final stabilized sites demonstrates a 2-fold difference (Table 2), which implies that the hybrid-induced dynamics of nucleotides significantly affects the hybridization modes of C60, quite similar to the food intake process from the mouth to the stomach.

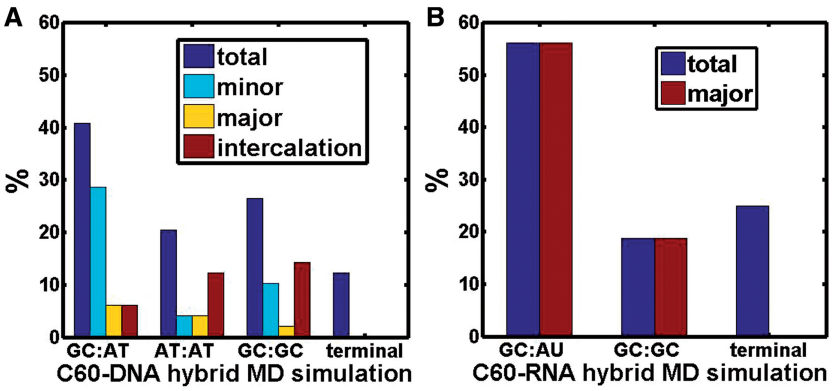

Figure 9. Dynamics hybridization characteristics of C60-DNA/RNA complexes. (**A**) shows the percentages of representative DNA sequences derived from the MD simulations that hybrid with C60 in the GC:AT, AT:AT, GC:GC and terminal regions, respectively. (**B**) The percentages of representative RNA sequences derived from the MD simulations that hybrid with C60 in the GC:AU, GC:GC and terminal regions, respectively.

Table 2. Calculation of binding free energy for dynamics hybridization of C60 with DNA/RNA

Nucleic acid	Binding modes	Starting identified sites	System	E_{vdW}		G_{solv}		G_{tot}	
				Mean (kcal mol^{-1})	Standard deviation	Mean (kcal mol^{-1})	Standard deviation	Mean (kcal mol^{-1})	Standard deviation
DNA	dsDNA twist	GC:GC:AT	1XRW	−34.26	3.55	9.21	1.01	−25.05	3.03
		AT:AT:AT	378D	−39.50	5.13	7.93	1.13	−31.56	4.27
	dsDNA unwinding	GC:GC:AT	1CP8	−31.55	5.51	7.86	0.84	−23.69	5.35
		GC:GC:AT	1I5V	−30.88	1.91	8.19	0.93	−22.69	1.78
	dsDNA stability	AT:AT:GC	108D	−40.60	2.52	7.85	0.57	−32.75	2.39
		GC:GC:AT	2ADW	−68.66	2.31	13.01	1.06	−55.65	2.23
	G-quadruplex disruption	–	2JT7	−51.38	3.16	10.89	1.07	−40.49	2.58
		–	1O0K	−45.89	2.97	6.49	0.60	−39.40	2.82
RNA	dsRNA curling	GC:AU:GC	1AKX	−33.73	4.34	13.04	1.75	−20.69	3.32
		GC:GC:GC	1ARJ	−55.98	3.21	21.17	1.78	−34.81	2.63
	Stabilized riboswitch	–	3NPB	−65.34	2.68	18.08	1.00	−47.27	2.74
		–	2GIS	−66.74	4.07	17.36	1.08	−49.38	4.02
	dsRNA stability	GC:GC:AU	2A04	−31.82	1.89	15.27	1.56	−16.55	1.58
		AU:AU:GC	2JUK	−20.05	4.96	9.82	1.32	−10.23	3.95

CONCLUSIONS

In this study, we have investigated the static and dynamic hybridization properties of C60 with DNA/RNA, and analyzed the potential toxic effects of the nanomolecule. Using statistical survey, MD simulations and thermodynamic analyses, we have found that:

(1) In the C60–dsDNA hybrids, C60 prefers the minor grooves of dsDNA involving three consecutive GC base pairs (GC_3), and the major grooves with three consecutive AT base pairs (AT_3). The presence of the base pair AT in the binding sites plays a key role in determining the groove binding specificity of C60.
(2) In the C60–dsRNA hybrids, C60 prefers the GC-rich regions of RNA, especially the GC-GC-AU sequences. More strikingly, the nanomolecule binds only to the major groove regions of RNA.
(3) The difference between the initial identified sites and the final stabilized sites implies that C60 initially binds to the initial identified sites of DNA/RNA to induce the structural changes of the nucleotides, such as DNA/RNA twist, unwinding and curling. Then, the C60 molecule moves to the final stabilized sites, which probably leads to potential toxic effects. This is similar to the process of food intake by mouth (initial) and then digestion in stomach (final).
(4) C60 hybridization enables to trigger the initiation of dsDNA unwinding, which probably inhibits the DNA discontinuous replication.
(5) C60 enables to disrupt the structure of G-quadruplex DNA, and thereby provides a possibility to activate the telomerase by facilitating its access to telomeres and in this way promotes the proliferation of tumor cells.
(6) C60 induces the conformational transition of HIV TAR RNA sequences from the stretch state to the curling state, which probably inhibits the HIV reverse transcription and represses the expression of HIV.
(7) C60 binds to the substrate-binding site of riboswitch RNA, showing great potential to be a new type of riboswitch substrate to regulate the gene expression.
(8) The nucleotides in the dsDNA stability, G-quadruplex disruption and stabilized riboswitch modes display much higher binding affinities to C60 than those in other modes, mainly due to the significant movement of C60, such as sliding.

SUPPLEMENTARY DATA

Supplementary Data are available at NAR Online.

ACKNOWLEDGEMENTS

Authors are grateful to Dr X.Z.Z. (Benkeman insititue, US) for English improvement.

FUNDING

High-Performance Computing Platform of Northwest A&F University, and is financially supported by the National Natural Science Foundation of China [31170796] and also the Fund of Northwest A&F University. Funding for open access charge: The National Natural Science Foundation of China (NSFC) is an organization directly affiliated to the State Council for the management of the National Natural Science Fund. And Northwest A&F University manages the Fund of Northwest A&F University.

Conflict of interest statement. None declared.

REFERENCES

1. Hess,H. and Tseng,Y. (2007) Active intracellular transport of nanoparticles: opportunity or threat? *ACS Nano*, **1**, 390–392.
2. Zuo,G., Huang,Q., Wei,G., Zhou,R. and Fang,H. (2010) Plugging into proteins: poisoning protein function by a hydrophobic nanoparticle. *ACS Nano*, **4**, 7508–7514.
3. Calzolai,L., Franchini,F., Gilliland,D. and Rossi,F.O. (2010) Protein–nanoparticle interaction: identification of the ubiquitin–gold nanoparticle interaction Site. *Nano Lett.*, **10**, 3101–3105.

4. Xu,X., Li,R., Ma,M., Wang,X., Wang,Y. and Zou,H. (2012) Multidrug resistance protein P-glycoprotein does not recognize nanoparticle C60: experiment and modeling. *Soft Matter*, **8**, 2915–2923.
5. Calvaresi,M. and Zerbetto,F. (2010) Baiting proteins with C60. *ACS Nano*, **4**, 2283–2299.
6. Tu,X., Manohar,S., Jagota,A. and Zheng,M. (2009) DNA sequence motifs for structure-specific recognition and separation of carbon nanotubes. *Nature*, **460**, 250–253.
7. Roxbury,D., Jagota,A. and Mittal,J. (2011) Sequence-specific self-stitching motif of short single-stranded DNA on a single-walled carbon nanotube. *J. Am. Chem. Soc.*, **133**, 13545–13550.
8. Xiao,Z., Wang,X., Xu,X., Zhang,H., Li,Y. and Wang,Y. (2011) Base- and structure-dependent DNA dinucleotide–carbon nanotube interactions: molecular dynamics simulations and thermodynamic analysis. *J. Phys. Chem. C*, **115**, 21546–21558.
9. Zhao,X., Striolo,A. and Cummings,P.T. (2005) C60 binds to and deforms nucleotides. *Biophys. J.*, **89**, 3856–3862.
10. Humphrey,W., Dalke,A. and Schulten,K. (1996) VMD: visual molecular dynamics. *J. Mol. Graphics*, **14**, 33–8, 27–28.
11. Schneidman-Duhovny,D., Inbar,Y., Nussinov,R. and Wolfson,H.J. (2005) PatchDock and SymmDock: servers for rigid and symmetric docking. *Nucleic Acids Res.*, **33**, W363–W367.
12. Lindahl,E., Hess,B. and van der Spoel,D. (2001) GROMACS 3.0: a package for molecular simulation and trajectory analysis. *J. Mol. Model.*, **7**, 306–317.
13. MacKerell,A.D., Bashford,D., Bellott,M., Dunbrack,R.L., Evanseck,J.D., Field,M.J., Fischer,S., Gao,J., Guo,H., Ha,S. *et al.* (1998) All-atom empirical potential for molecular modeling and dynamics studies of proteins. *J. Phys. Chem. B*, **102**, 3586–3616.
14. Mackerell,A.D. Jr, Feig,M. and Brooks,C.L. (2004) Extending the treatment of backbone energetics in protein force fields: limitations of gas-phase quantum mechanics in reproducing protein conformational distributions in molecular dynamics simulations. *J. Comput. Chem.*, **25**, 1400–1415.
15. Berendsen,H.J.C., Grigera,J.R. and Straatsma,T.P. (1987) The missing term in effective pair potentials. *J. Phys. Chem.*, **91**, 6269–6271.
16. Hoover,W.G. (1985) Canonical dynamics: equilibrium phase-space distributions. *Phys. Rev. A*, **31**, 1695–1697.
17. Parrinello,M. and Rahman,A. (1980) Crystal structure and pair potentials: a molecular-dynamics study. *Phys. Rev. Lett.*, **45**, 1196–1199.
18. Berk,H., Henk,B., Herman,J.C.B. and Johannes,G.E.M.F. (1997) LINCS: a linear constraint solver for molecular simulations. *J. Comput. Chem.*, **18**, 1463–1472.
19. Darden,T., York,D. and Pedersen,L. (1993) Particle mesh Ewald: an N.log(N) method for Ewald sums in large systems. *J. Chem. Phys.*, **98**, 10089–10092.
20. Hawkins,G.D., Cramer,C.J. and Truhlar,D.G. (1995) Pairwise solute descreening of solute charges from a dielectric medium. *Chem. Phys. Lett.*, **246**, 122–129.
21. Hawkins,G.D., Cramer,C.J. and Truhlar,D.G. (1996) Parametrized models of aqueous free energies of solvation based on pairwise descreening of solute atomic charges from a dielectric medium. *J. Phys. Chem.*, **100**, 19824–19839.
22. Dill,K.A. (1997) Additivity principles in biochemistry. *J. Biol. Chem.*, **272**, 701–704.
23. Srinivasan,J., Cheatham,T.E., Cieplak,P., Kollman,P.A. and Case,D.A. (1998) Continuum solvent studies of the stability of DNA, RNA, and phosphoramidate−DNA helices. *J. Am. Chem. Soc.*, **120**, 9401–9409.
24. Rohs,R., West,S.M., Sosinsky,A., Liu,P., Mann,R.S. and Honig,B. (2009) The role of DNA shape in protein-DNA recognition. *Nature*, **461**, 1248–1253.
25. Chargaff,E. and Davidson,J.N. (1955) *The Nucleic Acids: Chemistry and Biology*. Academic Press, New York.
26. Ogawa,T. and Okazaki,T. (1980) Discontinuous DNA replication. *Annu. Rev. Biochem.*, **49**, 421–457.
27. Tse,W.C. and Boger,D.L. (2004) Sequence-selective DNA recognition: natural products and nature's lessons. *Chem. Biol.*, **11**, 1607–1617.
28. Neidle,S. (1999) *Oxford Handbook of Nucleic Acid Structure*. Oxford University Press, Oxford, New York.
29. Mergny,J.L. and Helene,C. (1998) G-quadruplex DNA: a target for drug design. *Nat. Med.*, **4**, 1366–1367.
30. Richter,S., Ping,Y.-H. and Rana,T.M. (2002) TAR RNA loop: a scaffold for the assembly of a regulatory switch in HIV replication. *Proc. Natl. Acad. Sci. USA*, **99**, 7928–7933.
31. Toulme,J.J., Di Primo,C. and Moreau,S. (2001) Modulation of RNA function by oligonucleotides recognizing RNA structure. *Prog. Nucleic Acid Res. Mol. Biol.*, **69**, 1–46.
32. Montange,R.K. and Batey,R.T. (2008) Riboswitches: emerging themes in RNA structure and function. *Annu. Rev. Biophys.*, **37**, 117–133.
33. Lu,C., Ding,F., Chowdhury,A., Pradhan,V., Tomsic,J., Holmes,W.M., Henkin,T.M. and Ke,A. (2010) SAM recognition and conformational switching mechanism in the *Bacillus subtilis* yitJ S Box/SAM-I Riboswitch. *J. Mol. Biol.*, **404**, 803–818.
34. Yakovchuk,P., Protozanova,E. and Frank-Kamenetskii,M.D. (2006) Base-stacking and base-pairing contributions into thermal stability of the DNA double helix. *Nucleic Acids Res.*, **34**, 564–574.

C_{60} Binds to and Deforms Nucleotides

Xiongce Zhao,* Alberto Striolo,† and Peter T. Cummings*†
*Nanomaterials Theory Institute, Center for Nanophase Materials Sciences, Oak Ridge National Laboratory, Oak Ridge, Tennessee; and †Department of Chemical Engineering, Vanderbilt University, Nashville, Tennessee

ABSTRACT Atomistic molecular dynamics simulations are performed for up to 20 ns to monitor the formation and the stability of complexes composed of single- or double-strand DNA molecules and C_{60} in aqueous solution. Despite the hydrophobic nature of C_{60}, our results show that fullerenes strongly bind to nucleotides. The binding energies are in the range -27 to -42 kcal/mol; by contrast, the binding energy of two fullerenes in aqueous solution is only -7.5 kcal/mol. We observe the displacement of water molecules from the region between the nucleotides and the fullerenes and we attribute the large favorable interaction energies to hydrophobic interactions. The features of the DNA-C_{60} complexes depend on the nature of the nucleotides: C_{60} binds to double-strand DNA, either at the hydrophobic ends or at the minor groove of the nucleotide. C_{60} binds to single-strand DNA and deforms the nucleotides significantly. Unexpectedly, when the double-strand DNA is in the A-form, fullerenes penetrate into the double helix from the end, form stable hybrids, and frustrate the hydrogen bonds between end-group basepairs in the nucleotide. When the DNA molecule is damaged (specifically, a gap was created by removing a piece of the nucleotide from one helix), fullerenes can stably occupy the damaged site. We speculate that this strong association may negatively impact the self-repairing process of the double-strand DNA. Our results clearly indicate that the association between C_{60} and DNA is stronger and more favorable than that between two C_{60} molecules in water. Therefore, our simulation results suggest that C_{60} molecules have potentially negative impact on the structure, stability, and biological functions of DNA molecules.

INTRODUCTION

Several recent reports have highlighted the potentially hazardous nature of nanomaterials (1–3). For example, it has been shown that carbon nanotubes, arguably the best known nanomaterials, can accumulate in the lungs of rats, and possibly cause the development of granulomas in rats (4,5). The nanomaterials we consider in this work are buckminsterfullerenes (C_{60}) (6,7), because they show several promising potential applications in biology and pharmacology (8–11) and are regarded as one of the building blocks for nanotechnology applications.

The interest in biological applications of C_{60}, as well as that for possible applications in materials science and in other disciplines, has been tempered by concerns that fullerenes may exhibit adverse environmental and health impacts. Early studies showed low toxicity for the C_{60} molecule itself (12,13). Pharmacokinetic studies with radio-labeled water-soluble C_{60} showed that after intravenous injection into mice the compound quickly migrates through the body, accumulates in the liver after a few hours (14), and is excreted, either slowly or rapidly depending on the functionalization of the C_{60} surface (15). These and other studies suggested that fullerene molecules do not exhibit short-term toxicity (16). However, more recent studies suggest that fullerenes may induce oxidative stress in the brain of juvenile largemouth bass (17), and that certain types of C60 derivatives can be quite toxic in cell membrane (18), thus raising the specter of significant negative health impacts from exposure to fullerenes. It is widely believed that severely negative biological outcomes (e.g., replication errors, self-repair mismatches, abnormal functionalities, etc.) can occur when molecules bind to DNA and impact its shape. Such outcomes have the potential of leading to diseased conditions, including cancer. DNA damage of this kind typically requires long times to become detectable and, to the best of our knowledge, no long-term toxicity study related to DNA damage has been reported for fullerenes.

Fullerenes are known to be essentially insoluble in water. However, their solubility can be increased (up to 2 mM) through appropriate coatings (13) or by being suspended in colloidal solution (19). A colloidal solution of uncoated C_{60} in water can be very stable (up to nine months) at room temperature (20). Hence, it is useful to consider the exposure of biological molecules, such as DNA, to fullerenes in aqueous solutions. In this work, we are interested in investigating the potential long-term toxic effects of fullerenes by understanding how C_{60} derivatives approach and interact with nucleic acids. To this end, we performed molecular dynamics simulations of aqueous DNA fragments in the presence of C_{60}.

SIMULATION METHODOLOGY

The double-helix DNA molecule used in our simulations consists of 12 basepairs in the sequence of *d*[AGTCAGTCAGTC]$_2$. The length and sequence of the DNA molecule was chosen as a balance between computational efficiency

Submitted April 26, 2005, and accepted for publication September 8, 2005.

Address reprint requests to Xiongce Zhao, E-mail: zhaox@ornl.gov.

Alberto Striolo's present address is School of Chemical, Biological, and Materials Engineering, University of Oklahoma, Norman, OK 73019.

0006-3495/05/12/3856/07 $2.00

doi: 10.1529/biophysj.105.064410

and biological realism. In particular, a DNA chain of 12 basepairs shows most of the typical properties of a short DNA segment, including a complete 360° rotation in the double-helix in both the A- and B-forms and the ability to spontaneously transition from its A-form to its B-form. Although the simulation of longer chains is clearly desirable, 12 basepairs is approaching the current limit of feasibility for performing multi-nanosecond, atomistically detailed simulations of a DNA segment in an explicit aqueous solution. We chose the sequence $d[AGTCAGTCAGTC]_2$ because it includes and repeats the whole four types of basepairs. The rationale behind this choice consists in our desire to understand if C_{60} binds preferentially to one specific basepair.

DNA structures were obtained from the AMBER (21) utility software. The head-to-tail length of the DNA is ~4 nm. Single-strand DNA was obtained by taking one helix from the double-strand B-DNA created. Damaged double-strand DNA was obtained by removing a section of consecutive nucleotides from one helix of the undamaged B-DNA. The section of nucleotide removed contains four bases, together with the backbones connected to them. Resultant gap was of ~1.4 nm. The dangling bonds in the DNA helix resulting from the removal were saturated by hydrogen atoms. DNA and fullerenes were solvated in 4500–6100 (depending on the system size) TIP3P water molecules (22), within a cubic simulation box of initial size 7 nm. In the simulation box, at least 1.2 nm of water buffer separates the solute (DNA and C_{60}) surface and the box boundaries in any simulation cell directions. Periodic boundary conditions were applied in all three directions. Twenty-two Na^+ (11 Na^+ for single-strand DNA simulations) counterions were added to electrically neutralize the system. The simulations were performed in the NPT (constant pressure, constant temperature) ensemble; hence, the size of the simulation box is adjusted automatically during the course of the simulation to maintain the pressure at 1 bar.

The potential model for DNA was the all-atom AMBER force field, 1999 version (21). The sp^2 carbon atoms in the C_{60} molecule were modeled as Lennard-Jones (LJ) particle with $\varepsilon/k = 43.2$ K and $\sigma = 0.34$ nm (23). LJ interaction parameters between different atoms were calculated by the standard Lorentz-Berthelot combing rules. Lennard Jones interactions were computed within a 0.9-nm spherical cutoff without long-range corrections. TIP3P water model was chosen based on previous simulation works (24,25). The potential applied for Na^+ was the one built in AMBER. The particle-mesh Ewald method with a fourth-order interpolation was applied to evaluate electrostatic interactions. Initial configurations were obtained by placing one, two, or three C_{60} molecules near the DNA molecule. The nearest initial distance between the C_{60} and DNA surfaces was ~0.7 nm, which is within the LJ cutoff distance. The initial configurations permitted a clear separation between the fullerenes and DNA strands at the beginning of the simulation, while maintaining the simulation box size within a computationally manageable size.

Molecular dynamics simulations were performed within the constant pressure (1 bar) and temperature (300 K) (26) ensemble. The AMBER software package was employed to integrate the equations of motion. Each simulation includes 5000 steps of energy minimization, 40 ps of solvent relaxation, five cycles (each cycle with 1500 steps of energy minimization) of solutes relaxation, 20 ps of equilibration, and 5–20 ns of production. A time step of 2 fs was used and the structural configurations were saved every 2 ps for subsequent analysis.

The binding energy between one DNA and one C_{60} molecule is defined as

$$\Delta E = E_{\mathrm{DNA}+\mathrm{C_{60}}} - E_{\mathrm{DNA}} - E_{\mathrm{C_{60}}} - \Delta E_{\mathrm{deform}},$$

where $E_{\mathrm{DNA}+\mathrm{C_{60}}}$, E_{DNA}, and $E^0_{\mathrm{C_{60}}}$ represent the potential energy of the bound DNA-C_{60} pair, the potential energy of DNA in the bound pair, and the potential energy of the C_{60} in the bound pair. In our calculations, it is necessary to account for $\Delta E_{\mathrm{deform}}$ because significant deformations were observed for DNA segments and thus $\Delta E_{\mathrm{deform}}$ is not negligible compared to the total potential energy change. We define $\Delta E_{\mathrm{deform}}$ as

$$\Delta E_{\mathrm{deform}} = \left(E_{\mathrm{DNA}} - E^0_{\mathrm{DNA}}\right) + \left(E_{\mathrm{C_{60}}} - E^0_{\mathrm{C_{60}}}\right).$$

E^0_{DNA} and $E^0_{\mathrm{C_{60}}}$ represent the potential energy of DNA and C_{60} in their native conformations. We use the term ''native conformation'' to refer to the state that a free DNA or C_{60} takes when it is in the same solvent and ion environment but with no association interaction force on it. We performed very short simulations (200 ps for C_{60}, B-DNA, ssDNA, and damaged DNA, 10 ps for A-DNA because A-DNA tends to convert into its B-form under the simulation solvent conditions) of free DNA and C_{60} in water with counterions to calculate E^0_{DNA} and $E^0_{\mathrm{C_{60}}}$. We should point out that the binding energy reported in this work is not free energy. Free-energy calculations are preferable, but the tools available to us for the systems of interest can be highly approximate (such as the Poisson-Boltzmann/surface-area free-energy estimation techniques in MMTSB, The Scripps Research Institute) and we did not attempt to carry out such calculation.

The potential energies were computed from the simulation structures collected, using the software MMTSB. MMTSB operates on the equilibrated structures of DNA and C_{60} collected during molecular dynamics and invokes an instantaneous potential energy calculation, employing the AMBER package and its utilities. It reports the potential energies of the molecules of interest, or of the associated hybrids.

RESULTS AND DISCUSSION

Our results indicate that C_{60} forms stable complexes with aqueous DNA (Fig. 1). In our initial simulation configurations

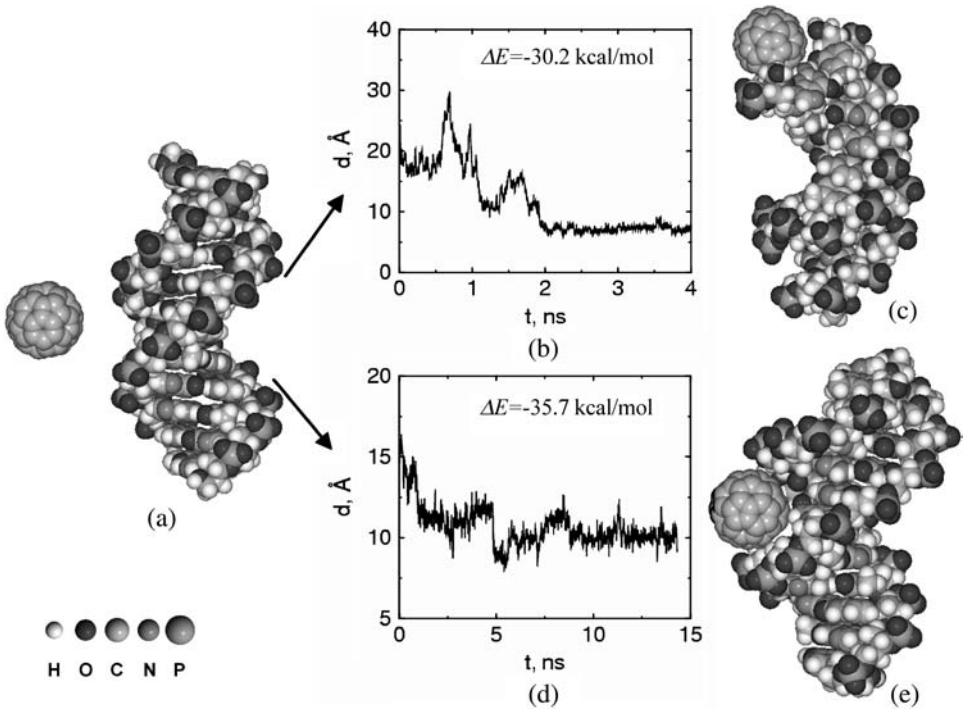

FIGURE 1 (*a*) A typical starting simulation configuration for a C_{60} molecule interacting with a double-strand DNA molecule in aqueous solution. Water molecules and Na^+ ions in the simulation cell are not shown for clarity. During the course of the simulation, C_{60} approaches either the hydrophobic end (*b* and *c*) or the minor groove (*d* and *e*) of the double-strand DNA. Once energetically favorable complexes are formed, fullerenes do not leave their docking site for the remainder of our simulations, suggesting that stable complexes are formed. Snapshots of final configurations are reported in *c* and *e*. The binding energy, ΔE, for the C_{60}-DNA hybrid is -30.2 or -35.7 kcal/mol for the structures shown in *c* and in *e*, respectively. By comparison, the thermal fluctuations of the system is in the order of 0.6 kcal/mol (300 K) and the binding energy between two C_{60} molecules in the same simulation condition is $\Delta E = -7.5$ kcal/mol. To visualize the progress of the simulation, we report the distance between the center of mass of the C_{60} molecule and that of one DNA end (defined as the center of mass of the DNA end basepairs C12–G13) as a function of simulation time (*b*). The same quantity for the C_{60} molecule and the minor groove site versus simulation time is shown in *d*. In both cases, it can be seen that after ~2 ns the fullerene is able to find a docking site in the nucleotide. Once the C_{60} molecule reaches the docking site, the hybrid remains stable for the remainder of the simulation.

C_{60} and DNA are separated, with solvent molecules in between. The first contact between the C_{60} molecule and the DNA typically occurs after 1–2 ns. Once the fullerenes diffuse and bind with the nucleotides, C_{60}-DNA complexes are formed and remain stable for up to 20 ns of the simulations. Initially it appeared that the C_{60} molecules are prone to bind only to the free ends of the double-strand DNA. However, extensive simulations indicate that association of C_{60} can also occur at the minor groove sites. No association has been observed at the major groove sites in our simulations. These observations are different from a recent experimental observation, according to which a water-soluble (i.e., functionalized) C_{60} derivative can interact strongly with DNA, the major groove of the double-helix and phosphate backbone acting as the binding sites (27). However, we observe that the C_{60} considered here is hydrophobic and not hydrophilic.

We note that the free ends of the double-strand DNA fragment are the explicit hydrophobic sites exposed in solution, and this may favor the diffusion of hydrophobic fullerenes toward their docking sites. The two free ends of our double-strand DNA segment are constituted by either A-T or G-C basepairs. We performed simulations with C_{60} in proximity of both ends and did not notice appreciable differences in the binding features. Careful calculation of the binding energy ΔE reveals that the hybrid C_{60}-DNA complexes are energetically favorable compared to the unpaired molecules (the binding energy goes from $\Delta E = -35.9$ kcal/mol, for C_{60} docked in the minor groove, to -30.4 kcal/mol, for C_{60} docked at the DNA ends). For comparison, the thermal fluctuations under the simulation condition are in the magnitude of 0.6 kcal/mol (300 K). We also found that the deformation energy of B-DNA is ~6.5 kcal/mol, which indicates that the C_{60}-DNA association causes an energetically unfavorable deformation in the DNA molecule. However, the deformation energy of C_{60} observed in simulations is <0.5 kcal/mol and so is negligible.

We also simulated the self-association of C_{60} molecules in the presence of DNA molecules in the same aqueous solution. The result is summarized in Fig. 2. In this simulation, we placed two C_{60} molecules and one B-DNA in the simulation box. Self-association between C_{60} molecules was observed at early stages during the simulation, with a binding energy of $\Delta E = -7.5$ kcal/mol. However, the stable configuration obtained after 5 ns of simulation indicates that the self-association between C_{60} molecules did not prevent one of the C_{60} molecules from binding to one end of the DNA. Both C_{60} molecules migrated to the end of the DNA, with one C_{60} docked to the DNA end; the other C_{60} remains associated with the DNA-docked C_{60}.

Despite the large deformation energies discussed earlier, visual observation of the simulation results suggests that the overall shape of the double-strand DNA molecule is not appreciably affected by the association of C_{60}, in agreement

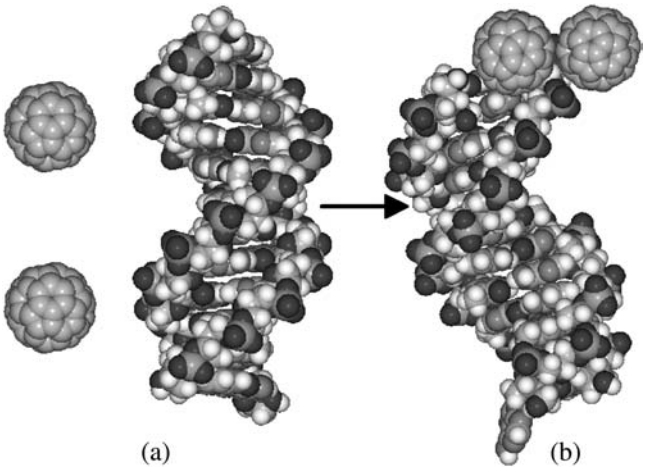

FIGURE 2 Self-association of C_{60} molecules in the presence of a DNA molecule. (*a*) The starting configuration of two C_{60} molecules and a B-DNA molecule. (*b*) The stabilized hybrid of C_{60}-DNA after 5-ns simulation. One C_{60} binds with an end of the DNA, while the other C_{60} associates with it. The binding energy between the two C_{60} molecules is −7.5 kcal/mol. It can be seen from the final configuration that the self-association of the two C_{60} molecules did not inhibit the binding between one C_{60} and one hydrophobic end of the DNA.

with experimental observations of DNA/fullerene derivative hybrid materials (28). However, the impact on the DNA structure is more pronounced when C_{60} interacts with a double-strand DNA fragment in the A-form (Fig. 3). DNA fragments in their A-form differ from their B-form counterparts in that more hydrophobic contacting surfaces are exposed at the end because of the open channel along the axis. The nucleotide segment modeled in this work is expected to transform into the narrower B-form under the solution conditions considered here (24,25). The simulation started from initial conditions similar to those for C_{60}/B-DNA simulations (see Fig. 1) except the initial DNA structure was replaced by its A-form counterpart. Our results (Fig. 3 *a*) indicate that a C_{60} molecule is able to penetrate into one free end of an A-form DNA fragment. A closer look at the basepairs being penetrated indicates that the hydrogen bonds between them are disconnected. The C_{60} molecule docked in the DNA end is able to come in contact with the face of the basepairs second from the end. The binding energy that corresponds to this docking amounts to −41.9 kcal/mol. The observed deformation energy of the A-DNA is ~−4.5 kcal/mol. We observe that the deformation energy is negative, while it was positive in our C_{60}/B-DNA simulations. The favorable deformation energy observed for A-DNA is due to the transition of the nucleic acid to its more stable B-form. Although it is known that the hydrogen bonds between the end basepairs of a double-strand DNA may in some cases break during the course of molecular simulation (24,25), such bond breakage is temporary and recovered through thermal fluctuations as the simulation proceeds. In contrast, in our study, we find that the hydrogen-bond breakage encountered when a C_{60} molecule docks into the end of the A-form

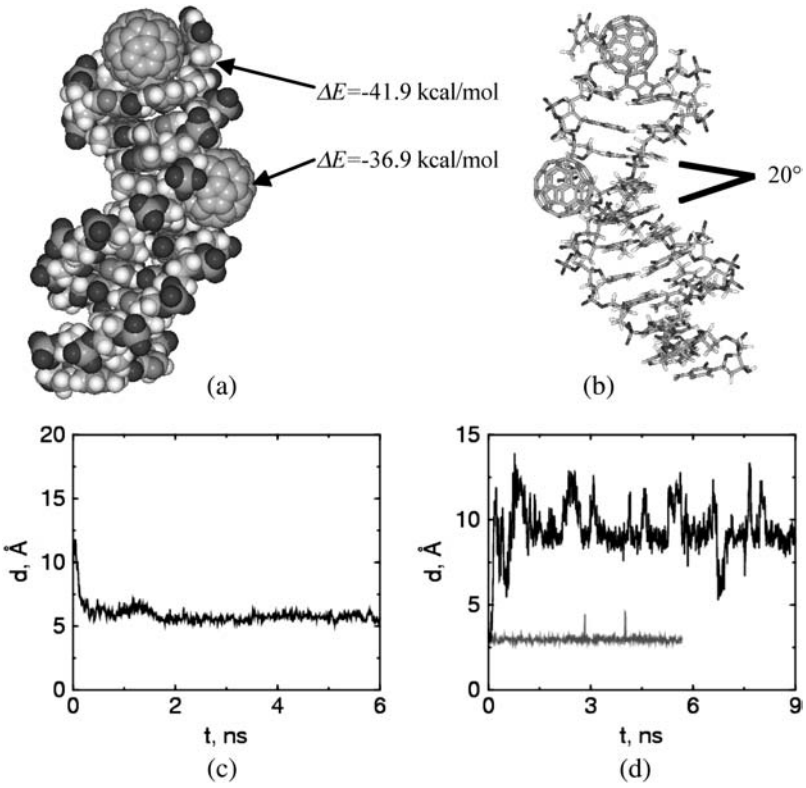

FIGURE 3 Deformation of an A-form DNA when it interacts with C_{60} molecules. (*a*) Two C_{60} are associated with the DNA molecule. One penetrates into the A1–T24 end of DNA, the other docked by the minor groove. This figure is the snapshot after 10-ns simulation. (*b*) The stick presentation of *a*. The docking of one C_{60} molecule on the minor groove perturbs the stacking of consecutive basepairs, resulting in an angle of ~20° between the basepair planes that bite the C_{60} molecule. (*c*) The C_{60} molecule penetrates into the first end basepairs (A1–T24) of the DNA and is able to contact with the second basepair (G2–C23) from the end. This is indicated by the distance *d* between the C_{60} molecule and center-of-mass of the second basepair as a function of simulation time. (*d*) The C_{60} molecule penetrating into one end of the DNA (A1–T24) disrupts the hydrogen bonds of the end basepairs. Here we show the length of one of the hydrogen bonds in the end basepairs A1–T24, with (*upper line*) and without (*lower line*) C_{60} docking into the DNA end. The hydrogen-bond length is defined as the distance between one pair of H-bonding atoms in the end basepairs.

DNA, is not restored during the course of the simulation, and appears to be permanent. The docked C_{60}–DNA complex is very stable and the broken hydrogen bonds are not reconnected even after 10 ns of simulation (see Fig. 3 *d*).

In addition, we observe an appreciable deformation on the basepair stacking angles of the A-form double-strand DNA when the C_{60} docks on its minor groove sites (Fig. 3 *b*). Although the A-form DNA under our simulation condition is expected to transform into its B-form with the stacking planes between consecutive basepairs parallel to each other (25), the docking of one C_{60} into the minor groove induces an angle of 20° between the basepair planes that bite the C_{60}. The deformation of the nucleotide structure results in a slightly greater binding energy (−36.9 kcal/mol) than that of C_{60} binding to the minor groove of a regular B DNA (−35.7 kcal/mol). Examining the structural details of C_{60}/B-DNA and C_{60}/A-DNA hybrids more carefully, we see that the binding of C_{60} on the minor groove of A-DNA is somewhat prohibited from fully relaxing into its B-form, as indicated by the nonparallel basepairs in the region near to where C_{60} docks. This allows the C_{60} molecule to contact deeper, and with a larger contact area into the A-DNA groove than it does with a B-DNA (see Fig. 4).

As might be expected on the basis of the double-strand DNA results, the docking of a C_{60} into a flexible single-strand DNA molecule causes significant deformations in the DNA (Fig. 5 *a*). We started additional simulations by placing three C_{60} and one single-strand DNA in the simulation box. After the system reaches equilibrium, we observe that all the C_{60} molecules in the system are essentially wrapped by nucleotides. One end of the single-strand DNA bends severely because of the two fullerenes docked inside. The other end maintains a relatively native conformation because no C_{60} molecule binds to it. The C_{60} docked in the central region of the single-strand DNA induces significant structural deformations on the two basepairs it contacts. The stacking of the base rings is completely deformed and the bases contact the C_{60} in a face-on pattern. We speculate that a sufficiently long single-strand DNA would completely wrap a C_{60}. However, we did not test this hypothesis, because of computing time limitations. The single-strand DNA and C_{60} hybrids observed in this work are energetically favorable, with binding energies in the range −27.7 to −39.3 kcal/mol, depending on atomistic docking details. The deformation energy computed for one single-strand DNA (Fig. 5) is ~5.1 kcal/mol. We noted that a free single-strand DNA is very flexible and therefore can experience large deformation. That helps to explain the relatively small deformation energy of single-strand DNA, even though significant deformation is seen in the ssDNA-C_{60} hybrids.

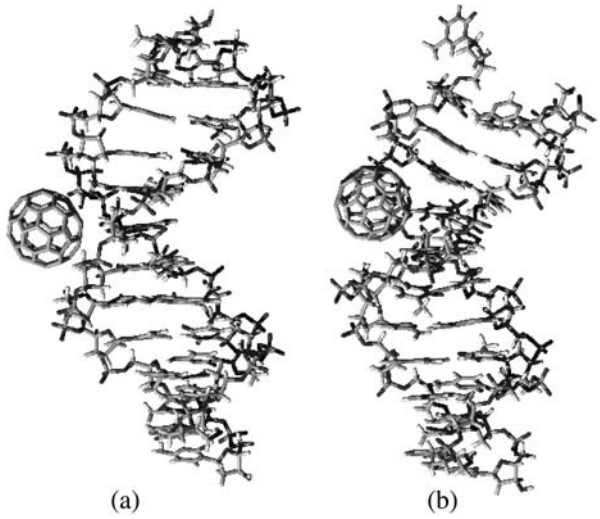

FIGURE 4 Complexes of C_{60} in the minor groove, starting from the B-DNA (*a*) and A-DNA (*b*) conformations. C_{60} has more contact with DNA starting from A-form than that from B-form, resulting in a slightly greater (more negative) binding energy.

We attribute the binding between the C_{60} and DNA molecules to the hydrophobic interaction between the C_{60} and hydrophobic sites on the DNA. As indicated previously, the binding energy being measured is not free energy, but includes contributions from both free energy ΔG and entropic term $T\Delta S$. For nonpolar molecules in an aqueous environment, the hydrophobic interaction is dominated by entropy change. This is due to the high entropy decrease

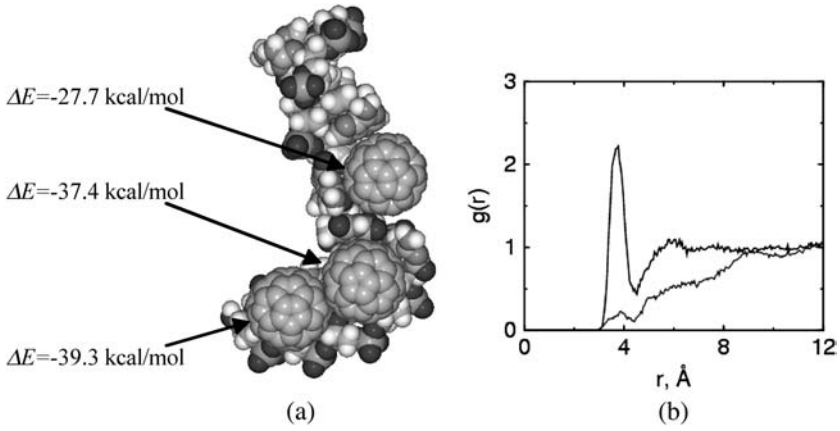

FIGURE 5 (*a*) Binding of C_{60} with a single-strand DNA. (*b*) Radial distribution of water molecules (O atom) around the hydrophobic site (*line* with *no peak*) and hydrophilic site (*line* with *peak around* $r = 4$) of DNA after the formation of DNA-C_{60} hybrid. Here the hydrophobic site is defined as one of the carbon atoms on the base ring of the binding end of the DNA; the hydrophilic site is defined as one of the phosphorus atoms along the sugar frame.

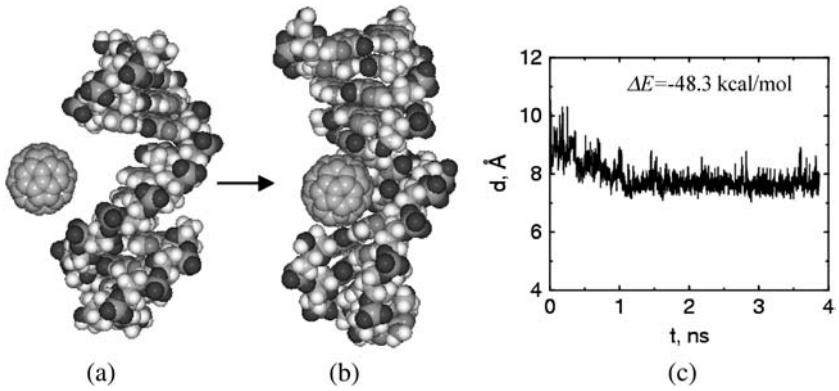

FIGURE 6 C_{60} occupies the defect site of the DNA. (*a*) Starting configuration of defected DNA and C_{60}. (*b*) The snapshot after 3.8-ns molecular dynamics simulation. The defect site occupied by the C_{60} molecule corresponds to the vacancy left when a section of the nucleotide was removed. The angles of the basepair planes above and below the buckyball were deformed after the C_{60} molecule binds to the defect. (*c*) Distance between the center of mass of the C_{60} molecule and the center of mass of the bases right above and below the C_{60} molecule.

during water structural rearrangement for the nonpolar solutes to disperse into the solvent (29). This is supported by our structural analysis of water molecules surrounding the binding sites in the nucleotide compared with a hydrophilic site (Fig. 5 *b*). Water molecules are completely displaced from the binding site after the docking process stabilizes. Our contention that hydrophobic forces dominate agrees with earlier observations according to which electrostatics are not the driving force for the association between fullerenes and nucleotides (30). Ideally, one could estimate the entropic contribution to the binding process by analyzing the system dynamics using techniques such as those of Smith and co-workers (31,32). However, such analysis is nontrivial and we did not attempt to estimate the entropic interactions.

The above described tendency of C_{60} to bind and form stable hybrids with the DNA segments led us to investigate the behavior of C_{60} in proximity of a damaged nucleotide. In this simulation, we removed a piece of nucleotide with the length of four bases from the central part of one DNA strand. The resulting double-strand DNA shows one defect gap in its structure (Fig. 6). The width of the defect gap is ~1.4 nm. C_{60} has a diameter of ~1 nm. We find that when a C_{60} diffuses near this structure it is rapidly attracted within the defect and forms a stable hybrid with a binding energy of −48.3 kcal/mol. The interaction between the DNA and C_{60} deformed the stacking of the binding bases for C_{60} to have a face-on contact with them, as found in C_{60} and single-strand DNA simulations. The significant deformation of the bases contacting the C_{60} molecule results in a deformation energy of 11.0 kcal/mol. The hybrid remains very stable during the entire course of simulation. The results suggest that C_{60} fills in the defect gap, and so thereby may impact the self-repairing process of the damaged nucleotide by blocking the repair sites.

CONCLUSIONS

In summary, we have shown, based on molecular dynamics simulations, that C_{60} can bind to nucleotides and form energetically stable hybrids in aqueous solution. The favorable binding sites in double-strand DNA are the free ends and minor grooves. The binding between C_{60} and B-form double-strand DNA does not affect the overall shape of the DNA. In contrast, C_{60} can penetrate into an A-form DNA from the free end and permanently break the hydrogen bonds between the end basepairs. Furthermore, the C_{60} docked on the minor groove of A-DNA deforms the stacking angles of bases contacting it. C_{60} binds strongly with single-strand DNA and results in a significant deformation of the nucleotides. In addition, we find that a C_{60} molecule can readily occupy a defect site in a double-strand DNA and form a stable complex. The set of simulation results presented here suggest the possibility that C_{60} molecules may interfere with the biological functions performed by DNA, and therefore cause long-term negative side effects in living organisms. However, additional studies are required to determine whether the binding events observed in these simulations have in vivo relevance.

The authors thank an anonymous referee for pointing out the role of the deformation energy in the total binding energies.

This research used resources of the Center for Computational Sciences at Oak Ridge National Laboratory, which is supported by the Office of Science of the U.S. Department of Energy under contract No. DE-AC05-00OR22725. X.C.Z. acknowledges the ORNL-ORAU postdoctoral programs operated by the Oak Ridge Associated Universities. A.S. and P.T.C. additionally acknowledge support of this research from the National Science Foundation through grant No. DMR-0103399 to Vanderbilt University.

REFERENCES

1. Service, R. F. 2003. Nanomaterials show signs of toxicity. *Science*. 300:243.
2. Brumfiel, G. 2003. Nanotechnology: a little knowledge.... *Nature*. 424:246–248.
3. Colvin, V. L. 2003. The potential environmental impact of engineered nanomaterials. *Nat. Biotechnol.* 21:1166–1170.
4. Lam, C. W., J. T. James, R. McCluskey, and R. L. Hunter. 2004. Pulmonary toxicity of single-walled carbon nanotubes in mice at 7 and 90 days after intratracheal instillation. *Toxicol. Sci.* 77:126–134.
5. Warheit, D. B., B. R. Laurence, K. L. Reed, D. H. Roach, G. A. M. Reynolds, and T. R. Webb. 2004. Comparative pulmonary toxicity

assessment of single-wall carbon nanotubes in rats. *Toxicol. Sci.* 77: 117–125.

6. Kroto, H. W., J. R. Heath, S. C. O'Brien, R. F. Curl, and R. E. Smalley. 1985. C_{60}—Buckminsterfullerene. *Nature.* 318:162–163.
7. Krätschmer, W., L. D. Lamb, K. Fostiropoulos, and D. R. Huffman. 1990. Solid C_{60}—a new form of carbon. *Nature.* 347:354–358.
8. Tokuyama, H., S. Yamago, E. Nakamura, T. Shiraki, and Y. Sugiura. 1993. Photo-induced biochemical activity of fullerene carboxylic acid. *J. Am. Chem. Soc.* 115:7918–7919.
9. Tabata, Y., Y. Murakami, and Y. Ikada. 1997. Photodynamic effect of polyethylene glycol-modified fullerene on tumor. *Jpn. J. Cancer Res.* 88:11108–11116.
10. Noon, W. H., Y. F. Kong, and J. P. Ma. 2002. Molecular dynamics analysis of a buckyball-antibody complex. *Proc. Natl. Acad. Sci. USA.* 99:6466–6470.
11. Gao, H. J., and Y. Kong. 2004. Simulation of DNA-nanotube interactions. *Annu. Rev. Mater. Res.* 34:123–150.
12. Nelson, M. A., F. E. Domann, G. T. Bowden, S. B. Hooser, Q. Fernando, and D. E. Carter. 1993. Effects of acute and subchronic exposure of topically applied fullerene extracts on the mouse skin. *Toxicol. Ind. Health.* 9:623–630.
13. Scrivens, W. A., J. M. Tour, K. E. Creek, and L. Pirisi. 1994. Synthesis of C14-labeled C_{60}, its suspension in water, and its uptake by human keratinocytes. *J. Am. Chem. Soc.* 116:4517–4518.
14. Yamago, S., H. Tokuyama, E. Nakamura, K. Kikuchi, S. Kananishi, K. Sueki, H. Nakahara, S. Enomoto, and F. Ambe. 1995. In vivo biological behavior of a water-miscible fullerene: ^{14}C labeling, adsorption, distribution, excretion and acute toxicity. *Chem. Biol.* 2:385–389.
15. Rajagopalan, P., F. Wudl, R. F. Schinazi, and F. D. Boudinot. 1996. Pharmacokinetics of a water-soluble fullerene in rats. *Antimicrob. Agents Chemother.* 40:2262–2265.
16. Rancan, F., S. Rosan, F. Boehm, A. Cantrell, M. Brellreich, M. Schoenberger, A. Hirsch, and F. Moussa. 2002. Cytotoxicity and phototoxicity of a dendritic C_{60} mono-adduct and a malonic acid C_{60} tris-adduct on Jurkat cells. *J. Photochem. Photobiol. B Biol.* 67: 157–162.
17. Oberdörster, E. 2004. Manufactured nanomaterials (Fullerenes, C_{60}) induce oxidative stress in the brain of juvenile largemouth Bass. *Environ. Health Perspect.* 112:1058–1062.
18. Bosi, S., L. Feruglio, T. Da Ros, G. Spalluto, B. Gregoretti, M. Terdoslavich, G. Decorti, S. Passamonti, S. Moro, and M. Prato. 2004. Hemolytic effects of water-soluble fullerene derivatives. *J. Med. Chem.* 47:6711–6715.
19. Andrievsky, G. V., V. K. Klochkov, A. B. Bordyuh, and G. I. Dovbeshko. 2002. Comparative analysis of two aqueous-colloidal solutions of C-60 fullerene with help of FTIR reflectance and UV-Vis spectroscopy. *Chem. Phys. Lett.* 364:8–17.
20. Deguchi, S., R. G. Alargova, and K. Tsujii. 2001. Stable dispersions of fullerenes, C-60 and C-70, in water. Preparation and characterization. *Langmuir.* 17:6013–6017.
21. Case, D. A., T. A. Darden, T. E. Cheatham III, C. L. Simmering, J. Wang, R. E. Duke, R. Luo, K. M. Merz, B. Wang, D. A. Pearlman, M. Crowley, S. Brozell, V. Tsui, H. Gohlke, J. Mongan, V. Hornak, G. Cui, and P. Beroza. P., C. Schafmerster, J. W. Caldwell, W. S. Ross, P. A. Kollman. 2004. *AMBER 8*. University of California, San Francisco.
22. Jorgensen, W. L. 1981. Quantum and statistical mechanical studies of liquids. 10. Transferable intermolecular potential functions for water, alcohols, and ethers. Application to liquid water. *J. Am. Chem. Soc.* 103:335–340.
23. Hummer, G., J. C. Rasaiah, and J. P. Noworyta. 2001. Water conduction through the hydrophobic channel of a carbon nanotube. *Nature.* 414:188–190.
24. Kalra, A., S. Garde, and G. Hummer. 2003. Osmotic water transport through carbon nanotube membranes. *Proc. Natl. Acad. Sci. USA.* 100: 10175–10180.
25. Cheatham III, T. E., and P. A. Kollman. 2000. Molecular dynamics simulation of nucleic acids. *Annu. Rev. Phys. Chem.* 51:435–471.
26. Cheatham III, T. E., and M. A. Young. 2001. Molecular dynamics simulation of nucleic acids: successes, limitations, and promise. *Biopolymers.* 56:232–256.
27. Berendsen, H. J. C., J. P. M. Postma, W. F. van Gunsteren, A. D. Nola, and J. R. Haak. 1984. Molecular-dynamics with coupling to an external bath. *J. Chem. Phys.* 81:3684–3690.
28. Pang, D. W., Y. D. Zhao, P. F. Fang, J. K. Cheng, Y. Y. Chen, Y. P. Qi, and H. D. Abruňa. 2004. Interactions between DNA and a water-soluble C60 derivative studied by surface-based electrochemical methods. *J. Electroanal. Chem.* 567:339–349.
29. Israelachvili, J. N. 1985. Intermolecular and Surface Forces: With Applications to Colloidal and Biological Systems. Academic Press, London. 102–107.
30. Cassell, A. M., W. A. Scrivens, and J. M. Tour. 1998. Assembly of DNA/fullerene hybrid materials. *Angew. Chem. Int. Ed. Engl.* 37: 1528–1531.
31. Smith, D. E., L. Zhang, and A. D. J. Haymet. 1992. Entropy of association of methane in water—a new molecular dynamics computer simulation. *J. Am. Chem. Soc.* 114:5675–5676.
32. Smith, D. E., and A. D. J. Haymet. 1993. Free-energy, entropy, and internal energy of hydrophobic interactions—computer simulations. *J. Chem. Phys.* 98:6445–6454.

The Painful Truth About Omega 3 Fatty Acids

Contrary to popular opinion, omega 3 and 6 fatty acids are not the amazing health items you've been told. I was just in the grocery store earlier today and found the "top brand" of fish oil on sale for $56! Little do these sad consumers know they are mostly being taken for a ride. How so? -A few months back I wrote **a similar article revealing the oxidative free radical damage and premature aging caused by omega 3 fatty acids**. Not too many people were happy to hear the painful truth that their favorite fish oil/krill oil supplement are really just potential free radicals in a bottle.

The Painful Truth About Polyunsaturated Omega 3

Polyunsaturated omega 3 and 6 are potentially harmful to the body in 3 primary ways:

1. **Through very rapid lipid peroxidation and free radical damage**
2. **Through the formation of pro-inflammatory prostaglandins**
3. **By forming trans-isomers and other ultra-unusual fatty acids**

Polyunsaturated oils are the most susceptible to the oxidative destruction of lipid peroxidation. Lipid peroxidation is the process of degradation of lipids. **Omega 6 and especially omega 3 cause very rapid cellular breakdown to take place. Wonderful news if you would like enormously high amounts of free radicals floating around inside of you**. Bad news if you are interested in maintaining your health. **Not only will omega 3 fatty acids cause a rapid and substantial loss of vitamin E in the body, omega 3 will rapidly oxidize, even before entering the blood itself. Omega 3 consumption can result in liver spots on the skin known as Lipofuscin, and this is especially true if vitamin E levels are low. Omega 3 fatty acids do have anti-inflammatory effects in the body, but these anti-inflammatory effects are short lived. And there may be long term pro-inflammatory effects associated with their consumption. Omega 3 works on what are called prostaglandins.** Prostaglandins are "messengers molecules" that play very substantial roles in the pro-anti/inflammatory responses in the body.--Essentially omega 3 temporarily blocks the conversion of PG2 prostaglandins. It is this class of prostaglandins which are responsible for so many inflammatory processes that result in pain, arthritis, autoimmune processes, migraine headaches, etc. **In fact, omega 3 blocks the same prostaglandin pathway that aspirin blocks, seeming to indicate that omega 3 has more of a drug like effect than a nutritive effect in the body**. The problem though with omega 3 and prostaglandins is that it is the oxidized omega 3 fats in the body that work on the prostaglandins. As we've already discussed, oxidation of omega 3 oils in the body is harmful because they will result in high amounts of free radical formation, **destruction**

of cells and loss of vitamin E. The other damaging aspect of omega 3 occurs when they are heated or oxidized. Omega 3 is a very heat and oxygen sensitive oil. **Heated omega 3 oils (such as in cooking fish, meat or nuts & seeds, or any other source of omega 3, or the heat extraction process of fish oil) results in the formation of trans-isomers or other unusual types of fatty acids, which are toxic to the liver and further contribute to free radical formation and lipid peroxidation**.

Making Sense of It All

in the body everything functions in balance. Balance between dualism:

- Sympathetic/parasympathetic
- Anabolic/catabolic
- Water/Electrolyte
- Anti-infammatory/pro-inflammatory
- Glucogenic/ketogenic
- Acid/alkaline
- Anti-oxidants/free radicals

The cells of your body are no different. Your cell membranes are made up of both **saturated fats as well as polyunsaturated fatty acids**. In order for things to work smoothly, there must be a balance. When the cells are too tight, too thick, they become hardened and anaerobic**. If the cell can't be penetrated, oxygen can't be used efficiently and excess lactic acid gets produced, leading to all sorts of problems.** To simplify, Polyunsaturated omega 3 maintains the permeability of cells, with other nutrients such as Vitamins A and D. **When cells become too loose, the cell membranes fall apart causing tremendous free radical formation. This is called dysaerobic metabolic imbalance or catabolism. Saturated fat and cholesterol as well as vitamin E maintains the proper stiffness of cells, preventing lipid peroxidation.** It makes sense to me that the people who will derive the most benefits of omega 3 fatty acids will be those with anaerobic diseases. What are some of the most common? **Cancer, arthritis, heart disease. This explains why some of the most brilliant physicians like Emanuel Revici and Johanna Budwig were so successful at treating cancer. Both used omega 3 fatty acids**.But the important point to remember is that dysaerobic diseases/conditions will only be exacerbated by high amounts of omega 3 oils. Should you take fish oil as a supplement? Personally I don't use it and don't recommend it to everyone as a 'one size fits all' recommendation. I might recommend omega 3 supplementation to some people in some instances, but this is only if I know they have anaerobic imbalances.

Fullerenes shown to penetrate healthy skin

(*Nanowerk Spotlight*) Nanoparticles exhibit unique properties that make them ideal for a wide-variety of applications. **Also unique, and largely unknown, are the interactions that occur between the biological environment and nanoparticles.** On the upside, the ability of quantum dots and fullerenes to penetrate intact skin provides potential benefits for the development of nanomaterial applications involving drug delivery. On the downside, this ability poses potential risks associated with manufacturing and handling such nanoparticles. **A new study now confirms that fullerene-based peptides can penetrate intact skin and that mechanical stressors, such as those associated with a repetitive flexing motion, increase the rate at which these particles traverse into the dermis. These results are important for identifying external factors that increase the risks associated with nanoparticle exposure during manufacturing or consumer processes**. Future assessments of nanoparticle safety should recognize and take into account the effect that repetitive motion and mechanical stressors have on nanoparticle **interactions with the biological environment.** Additionally, these results could have profound implications for the development of nanoparticle use in drug delivery, specifically in understanding mechanisms by which nanoparticles penetrate intact skin "**Our work investigates how a specific type of nanoparticle, an amino acid-derivatized fullerene, interacts with the biological environment both at the tissue and cellular levels**" Jillian Rouse, a student at the Center for Chemical Toxicology Research and Pharmacokinetics (CCTRP) at North Carolina State University, explains to Nanowerk**. "It is important to identify those nanoparticles that can penetrate intact skin and to determine the potential risk for toxicity once the particles are in the body.** Nanoparticles have the potential to provide great scientific developments; however, if there are inherent biological risks associated with their use, then safety evaluations need to be conducted." " Rouse is first author of a recent paper, titled "Effects of Mechanical Flexion on the Penetration of Fullerene Amino Acid-Derivatized Peptide Nanoparticles through Skin", that was published in the December 6, 2006 web edition of *Nano Letters*. This study was funded by the Environmental Protection Agency, the National Academies Keck Futures Initiative and the Robert A. Welch Foundation. Rouse, Nancy Monteiro-Riviere, professor of investigative dermatology and toxicology at NC State's College of Veterinary Medicine, and Dr. Andrew R. Barron, professor of chemistry and materials science at Rice University are the **first to show the ability of fullerenes to penetrate intact skin and to relate nanoparticle penetration to biomechanical stimuli**. "Our work was motivated by the discovery that mechanical stimuli applied during standard **physiological processes, such as walking, increase the penetration of particles found in soil and result in a higher prevalence of podoconiosis in the African rift valleys"** says Rouse. "**The ability of normal biomechanical movements to increase nanoparticle penetration solidifies the need for risk assessment, especially in occupational settings where constant, repetitive motions are**

involved." **The researchers have previously reported the synthesis of the phenylalanine-based fullerene amino acid, Bucky amino acid (Baa), and the uptake and interaction of Baa with human epidermal keratinocytes (**"**Fullerene-based amino acid nanoparticle interactions with human epidermal keratinocytes**"**)**. The presence of the fullerene substituent has a significant effect on the intracellular transport of peptides containing Baa. **The addition of a fullerene-derived amino acid to a cationic peptide results in the peptide showing cellular uptake, whereas the same peptide sequence in the absence of Baa shows no transport across the cell membrane. The peptide sequence used is based on on the nuclear localization sequence (NLS).** After the NLS sequence (Pro-Lys-Lys-Lys-Arg-Lys-Val) was completed, a Lys(Mtt) residue was coupled to the end to allow attachment of the fluorescein isothiocyanate (FITC) fluorescent marker. The individual Baa-Lys(FITC)-NLS particles measured ca. 3.5 nm in size. **Because of its physiological and structural similarities to human skin, porcine skin was used a model for human skin in this study**. To determine the effects of flexing on skin penetration, the dermatomed skin was dosed with 20 µL of Baa-Lys-(FITC)-NLS in 1% PBS, and the dosed areas were subsequently flexed for 60 or 90 min or left unflexed (control) to investigate nanoparticle penetration.

Carbon nanotubes introduced into the abdominal cavity of mice show asbestos-like pathogenicity in a pilot study

- Craig A. Poland
- , Rodger Duffin
- , Ian Kinloch
- , Andrew Maynard
- , William A. H. Wallace
- , Anthony Seaton
- , Vicki Stone
- , Simon Brown
- , William MacNee
- & Ken Donaldson

Nature Nanotechnology **volume 3**, pages 423–428 (2008) | Download Citation

Abstract

Carbon nanotubes[1] have distinctive characteristics[2], but their needle-like fibre shape has been compared to asbestos[3], raising concerns that **widespread use of carbon nanotubes may lead to mesothelioma, cancer of the lining of the lungs** caused by exposure to asbestos[4]. Here we **show that exposing the mesothelial lining of the body cavity of mice, as a surrogate for the mesothelial lining of the chest cavity, to long multiwalled carbon nanotubes results in asbestos-like, length-dependent, pathogenic behaviour. This includes inflammation and the formation of lesions known as granulomas**. This is of considerable importance, because research and business communities continue to invest heavily in carbon nanotubes for a wide range of products[5] under the assumption that they are no more hazardous than graphite. Our results suggest the need for further research and great caution before introducing such products into the market if long-term harm is to be avoided.

Figure 3 Effect of fibre length on phagocytosis by peritoneal macrophages. a,**b**, Histological sections show incorporation of LFA (**a**, arrow) leading to 'frustrated phagocytosis', but SFA (**b**, see inset) is successfully phagocytosed. **c**, Representative image of an FBGC after injection of LFA containing short fragments of fibre (see inset). **d**, Like LFA, NT_{long2} also leads to frustrated phagocytosis (E-erythrocytes). **e**, In contrast, NT_{tang1} can be readily phagocytosed (see inset). **f**, FBGC is also present after injection of NT_{long2} (see inset for internalized fibres) (PMN, polymorphonuclear leukocyte; L, lymphocyte). All images are shown at ×1,000 magnification with a 5 μm scale bar.

Carbon NanoTubes--will not be detected in water bodies using currently available monitoring equipment and hence will not be identified as a pollutant, were they to be present.

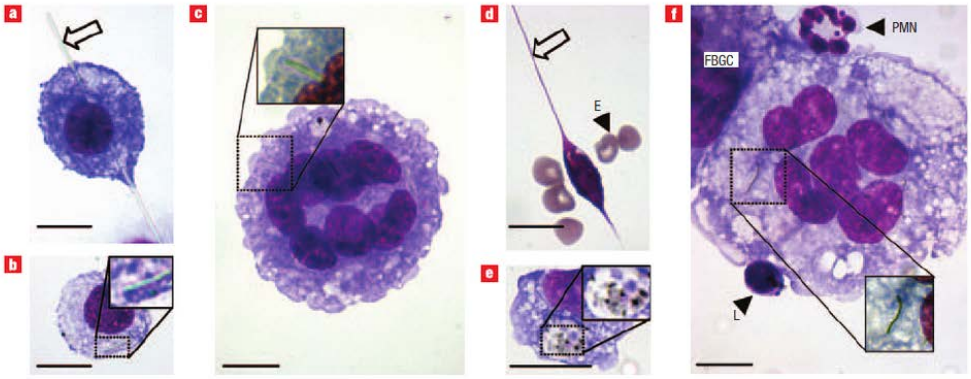

Toxicity Studies of [60]Fullerene and Carbon Nanotubes: State of the Art

Chapter · July 2012
DOI: 10.1142/9789814401449_0002

4 authors:

Jelena Kolosnjaj Tabi
IPBS - Institut de Pharmacologie et de Biologie Structurale
38 PUBLICATIONS **1,250** CITATIONS
SEE PROFILE

Tarek Baati
30 PUBLICATIONS **3,841** CITATIONS
SEE PROFILE

H. Szwarc
Université Paris-Sud 11
167 PUBLICATIONS **3,123** CITATIONS
SEE PROFILE

Fathi Moussa
Université Paris-Sud 11
125 PUBLICATIONS **1,697** CITATIONS
SEE PROFILE

Chapter 2

Toxicity Studies of [60]Fullerene and Carbon Nanotubes: State of the Art

*Jelena Kolosnjaj-Tabi, Tarek Baati, Henri Szwarc and Fathi Moussa**

UMR CNRS 8612 and LETIAM, EA 4041
University of Paris Sud, France

*Corresponding author. Email: fathi.moussa@u-psud.fr

1. Introduction

Since the U.S. National Nanotechnology Initiative,[1] toxicity studies on nanomaterials attracted considerable interest and the term "nanotoxicology" was coined likely to attract the attention to the potential dangers of nanotechnology.[2,3] The first concerned material was [60]fullerene (C_{60}), which is widely considered as the building block of nanotechnology, together with carbons nanotubes (CNTs). The growing use of these two kinds of fullerenes and their mass production raised concerns about their safety and environmental impacts. In fact, research groups that pioneered fullerene studies started to investigate C_{60} toxicity since 1993, after the first method of production in significant amount was available.

Available data provided by several international independent research groups clearly show that pristine C_{60} has no toxicity in a large panel of experimental models. In contrast, CNT toxicity remains a matter of debate. This is mainly related to the large heterogeneity of this carbon material family. Anyway, it is to be expected that C_{60} and CNTs behave differently, because C_{60} forms plastic crystals at ambient temperature, while CNTs form rigid entities, which has been soon compared to asbestos fibers.

Here we will summarize the relevant knowledge in the field. As a great number of publications have been devoted to this subject (On November 29, 2011, key words "fuller* AND toxic*" and "nanotube AND toxic*" resulted in 669 entries and 2474 entries, respectively, on Web of Science for the timespan 1993–32011), we cannot quote all of them in this chapter. We will mainly focus on *in vivo* studies.

2. Toxicity Studies of [60]Fullerene

2.1. General considerations

When C_{60} became available in significant amount in the early nineties it was naïvely considered as a three-dimensional benzene, and researchers raised the question about its safety. Preliminary experiments on C_{60} toxicity were conducted with a C_{60}-benzene solution.[4] Of course benzene is highly toxic, and it is not the appropriate solvent for studying the toxicity of C_{60}. But since the scientists working in the area of fullerenes were daily exposed to such C_{60}-solutions, this experiment was highly relevant. At the same time, the discovery of the chemical reactivity of this intrinsically three-dimensional molecule led researchers to look for possible biomedical applications.[5] Soon C_{60} derivatives demonstrated many interesting potential biological applications, including DNA cleavage, HIV protease inhibition, photodynamic

therapy, free radicals-scavenging as well as imaging and radiotherapy.[5–9] Thus it became important to investigate the toxicity and the *in vivo* fate of C_{60} and derivatives. Besides, as underivatized and derivatized fullerenes are becoming increasingly available, it is of great importance to assess their safety and environmental impact.

C_{60} is a dark-brown crystalline powder, which is not soluble in aqueous media.[10] Thus most authors resorted to its water-soluble derivatives in order to investigate its toxicity as well as its biological effects. Other ways of solubilization used the encapsulation or micro-encapsulation in carriers (such as γ-cyclodextrines, calixarenes or liposomes) or the addition of PVP, octanol, Triton X or lecithin, Tweens and phospholipids.[5] However, it is obvious that such modifications lead to different compounds with different properties. Curiously, some studies seem to have missed this point. Besides some modifications, sometimes even non-covalent interaction with a solubilizing agent (like, for example, polyvinylpyrrolidone,[11] PVP, which forms a charge transfer complex with fullerene), can have a considerable impact on the general behavior of this fullerene.

In order to study the toxicity of pristine C_{60}, several authors used highly stable aqueous suspensions or molecular colloid systems of C_{60} in water. Similar molecular colloid systems can be prepared by using intermediate organic solvents, notably THF. However, the molecular colloid resulting complex can lead to surface modification and hence a different toxicological profile.

On another hand, C_{60} is an efficient singlet oxygen sensitizer under light exposure.[12] C_{60} and derivatives can be then highly toxic through $^1O_2$ formation.[13,14]

Thus, in this section we will first describe toxicity studies of unmodified C_{60} before considering the toxicity of its modified forms, including C_{60} derivatives. An additional subsection will be also devoted to the environmental impact of C_{60}.

2.2. Toxicity studies of pristine C_{60}

In the course of the first toxicity study of pristine C_{60},[4] as mentioned earlier, a C_{60}-benzene solution was used to determine the effects of acute and subchronic exposure of topically applied fullerene extracts on mouse skin. No acute toxic effects on mouse skin epidermis were observed.[4]

One year later,[14]C-labeled C_{60} was synthesized, suspended it in water, and its uptake by cultured human keratinocytes was studied.[15] Although the authors did not prove the internalization of the fullerene inside the cells, they

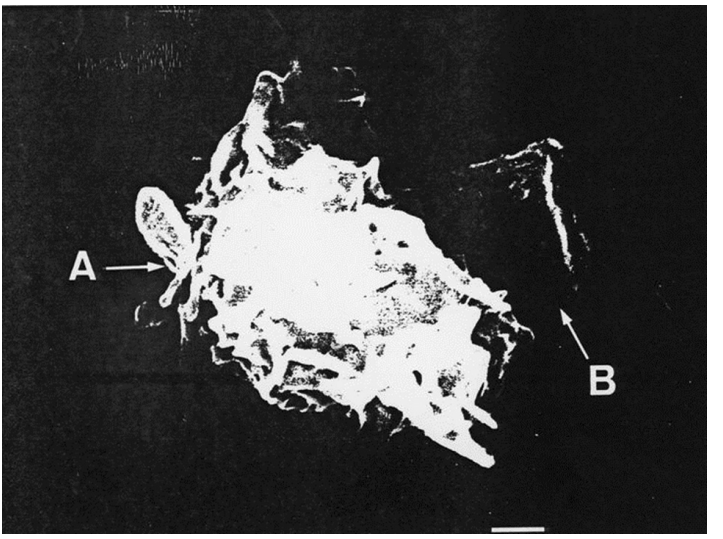

Figure 1. Scanning electron microscopy (SEM) micrograph of a human leucocyte (A) trying to engulf a C_{60} crystal (B). Taken from Ref. 17, with permission of Taylor & Francis.

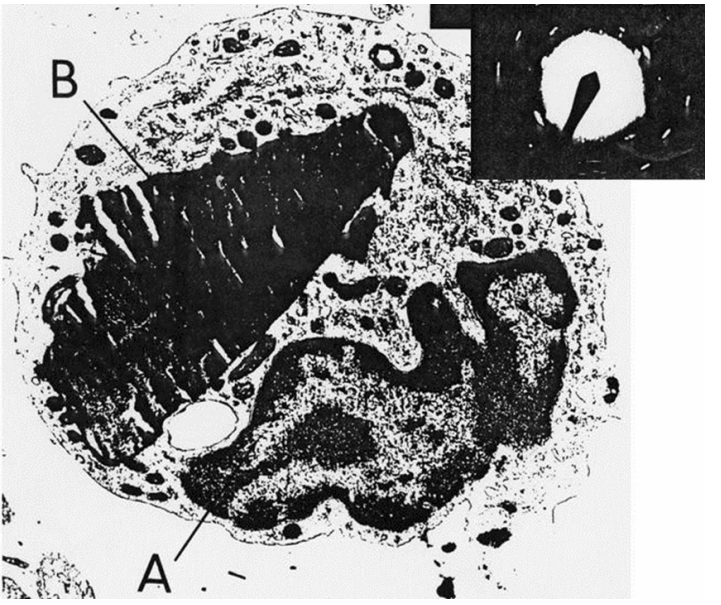

Figure 2. Transmission electron microcopy (TEM) micrograph of (B) a C_{60} crystal inside the cytoplasm of a human leucocyte (A = nucleus). (Inset) Electron diffraction was used to characterize the C_{60} crystal. Taken from Ref. 17, with permission of Taylor & Francis.

did not observe any sign of acute toxicity. At the same time, the absence of genetic toxicity of C_{60} was demonstrated by a Russian team by using the somatic mosaïcism model.[16]

In 1995, it was proved, using hand-grinded $C_{60,}$ that C_{60} can be internalized by normal human phagocytes (Figures 1 and 2)[17] without any sign of acute toxicity, which confirmed the results described above.[15]

In 1996, the absence of cytotoxic effects on cultured bovine alveolar macrophages and HL-60-macrophages was confirmed and the effects of C_{60} on the production by these cells of tumor necrosis factor and interleukin-8 as well as on superoxide anion release were measured.[18]

Also in 1996, the *in vivo* toxicity of this fullerene was studied after intraperitoneal injection to rodents of a highly concentrated aqueous suspension of micronized C_{60} (100 mg/ml) (Figure 3).[19,20]

The amounts injected were very large (2.5 to 5.0 g/kg of body weight), but no toxicity, either lethal or acute[19] or sub-acute,[20] was observed. Moreover this work clearly demonstrated that C_{60} can cross membrane barriers *in vivo* (Figure 4).[5,20] In spite of the induction of hypertrophy and hyperplasia of hepatic stellate cells (HSCs) (Figure 4), the mouse liver structure remained normal and no fibrosis either sinusoidal or portal developed.[19] Fifty-six days after C_{60}-treatment, the number of HSC decreased without any transformation into myofibroblast-like cells (MFCs),[21] which may be attributed to the free radical–scavenging properties of C_{60}.[21]

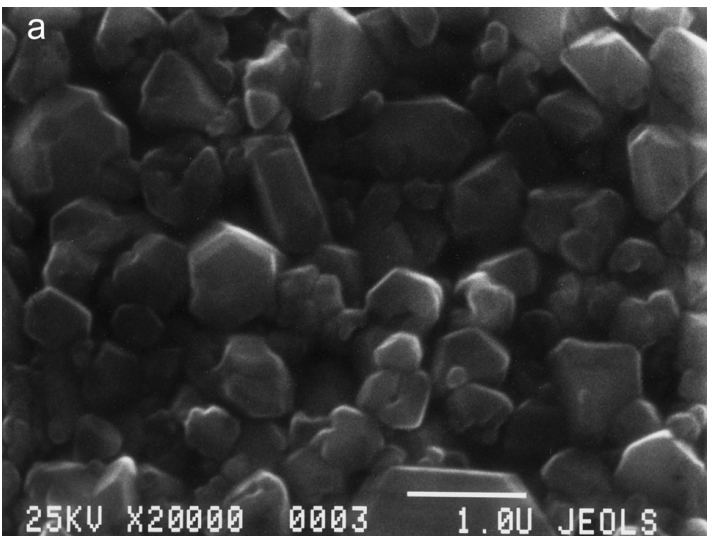

Figure 3. SEM micrograph of the micronized C_{60} aqueous suspension (100 mg/ml) used for *in vivo* toxicity studies of C_{60}. Taken from Ref. 21, with permission of ACS Publications.

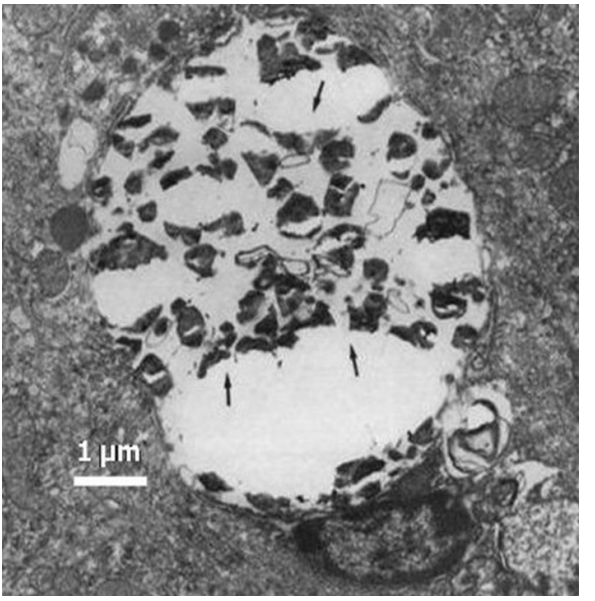

Figure 4. TEM micrograph of a liver section from a C_{60}-treated mouse showing a liver fat storing cell laden with C_{60} crystals (arrows). Taken from Ref. 24, with permission of Taylor & Francis.

Soon afterward, the absence of mutagenic effect of C_{60} in a prokaryotic *in vitro* test was confirmed using the *Escherichia coli* PQ37 strain and in an eukaryotic *in vivo* system on somatic wing cells of *Drosophila melanogaster* larvae.[22] In another way, an English group showed during the same period that fungal can grow on C_{60}.[23] At the same time, it was observed that C_{60} does not induce interleukin1-β secretion in cultured human leukocytes[24] and for the first time the reaction of C_{60} with vitamin A inside liver cells was observed,[25] which is the first Diels–Alder–like reaction ever observed *in vivo* to our knowledge (Scheme 1 and Figure 5).

A study conducted later in France on the microbial growth of 22 collection strains including *E. coli* ($n = 5$); *Pseudomonas aeruginosa* ($n = 2$); *Salmonella typhimurium* ($n = 6$); *Staphylococcus aureus* ($n = 2$); *Listeria monocytogenes* ($n = 2$) *Enterococcus hirae* ($n = 1$); *Bacillus cereus* ($n = 1$); *Bacillus subtilis* ($n = 1$); *Bacillus pumilis* ($n = 1$) and *Candida albicans* ($n = 1$) showed that C_{60} has no effect on the normal growth of these micro-organisms.[26]

In 2005, the absence of acute and sub-acute toxicity was confirmed in another species of rodents (Figures 5 and 6).[21]

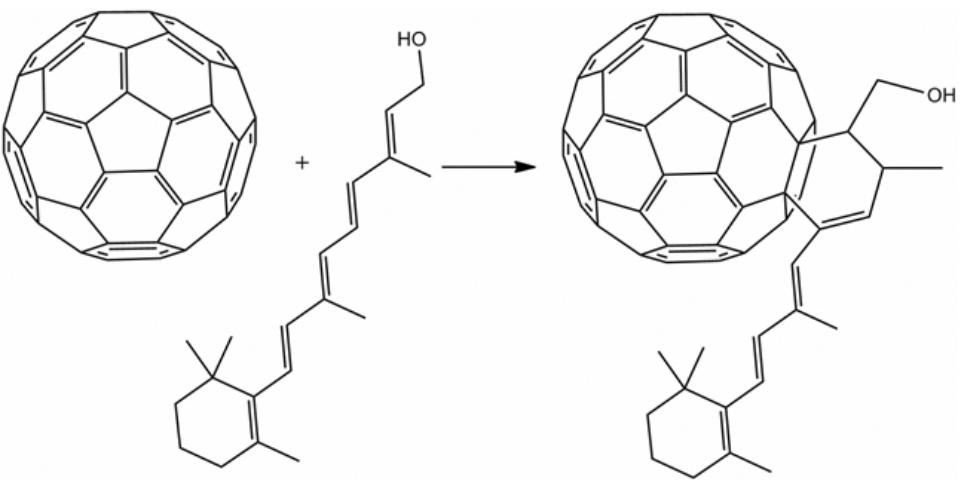

Scheme 1. *In vivo* Diels–Alder–like reaction between C_{60} and vitamin A occurring inside the livers of C_{60}-treated mice. Adapted from Ref. 25.

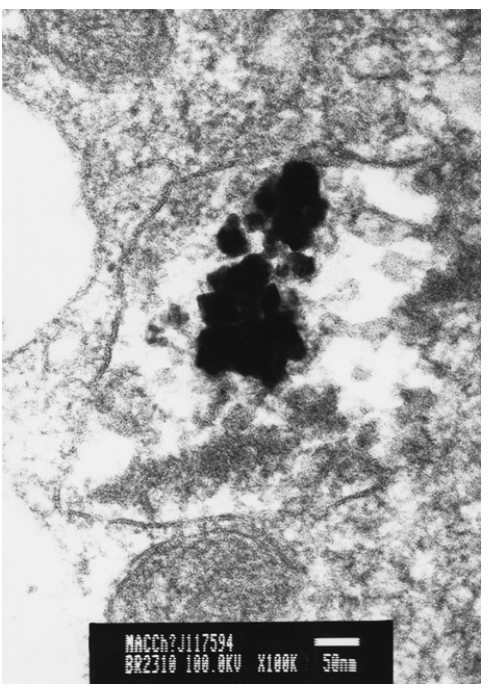

Figure 5. TEM micrograph showing C_{60} crystals inside a vacuole of a C_{60}-treated rat liver cell. Taken from Ref. 21, with permission of ACS Publications.

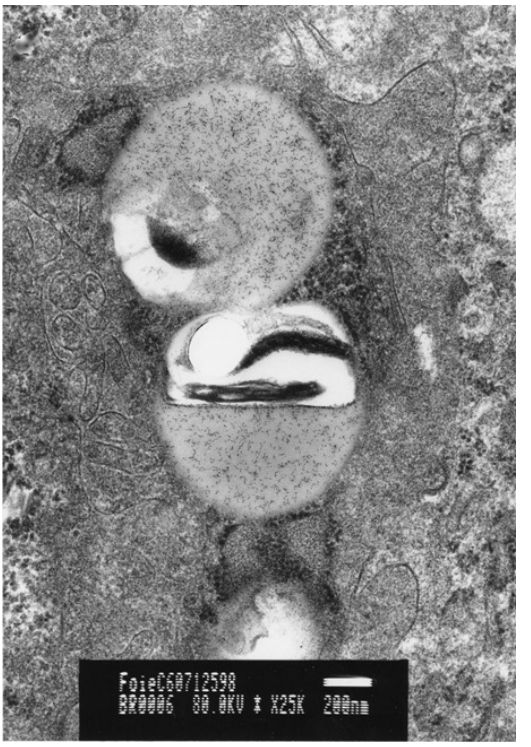

Figure 6. TEM micrograph showing the dissolution of C_{60} crystals inside the lipid droplets of a C_{60}-treated rat liver cell. Taken from Ref. 21, with permission of ACS Publications.

Moreover, the authors showed that C_{60} can be partly eliminated through the bile ducts. They also observed that the *in vivo* Diels–Alder–like reaction leading to C_{60}-retinyl adducts occurs in rats as was previously observed in mice (Scheme 1 and Figure 7).[25]

In 2006, the absence of toxicity in rodents was confirmed by a Japanese group.[27] The authors used the same C_{60} aqueous suspension as that described by Moussa *et al.*[19–21] and administered it orally as a single dose of 2 g/kg of body weight to male and female Sprague Dawley rats. In all cases, no death was observed in treated rats and the growths were normal. Thanks to a bacterial reverse mutation assay (Ames test) and to the chromosomal aberration test in cultured Chinese hamster lung (CHL/IU) cells, the same group also assessed the absence of genotoxicity.

All these studies performed on various experimental models by different groups from different countries showed that pristine C_{60} has neither acute nor sub-acute toxicity. These studies used well-characterized pure C_{60} suspended in aqueous media, but other C_{60} preparations can be used. Polar organic solvents

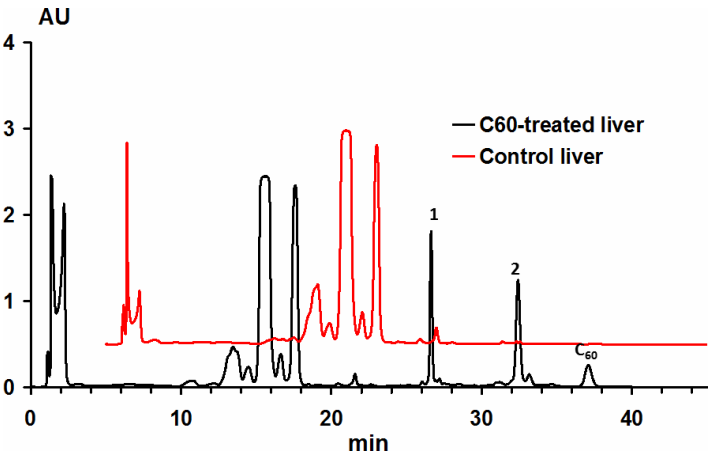

Figure 7. Chromatographic profile of a hepatic extract from a C_{60}-treated rat showing additional peaks (1 and 2) corresponding to C_{60}-retinyl adducts. Taken from Ref. 21, with permission of ACS Publications.

like THF can also lead to aqueous C_{60}-suspensions. On the other hand, C_{60}-solutions can be prepared with solubilizing agents leading to charge-transfer complexes such as C_{60}-PVP.[28] Such charge-transfer complexes formed in aqueous media usually exhibit either one or multiple coordinating nitrogen atoms, depending on the concentration of the ligand and its ionization potential.[28] Then, a C_{60}/PVP complex could bind to different receptors in biological media resulting in different effects. In 1995, Satoh *et al.* studied the effects of acute and short-term repeated application of a PVP-solution of fullerene C_{60} (4 μM) on agonist-induced responses in various tissues of Guinea pigs and rats. They reported that sub-chronic exposure decreased responsiveness toward drug receptors. This was the first study pointing out a possible negative effect of C_{60}.[29]

As a matter of fact, the first real harmful effect of C_{60}-PVP solutions was observed in 1996 by Tsuchiya *et al.* on mouse embryos *in vitro* as well as *in vivo*.[30] *In vitro*, it was observed that the incubation of C_{60} with various PVP concentrations inhibited cell differentiation and proliferation in a mouse midbrain but the effect was weaker than the vehicle controls. But *in vivo*, it appeared that C_{60}-PVP solutions strongly alter embryogenesis while PVP alone has no effect.[30] At the time, ignoring the strong interactions between C_{60} and PVP, which were still unknown, Tsuchiya *et al.* attributed this harmful effect to C_{60}.[30] In fact, C_{60}-PVP complexes can cross the placental barrier while PVP, which is also toxic *in vitro,* cannot. The authors wrote that this is a "serious harmful effect of C_{60}," but, surprisingly, the media failed to notice, perhaps because the production of fullerenes was still confidential.

But the media did notice in 2004, when a study performed in the Southern Methodist University in Dallas (Texas, USA) linked a fullerene aqueous suspension (nano-C_{60} aggregated water-soluble fullerenes or nC_{60}) to brain damage in fish.[31] The same group carried on their study and they concluded that nano-C_{60} is cytotoxic to human dermal fibroblasts (HDFs) and human liver carcinoma (HepG2) cells at the 20 ppb level[32] which is among the lowest known LC50 values for any organic compound. This article made international headlines with coverage in a number of newspapers.[33,34]

These headlines raised concerns about the alleged dangers of fullerenes and nanotechnologies.[33] In particular; the safety of C_{60} and its environmental innocuousness were seriously questioned. Probably because it permitted to bypass the water insolubility of C_{60}, the same nC_{60} preparation continued to be used by a limited group of authors and it soon was reported that pristine C_{60} might be very toxic in living systems such as bacteria, algae and fishes by inducing oxidative stress,[31,35–38] and that C_{60} derivatives are less toxic than pristine C_{60}, which was contrary to all previous studies.[39–45]

In fact the origin of these observations lay in the preparation of the nC_{60} suspensions used in these alarming studies. First fullerene powder was dissolved in THF. Then the resulting solution was mixed with water and the organic solvent was evaporated, leading to a stable colloidal suspension of nC_{60} clusters in water.[46] But these clusters did not contain C_{60} and water only. In 2005, using FTIR analysis, G. Andrievsky, the Ukrainian pioneer of biological applications of nC_{60},[47] and his group showed that organic groups remained in nC_{60} structures prepared using organic solvents, and that, in this case, THF was present indeed.[48] So they assumed that "the reason of the revealed negative effects should be explained by the presence in dispersions of THF and products of its modification, but not of fullerenes." Independently, Brant *et al.*,[49] through electrokinetic studies, showed that THF was still present in these clusters and asked for a reinterpretation of the previous toxicity conclusions about THF-prepared solutions. One year later, NMR studies confirmed the presence of THF.[50]

A number of studies were performed to confirm or invalidate the assumed toxicity of nC_{60} clusters. It was demonstrated that gamma-irradiation of THF/nC_{60} resulted in a complete loss of its cytotoxic effect and even led to its conversion to a cytoprotective agent,[51] and that avoiding the use of THF during the preparation of nC_{60} suspensions prevented the toxic effects observed with THF/C_{60}.[52] In the same way, Jia *et al.*[53] a Chinese group, did not observe any significant toxicity for C_{60} up to a dose of 226 $\mu g/cm^2$ on alveolar macrophage cell lines after 6 h exposure. As we wrote above,

Gharbi *et al.* had confirmed the absence of acute and sub-acute toxicity in rodents.[21] One year later, an Italian–French collaborative study explored the inflammatory response of murine and human macrophage cells *in vitro*.[54] The authors showed that C_{60} does not stimulate the release of NO by murine macrophages in culture and that this fullerene has no toxicity against human macrophages. Furthermore, Brant *et al.*[55] showed that the "*n*C_{60} produced *via* the different methods were unique from each other with respect to size, morphology, charge, and hydrophobicity. The greatest dissimilarities were observed between the *n*C_{60} produced by extended mixing in water alone and the *n*C_{60} produced by solvent exchange processes." So it was impossible to generalize *n*C_{60} properties, "particularly as they vary in potential toxicity considerations".[55]

In 2007, the first author of a 2004 paper that reported that C_{60} was more toxic than its derivatives,[32] claimed that *n*C60 has no lung toxicity in an *in vivo* experimental model that is not consistent with the previously reported *in vitro* effects.[56] Surprisingly, this implicit error admission did not prevent some toxicological reviews to continue to claim that C_{60} is very toxic.[57]

Anyway, it took three years to demonstrate that the observed deleterious effects on survival and gene expression in larval zebrafish *Danio rerio* was due to degradation by-products of THF: gas chromatography–mass spectrometry detected THF oxidation products gamma-butyrolactone and tetrahydro-2-furanol, so that the effects of THF treatments could result from gamma-butyrolactone toxicity.[58] The deleterious effects of degradation by-products of THF were confirmed by others[59–61] and the innocuousness of nC_{60} prepared without THF was also illustrated with respect to human epidermal and bacterial cells[62] and in the cases of the growth of *Saccharomyces cerevisiae or E. coli*.[63] Nevertheless studies using *n*C_{60} prepared with THF continued to be published.[64,65]

2.3. Toxicity studies of C_{60} derivatives

As to the fullerenes derivatives, whose potential of medicinal applications has been extensively studied,[5,9,40,46,66–82] no general trend can be deduced. This is obvious because in every case we deal with a new compound.[55] As a matter of fact, it has been shown in the case of daphnids that toxicity changes with functionalization of the same core material (*n*C_{60}). Functionalization (hydroxylation and hydrogenation) significantly affected the production of the toxicity biomarkers glutathione-S-transferase and catalase.[83]

To illustrate the range of behaviors as a function of functionalization, we will consider the effects on the lifespan. Polyhydroxyfullerenes have beneficial

and/or specific effects on model organisms representing four kingdoms, including the green algae *Peudokirchneriella subcapitata*, the plant *Arabidopsis thaliana*, the fungus *Aspergillus niger* and the invertebrate *Ceriodaphnaia dubia*. In particular, the lifespan of *Daphnia* underwent an extension of about 38%.[84] In the same way, a carboxyfullerene SOD mimetic extended the median lifespan of non-transgenic mice by 15%.[85] On the contrary, a tris carbonyl fullerene adduct ($C_{60}[C(CO_2H)_2]_3$) induced premature senescence in human epidermal keranocyte cells.[86] In extreme cases, some C_{60} derivatives can be highly toxic.[44]

2.4. Environmental impact of C_{60}

It could be feared that C_{60} could impact the environment through the generation of oxygen reactive species (ROS) by the action of sunlight on nC_{60} in aqueous media. But in a recent review in which they insist on the fact that nC_{60} is of low toxicity in fish,[87] the authors emphasize that nC_{60} generates minimal reactive ROS.[55] However, they draw the attention of the community on the ability of nC_{60} to affect the environmental fate. In particular, they showed that mixtures of 17α-ethinylestradiol (EE2) and nC_{60} decreases bioavailability of EE2 in zebrafish, which indicates that EE2 associates with nC_{60} and becomes unavailable to fish.[88] This is another example of the association of nC_{60} with co-contaminants,[89–91] which could lead to persistence of co-contaminants in the environment.

Moreover, a number of studies show that nC_{60} undergoes photochemical transformations under sunlight exposure (simulated or not) to yield unknown compounds.[92–95] Such transformations, including breakdown of C_{60} cages,[96] are an important factor controlling nC_{60} physical and chemical properties as well as its fate and transport in the natural aqueous environment.

Furthermore, plants in aquatic systems[97] and worms in soils[98] tend to bioabsorb and accumulate C_{60}, which also could influence the fate of C_{60} in the environment.

Finally, in their review,[87] the authors list a number of oxidative stress effects on fish that they suggest as resulting from false positives but they conclude that "C_{60} may have important effects on environmental fate, transport, and bioavailability of co-contaminants… similar to that observed for microplastics."

2.5. Conclusion

This review shows that pristine C_{60} has no acute or sub-acute toxicity in a large variety of living organisms, from bacteria and fungal to human leukocytes, and also in drosophila, mice, rats and guinea pigs.

As to nC_{60} aggregates, the effects of THF oxidation by-products trapped inside these aggregates has been recently thoroughly reviewed.[88] The authors state: "Future studies should acknowledge that current evidence indicates low toxicity of nC(60) and refrain from citing articles that attribute toxicity in fish to nC(60) based on methods shown to be compromised by experimental artefacts".[88] Independently, another paper reached the same conclusions.[6]

While pristine C_{60} is non-toxic, it has to be stressed that chemically — either covalently or non-covalently — modified fullerenes, can be toxic. Furthermore, under light exposure, C_{60} is an efficient singlet oxygen sensitizer. Therefore, if pristine C_{60} is absolutely non-toxic under dark conditions, this is not the case under UV-visible irradiation in the presence of O_2, where *fullerene molecules* can be highly toxic through $^1O_2$ formation.

As to C_{60}-preparations and C_{60} derivatives devoted to biomedical applications, they have to undergo the same controls as every new drug.[99]

Finally, the general rules of C_{60} toxicity are well known now:[100]

1- Pristine C_{60} is not toxic. But, of course, a certified toxicity study is still needed.
2- C_{60} aggregates may convey toxic elements as any other aggregated material.
3- In contrast with pristine C_{60} some of its derivatives, notably cationic ones may be highly toxic.

3. Toxicity Studies of Carbon Nanotubes

3.1. General considerations

Pristine (unmodified) CNTs are hardly dispersible in water and biological media. The tubes are often entangled and the ropes of single-walled CNTs (SWNTs) are held together by van der Waals forces. Non-covalent or chemically covalent functionalization was widely used in order to enhance the dispersion of CNTs in biological media.[101]

CNTs are a heterogeneous carbon family. The diameter of CNTs generally varies from 0.4 to 100 nm, while the length usually reaches several micrometers.[102] Besides, raw CNT materials generally contains up to 30% metal catalyst particles, mainly iron and nickel, and some amorphous carbon. The most commonly used technique of purification is based on strong acid treatments, which allows solubilization and removal of a large part of the metallic impurities.[103] However, such treatment generally result in cutting the tubes in shorter pieces and in generating carboxylic functions at the tips and around the sidewalls, where the curvatures of the tubes present a higher strain.[104]

Due to their asbestos-like structures, airborne CNTs[105] might represent a danger to people handling these materials on daily basis either by crossing their skin barrier or entering and residing in their lungs. Thus early studies concentrated on the exploration of CNT toxicity through classical routes of exposure at work place.

As possible biomedical applications of CNTs have attracted considerable attention, during the last decade, several studies were recently conducted on the toxicity and the *in vivo* behaviour of these materials after enteral and parenteral administrations.

In this section, toxicity studies on CNTs will be reviewed as a function of the exposure route.

3.2. *In vitro* studies of CNT toxicity

Many *in vitro* toxicity studies have been performed on different types of CNTs, during last decade, but their results remain controversial.[6] Preliminary investigations of the effects of CNTs on living cells showed that the toxicity of these materials mainly depends on the type of CNTs, including the method of production, impurities and purification process, lengths, aggregation states, surface coatings and chemical modifications.[106] Moreover, CNTs may interact with assay reagents and even dispersion agents, potentially resulting in a secondary rather than primary toxicity.[107,108]

3.3. Toxicity studies related to the exposure at work place

Early *in vivo* studies were conducted in order to evaluate the safety of CNTs at work place. The first study on the potential of CNTs to induce skin or eye irritation was performed in 2001 by two classical dermatological tests.[109] No irritation effect was observed in comparison to a CNT-free soot control and it was concluded that "no special precautions have to be taken while handling these nanostructures".[109] These results have been recently confirmed with SWCNTs and MWCNTs in two animal species, rabbits and Guinea pigs.[110]

In 2004, the physical nature of the aerosol formed from SWNTs during mechanical agitation was evaluated.[111] The authors also conducted a study in which airborne and dermal exposure to SWNTs was evaluated while handling unrefined material. Estimates of the airborne concentrations of CNT materials generated during handling suggest that concentrations were very low (less than 53 $\mu g/m^3$). In another way, glove deposits of SWNTs during handling were estimated at between 0.2 mg and 6 mg per hand.[111]

In the same year, two other studies were conducted in order to assess the pulmonary toxicity of CNTs.[112,113] The first study was performed on mice after intra-tracheal instillation of three kinds of SWNTs raw and purified HiPco and CarboLex CNTs.[112] While the first material contains only iron impurities, the third one contains nickel and yttrium impurities. CNTs were dispersed by brief shearing and sonication in heat-inactivated mouse serum. Mice were instilled with CNTs or carbon black or quartz particles used as negative and positive controls, respectively. Seven and ninety days after this single treatment, the animals were sacrificed for histopathological examination of the lungs. In the animals euthanized after seven days, all CNT treatments induced dose-dependent epithelioid granulomas and, in some cases, interstitial inflammation. These lesions were more pronounced in the group euthanized after 90 days.[112] The lungs of carbon black–treated mice were normal, whereas those treated with quartz high-doses revealed mild to moderate inflammation. The authors concluded that, on an equal-weight basis, if carbon nanotubes reach the lungs, they are much more toxic than carbon black and can be more toxic than quartz. According to the authors, these results indicate that chronic inhalation of CNTs can be considered as a serious occupational health hazard.[112]

The second study was conducted in rats after intra-tracheal instillation of SWNTs produced by laser ablation and containing about 30% to 40% amorphous carbon (by weight) and 5% each of nickel and cobalt.[113] As controls, the authors used quartz, carbonyl iron and graphite particles as well as the vehicle (1% Tween 80 — phosphate buffered saline (PBS)). The effects on lungs were then assessed by bronchoalveolar fluid (BALF) biomarkers analysis and histopathological examination of tissue at 24 h, 1 week, 1 month and 3 months post-instillation. The authors observed a granulomatous reaction similar to that observed in mice.[112] As the series of multifocal granulomas were non-uniform and as there were a lack of dose–response relationship and a lack of lung toxicity by assessing BALF and cell proliferation parameters, the authors concluded that the granulomatous reaction is a non-specific foreign tissue body reaction.[113]

The differences between the two studies may be attributed in part to species differences (rat *vs.* mouse), but are more likely due to the differences in the experimental designs.[113]

One year later, another group studied the effects of MWNTs after intratracheal administration to rats.[114] CNTs induced inflammatory and fibrotic reactions and stimulated the production of TNF-α. Two months after administration, CNTs persisted in lungs and the lesions were characterized by the formation of collagen-rich granulomas protruding in the bronchial lumen, in

association with alveoli in the surrounding tissues. These lesions were attributed to the accumulation of large MWNT agglomerates in the airways.[114]

The physiological relevance of intra-tracheal instillation of CNTs is questionable since physiologically inspired particles would probably encounter several barriers in the upper respiratory tract before reaching the trachea and the lungs. Nevertheless, purified HiPco SWNTs with less than 1% of iron catalyst impurities elicited inflammation, fibrosis and granuloma formation in mice even when administered by pharyngeal aspiration.[115] Moreover, functional respiratory deficiencies and decreased bacterial clearance were found in SWNTs-treated mice.[115]

Three years later, a study tried to investigate the physicochemical parameters involved in MWNT toxicity mechanism.[116] The authors evaluated the toxicity after intra-tracheal instillation to rats of MWNTs heated at 600°C (which allowed loss of oxygenated carbon functionalities and reduction of oxidized metals) or at 2400°C (which hardened structural defects and eliminated metals) before and after grinding (introduction of structural defects in a metal-deprived framework). According to the authors, the pulmonary toxicity as well as *in vitro* genotoxicity of MWNTs were reduced upon heating but restored upon grinding, indicating that the intrinsic toxicity of the tubes was mainly mediated by the presence of defective sites in the carbon framework.[116]

Recently, in order to check the hypothesis linking lung toxicity to the degree of CNT aggregation, unpurified aggregated or highly dispersed SWNTs (in 1% Pluronic F 108NF) were intra-tracheally instilled to mice.[117] According to the authors, lung inflammation induced by SWNTs is significantly lower than that induced by urban particulate matter or asbestos fibers used as positive controls. Aggregated SWNTs in PBS caused areas of chronic inflammation, while highly dispersed SWNTs did not cause any inflammation or fibrosis. Moreover, nanoscale-dispersed SWNTs were taken up by alveolar macrophages and cleared from the lung over time.[117] Thus, administering unpurified CNTs avoided a potential effect due to surface defects of tube sidewalls,[104] which might contribute to an increase in collagen deposition.[118] These results agree with those obtained the same year with individually dispersed MWNTs in Tween 80.[119] The authors did not find any evidence of chronic inflammation, such as angiogenesis or fibrosis, induced by MWNT instillation.[119]

In contrast, depending on the route of administration (*i.e.*, intratracheal instillation or inhalation) and on the dose, a more recent study reported that highly dispersed MWNTs could produce pulmonary lesions.[120] The MWNTs used in this study were ground in a fructose mold and the fructose was rinsed

afterward with water and hydrogen peroxide. According to the authors, this process slightly oxidized the tubes. The rats were instilled intra-tracheally with two single doses (0.2 mg or 1 mg of 1.1 μm of mean particle length) and the study was conducted up to six months. While only a transient infiltration of inflammatory cells was observed for the lowest dose, the highest dose caused small granulomatous lesions and transient collagen depositions. In parallel, the authors conducted an inhalation study of dispersed MWNTs in a daily average mass of 0.37 ± 0.18 mg/m^3. [120] The rats were exposed to aerosol particles for 6 h per day, 5 days a week for 4 weeks. At the end of the experiment, the dispersed MWNTs with the average length of 1.1 μm caused only a minimal transient inflammation without neutrophil infiltration. Moreover, granulomatous lesions or collagen depositions were not observed.[120]

In conclusion, recent studies indicate that nanoscale-dispersed SWNTs or MWNTs at a dose of 1.6 mg/kg,[117] or 0.66 mg/kg,[120] respectively do not induce lung toxicity after intra tracheal instillation to rodents. It must be noted that these doses would be equivalent to a single instilled dose of approximately 112 g or 46 g, respectively, in an average weighting human.

3.4. Toxicity studies related to the asbestos fibres analogy

The analogy between CNTs and asbestos fibres was pointed out for the first time in the late nineties.[105] Asbestos fibres have a high aspect ratio and they are characterized by high chemical stability in physiological environment.[121] The pathologies related to asbestos exposure, especially lung fibrosis (asbestosis) and lung cancer (mesothelioma) that most often originates in the pleura, the outer lining of the lungs, have caused a major worldwide occupational health disaster and founded reasonable fear of these airborne fibres.[122]

The pleural mesothelium is the primary mesothelial target for inhaled fibres.[123] The space between the visceral and the parietal pleura contains the pleural fluid and a population of pleural macrophages. The pleural liquid is derived mainly from capillaries in the parietal pleura and is principally removed by lymphatic stomata in the parietal pleura,[124] which drains the pleural fluid to the lymph nodes. This turnover is important for clearance of particles and fibres that reach the pleural space.[123] While the exact mechanism of fibre deposition in the pleural mesothelium remains unclear, the retention of bio-persistent fibres at the parietal pleura is known to initiates mesothelial injuries and inflammation that, overtime, lead to mesothelioma, a deadly cancer.

When the fibre diameter is small, the fibre will align with the flow and deeply penetrate the lungs. The fibres are more or less cleared by macrophages,

depending on their length. If the fibres are too long, they cannot be entirely phagocytized. This "frustrated" phagocytosis is a pro-inflammatory condition, characterized by the release of inflammatory mediators into the environment. These mediators may recruit other cells (for example collagen synthesizing fibroblasts) or cause DNA damage and mutations to proliferating cells, which may in term cause tumour development.[125]

Carbon nanotubes are fiber-shaped; however, SWNTs are flexible and bendable, and often entangled. These particle-sized tangles would not obey the fiber toxicity paradigm because of their non-fibrous geometry.[121,123] MWNTs, on the other hand, are much stiffer and generally less entangled; therefore, if long enough, they might present a risk.[123]

A study performed with nickel containing milled pluronic-suspended MWNTs[126] with a length ranging between 100 nm and 10 μm showed that the nanotubes are observed inside the sub-pleural tissue macrophages after a single 30 mg/m^3 inhalation exposure of 6 h. Fibrotic lesions, which increased two and six weeks after exposure, remained focal and regional. This effect did not occur after exposure to a dose of 1 mg/m^3, which, according to the authors, corresponds to 0.2 mg/kg body-weight. While the authors did not find MWNTs-loaded macrophages inside the pleura, they did notice an increased number of pleural mononuclear cells.

At the same time, another study reported that MWNTs could reach the pleura after pharyngeal aspiration.[127] The inflammation extended from lungs to pleura in half of the MWNT-exposed mice. At 56 days post exposure, MWNTs penetrated the pleura in two out of four mice treated with the highest MWNT dose. The inflammation induced by the nanotubes was transient at low doses but persistent through day 56 at a dose of 40 μg.

In another study performed by the same group,[128] the authors reported an initial high density of penetrations into the sub-pleural tissue and the intra-pleural space one day following aspiration of MWNTs (80 μg per mice). The kinetics of penetration decreased due to the clearance by alveolar macrophages by day 7 and reached steady state levels in the sub-pleural tissue and intra-pleural space from days 28 to 56. The majority of the tubes (62% of the dose) resided in alveolar macrophages, while 0.6% of tubes, reached the visceral pleura region (sub-pleura and intra-pleural space).

As it has been already emphasized,[123] the question that we should ask with regard to any fibre in relation to mesothelioma is not "Do fibres reach the pleura?" but "Are fibres retained in the parietal pleura", which is the site of origin of pleural mesothelioma.

In a recent study, long and short CNTs or asbestos fibres were injected directly into the pleural space.[129] The authors reported evidence

of length-related inflammation, with no significant inflammation when short tubes or fibres were administered. While no short samples were visible at day 1 or day 7, the mesothelium, that was thicker on day 1, returned to its normal thickness by day 7. While short tubes and fibres cleared from the pleura through stomatal openings, long tubes and fibres remained inside the pleura near stomata, where they persisted and caused inflammation and progressive fibrosis.

3.5. Toxicity studies after enteral and parenteral administrations

While pulmonary toxicity studies clearly indicate that inhalation of CNTs aggregates represents a possible occupational health hazard, the toxicity of CNTs after administration through bio-medically relevant routes is still a matter of debate.

Subcutaneous implantations of clusters of MWNTs of different lengths (220 nm and 825 nm) in rats showed that the degree of inflammatory response around the shorter MWNTs was slighter than that observed around the longer ones, thus indicating that macrophages could envelop the shorter nanotubes more readily than the longer ones.[130] However, no severe inflammatory response such as necrosis, degeneration or neutrophils infiltration was observed around both types of MWNTs.[130]

These biological responses have also been described after subcutaneous implantations in mice of 2 mg/animal of SWNTs, two different types of MWNTs (20 and 80 nm of average diameter) and cup-stacked carbon nanotubes (CSNTs made with stacked truncated cones), for up to 3 months.[131] The nanotubes used in this study were purified by thermal treatment process during which the metal particles evaporate. After 1, 2, 3 weeks, 1 month, 2 months and 3 months post-implantation, the animals were sacrificed, blood was collected for CD4+ and CD8+ T-cells counting by flow-cytometry and tissue of skin (including muscle layers) were collected for histopathological examination. All mice survived, and no large changes in their weights were observed during the experimental period. After one week of implantation, only SWNTs activated the major histocompatibility complex (MHC) class I pathway of antigen-antibody response system (higher CD4+/CD8+ value), leading to the appearance of an oedematous aspect. After two weeks, significantly high values of CD4+ without changes in CD8+ signified the activation of MHC class II for all samples. The authors noted that antigenic mismatch becomes less evident with time, notably one month post-implantation, indicating an establishment of granuloma formation. Furthermore, it must be

stressed that the toxicological response of CNTs was absolutely lower than that of asbestos.

Among different routes of administration, the intra-peritoneal way has several advantages: first it offers the possibility to administer larger doses of suspended nanoparticles and secondly, the peritoneal cavity has a recognized particle-clearance mechanism.

Particles leaving the peritoneal cavity pass *via* the retrosternal route through stomata (pore like structures) to the parathymic (mediastinal) nodes to the upper terminal thoracic duct or right lymphatic duct.[132] Moreover, the peritoneal cavity and its mesothelium-covered viscera were recognized as a convenient substitute for pleural cavity mesothelium in fibre toxicity studies.[123]

The first study of *in vivo* toxicity of CNTs after intra-peritoneal administration was conducted in 2007.[133] The authors compared the acute toxicity of full-length and ultra-short SWNTs suspended in a Tween 80 aqueous solution, under the same conditions they used since 1996 to study the acute and sub-acute toxicity of [60]fullerene in mice.[19] Preliminary results showed that irrespective of the length of the administered SWNT material, SWNT aggregates induced a granulomatous response inside the organs like that which occurs in lungs after inhalation or intra-tracheal instillation.[133]

In 2008, a Japanese team observed for the first time that MWNTs could induce mesothelioma after intra-peritoneal administration to p53 heterozygous mice.[134] This type of mice are, however, more sensitive and have a shorter tumor onset rate than standard wild-type rodents. Indeed, some authors contested this study[122,135] but Takagi *et al.* explained and justified their experimental choices letting other studies to confirm mesothelium threats.[136] The authors administered intra-peritoneally 3 mg of CNTs per mouse suspended in 1% Tween 80 and 0.5% methyl cellulose-aqueous solution. While the samples of crocidolite asbestos were evenly dispersed, MWNTs contained aggregates and fibres. The mice were monitored until one of the groups (MWNTs treated group) reached 100% mortality, which happened on day 180. The mice treated with MWNTs exhibited moderate to severe fibrous peritoneal adhesions, slight ascites, fibrous peritoneal thickening and a high incidence of macroscopic peritoneal tumours. Similar, but less severe findings were noted in the asbestos group. As the authors emphasized, it is important to limit the significance of this study to the monitoring of biological activity of a compartment of MWNTs longer that 5 μm. There is no information that this study method would be sensitive to pure nanometer-sized particles within the same timeframe.[134]

An analogous study was made, in time, on wild-type rats[137] in a two-year exposure period, where up to 20 mg of MWNTs with and without sidewall defects (induced by grounding of the raw material) suspended in phosphate buffer were intraperitoneally injected to a large number of rats. After 24 months, crocidolite induced mesothelioma in 34.6% animals, whereas mesothelioma occurred only in 3.8% in the vehicle-treated rats. MWNTs with or without structural defects did not induce significant mesothelioma in this study, as mesothelioma occurrence was detected in up to 6% of MWNT-treated rats, which is in line with the spontaneous incidences of mesothelioma in rats (up to 6%). The incidence of tumours other than mesothelioma was not significantly increased across the groups.[138]

In contrast to that observed after intra-peritoneal administration to wild-type rats,[137] MWNTs injected in a single intra-scrotal dose to rats induced mesothelioma 37 to 40 weeks after treatment.[139] In the latter experiment, MWNTs were suspended in a 2% carboxymethyl cellulose aqueous solution and administered to rats at a dose of 0.24 mg/animal. According to the authors, this dose corresponds to the maximal value recommended by the guideline for man-made mineral fibres.[139]

In conclusion, the ability of MWNTs to induce mesothelioma in experimental models in rodents is still a matter of debate. This cancer is a highly specific response to bio-persistent fibres and may occur in the pleura (outer lining of the lungs and internal chest wall), peritoneum (the lining of the abdominal cavity), pericardium (a sac that surrounds the heart), or *Tunica vaginalis* (a sac that surrounds the testis).[140] Considered together these findings show that under some experimental conditions, MWNTs may induce mesothelioma formation. Thus, further investigations are urgently needed.

In 2008, in a comparative study of MWNTs and asbestos fibres, it was reported that MWNTs exhibit a length-dependent pathogenic behavior, including granuloma formation and inflammation.[141] The overall conclusion of the study was that short MWNTs do not mimic the behavior of long asbestos, but that their data cannot preclude the possibility that short MWNTs may do by some other mechanism that was not assessed in this study. Long MWNTs produced inflammation, foreign body giant cells and granulomas that were qualitatively and quantitatively similar to the foreign body inflammatory response caused by long asbestos fibres. However, for the specimen treated with shorter MWNTs that did exhibit granuloma, the authors concluded that it may be due to the fact that the sample they injected was contaminated with long fibres, caused by some other unidentified component specific for the precise MWNTs sample, or the granulomas could have arisen spontaneously by chance.[141]

Preliminary studies[133] showed that intra-peritoneal (i.p.) administration of large aggregates of CNTs (>10 μm) of Tween-suspended ultra-short (20–80 nm long) and full-length SWNTs irremediably induce granuloma formation, irrespective of the administered dose (50 to 1000 mg/kg b.w.), length, or surface state of the administered material (Figure 8 and 9).[106,142]

Smaller agglomerates (<300 nm), on the other hand, did not induce granuloma formation nor did they induce any major life-threatening condition under the experimental conditions (Figure 10).[142]

A large portion of well-dispersed CNTs was eliminated through the kidney and the bile ducts (Figure 11). However, the aggregated part of the administered dose was not cleared from the body and persisted inside cells five months after administration (Figure 11).[142] The persistence of the nanotube aggregates inside the cells was probably due to the slow disaggregation and slow elimination of larger aggregates.[142]

The first report on the effects of SWNTs after intravenous administration to mice (3 mg/kg) monitored for over four months indicated normal blood chemistries and normal histological examinations.[143] The animals did not show significant inflammatory lesions and SWNTs accumulated in liver and spleen as evidenced by Raman spectroscopy. The CNTs used in this study were highly dispersed with polyethylene glycol (PEG). CNT aggregates were eliminated with ultracentrifugation before administration to the animals.

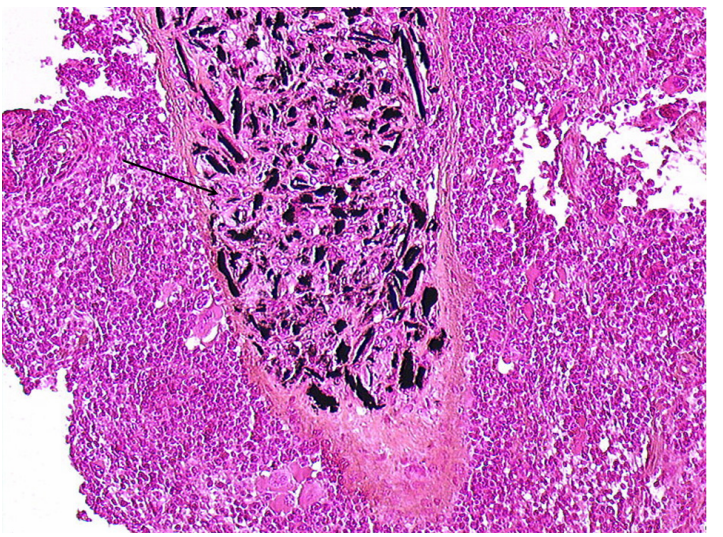

Figure 8. Optical microscopy after eosin-haematoxilin staining of a spleen section from a SWNT-treated mouse showing a granuloma laden with large SWNT aggregates (arrow) (Magnification × 1000). Taken from Ref. 142, with permission of ACS Publications.

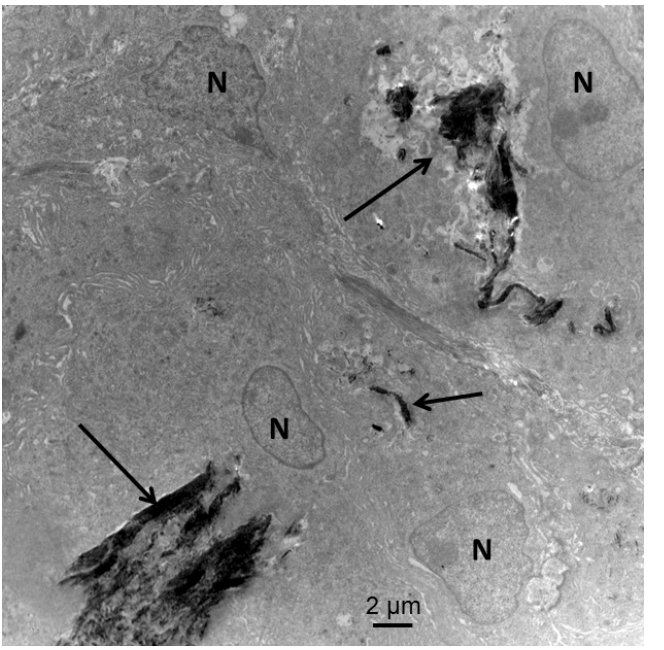

Figure 9. TEM micrograph of a granuloma laden with large SWNT aggregates (arrows) (N = nucleus).

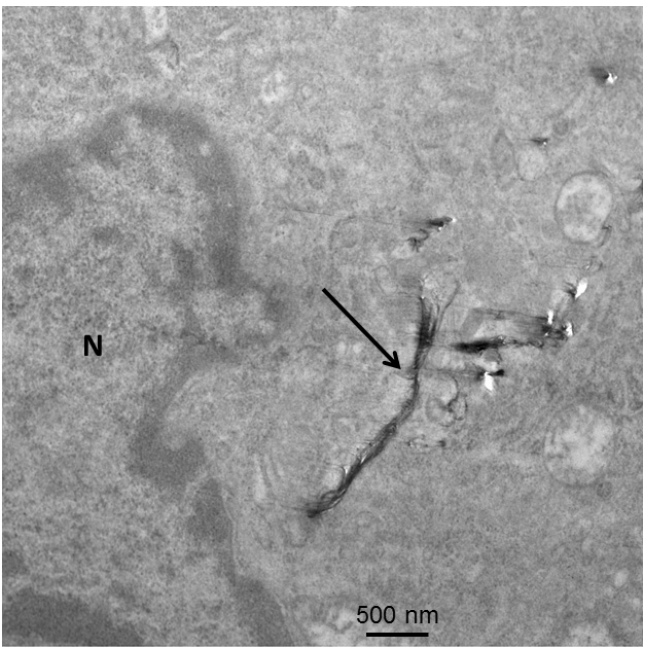

Figure 10. TEM micrograph of a small SWNT aggregate (arrow) inside a Kuppfer cell (liver macrophage) near the nucleus.

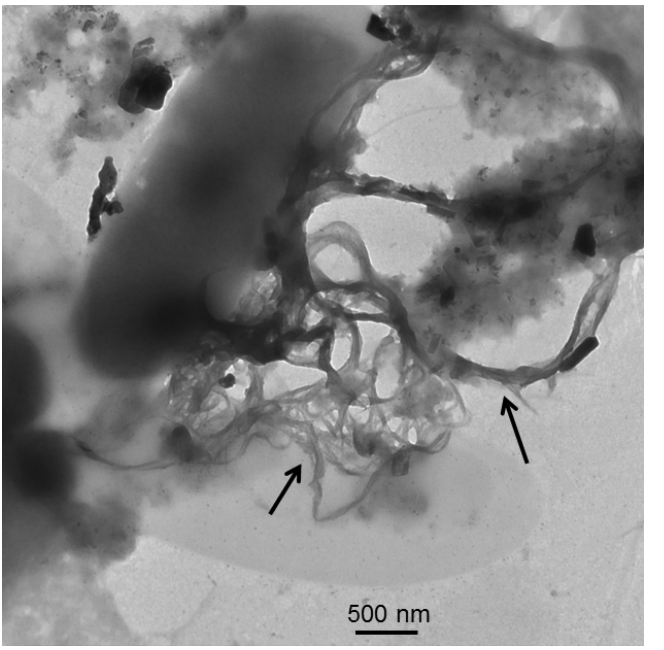

Figure 11. TEM micrograph of a fecal extract from a SWNT-treated mouse showing SWNT aggregates (arrows) eliminated via the bile ducts. Taken from Ref. 142, with permission of ACS Publications.

Another study used highly dispersed pristine HiPco SWNTs with different PEGylated phospholipids.[144] Big bundles and impurities were removed by centrifugation, and individually suspended tubes or small bundles were administered intravenously at a dose of approximately 20 μg or 100 μg per mouse. Blood, tissue and organ distribution and elimination in urines and feces were evaluated by Raman spectroscopy, by assessment of the tangential graphite-like phonon mode (G band). Administered SWNTs accumulated mainly in liver and spleen, however the quantity decreased over a three-month period. The authors concluded that SWNTs were mainly eliminated by the biliary pathway; only a small portion of short tubes (<50 nm in length) was eliminated in the urines. Finally, the authors did not report any obvious sign of toxicity.

Other authors also reported low toxicity of very low doses of SWNTs in mice over a three-month period.[145] Purified SWNTs were suspended in 1% Tween 80 aqueous solution and sonicated for 30 minutes prior administration to animals at various doses from 40 μg to 1 mg per mouse. Some of the serum biochemical parameters (ALT, AST and LDH) were higher in SWNT-treated animals compared to the control group 90 days post-exposure, indicating that

induced hepatic injury and tissue breakdown were dose-dependent. The long-term accumulation of aggregated SWNTs was evidenced in histological sections of lungs, livers and spleens and was confirmed by Raman spectroscopy and transmission electron microscopy in organ lysates. However, no fibrosis was detected in the organs.

Embriotoxicity was recently reported as an effect caused by intravenous administration of SWNTs in mice (30 μg/mouse).[146] The authors used pristine, oxidized or ultra-oxidized by acid treatment SWNTs. Cobalt was the only impurity that was released in the medium in which the tubes were dispersed (DMEM cell culture medium with fetal bovine serum). Before the end of gestation, the animals were sacrificed, and uteri, placentas and fetuses were examined. A high percentage of early miscarriages and fetal malformations were observed in females exposed to oxidized SWNTs, while lower percentages were found in animals exposed to the pristine material. The lowest effective dose was 100 ng per mouse. Extensive vascular lesions and increased production of reactive oxygen species (ROS) were detected in placentas of malformed but not of normally developed fetuses. Increased ROS levels were likewise detected in malformed fetuses. No increased ROS production or evident morphological alterations were observed in maternal tissues.[146]

MWNTs dispersed in mouse-serum (10 min of sonication) and injected to mice at a dose of 200 or 400 μg per mouse showed no severe acute response, 24 h after administration.[147] However, mice treated with pristine MWNT aggregates exhibited subdued behavior, hunched posture and signs of respiratory distress. While serum biochemistry data did not show significant increase, optical microscopy revealed aggregate accumulation, mostly in livers and lung vessels, which were probably responsible for respiratory distress. Nevertheless, no tissue degeneration, inflammation, necrosis or fibrosis occurred 24 h after injection.

The effects of Tween-suspended pristine MWNTs and PBS-suspended acid-oxidized MWNTs up to 2 months were investigated after i.v. administration to rats at a dose level of 10 or 60 mg/kg.[148] The authors reported an impact on body weight gain of the highest dose. Severe inflammatory cell infiltration in the portal region, cellular necrosis and focal necrosis were seen at a dose of 60 mg/kg in the MWNT-treated group 15 and 60 days following the treatment. Moreover, severe mitochondrial swelling, bile canaliculi expansion, mitochondrial destruction, loss and lysis of mitochondrial crest were also observed. In the acid-treated (oxidized) MWNTs group only slight inflammatory cell infiltration was observed after two months. A slight increase of AST activity used as biochemical marker of liver injury was also reported

in treated animals, but it did not increase more than twofold. Interestingly, 329 genes were upregulated and 31 genes were downregulated more than twofold in MWNT-treated mice, while 1139 genes were upregulated and 505 genes were downregulated over twofold in the mice treated with oxidized MWNTs.

In order to avoid mechanical blockage by the administered material, it is of capital importance to administer only individually suspended, short CNTs. Thus, further studies with individually suspended CNTs have to be made in order to confirm the direct effect of these materials after administration by the intravenous route.

3.6. Toxicity studies after oral administration

Oral administration of 1000 mg/kg of body weight of SWNTs to mice resulted in neither animal death nor behavioral abnormalities.[142] Compound-colored stool was found 24 h after gavage in all treated groups. Two weeks after treatment, regardless of the length or of the iron content, the nanotube materials did not induce any abnormalities after pathological examination, indicating that under these conditions, the lowest lethal dose (LDLo) is greater than 1000 mg/kg b.w. in Swiss mice.

Very recently, the potential effects of MWNTs after oral administration were also investigated on pregnant dams and embryo-fetal development in rats.[149] MWNTs were administered to pregnant rats by gavage at 0, 40, 200 and 1000 mg/kg/day. All dams were subjected to Cesarean section on day 20 of gestation, and the fetuses were examined for morphological abnormalities. A decrease in thymus weight was observed in the high dose group in a dose-dependent manner. However, maternal body weight, food consumption, and oxidant-antioxidant balance in the liver were not affected by treatment with MWNTs. No treatment-related differences in gestation index, fetal deaths, fetal and placental weights, or sex ratio were observed between the groups. Morphological examinations of the fetuses demonstrated no significant difference in incidences of abnormalities between the groups.

Intriguingly, it has been reported that CNTs may be involved in oxidative stress with oxidative damage of DNA in the colon mucosa, liver, and lung of rats after oral administration of SWNTs in a dose of 0.064 or 0.64 mg/kg body weight suspended in saline solution or corn oil.[150] Suspensions of particles in saline solution or corn oil yielded a similar extent of genotoxicity. However, corn oil per se generated more genotoxicity than the particles.[150]

3.7. Conclusion

Considered together, the diverging results concerning CNT toxicity highlight the difficulties in evaluating the toxicity of this heterogeneous carbon family. While the toxicity is certainly governed by the state of aggregation, length and stiffness of CNTs, other parameters might be involved. Most of them probably depend of the method of production of the sample, the method of purification and the method of preparation of the tested formulations. As the reactivity and the general behaviour of CNTs in biological media are not completely understood, assessing the safety of these nanoparticles should also include a careful selection of appropriate experimental methods. Thus, more studies are needed in order to determine the safety of CNTs. For the time being, precaution is necessary notably in case of CNT-exposure at workplace.

4. Conclusion

This review devoted to the toxicity studies of fullerenes and carbon nanotubes shows that it is no longer possible to generalize the biological behavior of this heterogeneous family of carbon materials. This underline the irrelevance of generalizing the paradigm of nanoparticle toxicity according to which toxicity depends on sizes whatever the nature of the so-called nanoparticle. In the field of nanomaterials, the dimension is the characterizing parameter but it is not the only relevant one as to what concerns the toxicity of a given material. It is necessary to consider every compound separately in order to avoid any confusion. The number and the nature of involved nanomaterials increases and it is no longer possible to encompass all of them in a sole scheme.[6]

References

1. Available at http://www.nano.gov/about-nni.
2. Kipen, H. M.; Laskin, D. L. *Am. J. Physiol. Lung Cell. Mol. Physiol.* **2005**, *289*, 696.
3. Oberdörster, G.; Oberdörster, E.; Oberdörster, J. *Environ. Health Perspect.* **2005**, *113*, 7.
4. Nelson, M. A.; Domann, F. Ò.; Bowden, G. T.; Hooser, S. B.; Fernando, Q.; Carter, D. E. *Toxicol. Ind. Health* **1993**, *9*, 623.
5. Jensen, A. W.; Wilson, S. R.; Schuster, D. I. *Bioorg. Med. Chem.* **1996**, *4*, 767.
6. Szwarc, H.; Moussa, F. In: R. F. Verner and C. Benvegnu (Eds.). *Handbook on Fullerene: Synthesis, Properties and Applications*, Nova Science, New York, NY, USA, **2011**, p. 405.
7. Baati, T.; Szwarc, H.; Moussa, F. *Recent Patents Nanomed.* **2011**, *1*, 101.
8. Wilson, L. J.; Cagle, D. W.; Thrash, T. P.; Kennel, S. J.; Mirzadeh, S.; Alford, J. M.; Ehrhardt, G. J. *Coord. Chem. Rev.* **1999**, *192*, 199.

9. Tsao, N.; Kanakamma, P.; Luh, T. Y.; Chou, C. K.; Lei, H. Y. *Antimicrob. Agents Chemother.* **1999**, *43*, 2273.
10. Hirsh, A. *The Chemistry of Fullerenes*; 1st edn., George Thieme Verlang: NY, **1994**.
11. Yamakoshi, Y. N.; Yagami, T.; Fukuhara, K.; Sueyoshi, S.; Miyata, N. *J. Chem. Soc. Chem. Commun.* **1994**, *4*, 517.
12. Krusic, P. J.; Waserman, E.; Keizer, P. N.; Morton, J. R.; Preston, K. F. *Science* **1991**, *254*, 1183.
13. Yamago, S.; Tokuyama, H.; Nakamura, E.; Kikuchi, K.; Kananishi, S.; Sueki, K.; Nakahara, H.; Enomoto, S.; Ambe, F. *Chem. Biol.* **1995**, *2*, 385.
14. Boutorine, A. S.; Tokuyama, H.; Takasugi, M.; Isobe, H.; Nakamura, E.; Helene, C. *Angew. Chem., Int. Ed.* **1994**, *33*, 2462.
15. Scrivens, W. A.; Tour, J. M.; Creek, K. E.; Pirisi, L. *J. Am. Chem. Soc.* **1994**, *116*, 4517.
16. Zakharenko, L. P.; Zakharov, I. K.; Lunegov, S. N.; Nikiforov, A. N. *Doklady Biolog. Sci.* **1994**, *335*, 153.
17. Moussa, F.; Chrétien, P.; Dubois, P.; Chuniaud, L.; Dessante, M.; Trivin, F.; Sizaret, P. Y.; Agafonov, V.; Céolin, R.; Szwarc, H.; Greugny, V.; Fabre, C.; Rassat, A. *Fullerene Sci. Technol.* **1995**, *3*, 333.
18. Baierl, T.; Seidel, A. *Fullerenes Sci. Technol.* **1996**, *5*, 1073.
19. Moussa, F.; Trivin, F.; Céolin, R.; Hadchouel, M.; Sizaret, P. Y.; Greugny, V.; Fabre, C.; Rassat, A.; Szwarc, H. *Fullerenes Sci. Technol.* **1996**, *4*, 21.
20. Moussa, F.; Pressac, M.; Hadchouel, M.; Sizaret, P. Y.; Céolin, R.; Szwarc, H. In: Kadish, K. and Ruoff, R. (Eds.). *Fullerenes. Proc. Series of the 191st Meeting of The Electrochem. Soc.* Pennington, NJ, USA, **1997**, *97–42*, 332–336.
21. Gharbi, N.; Pressac, M.; Hadchouel, M.; Szwarc, H.; Wilson, S. R.; Moussa, F. *Nano Lett.* **2005**, *5*, 2578.
22. Zakharenko, L. P.; Zakharov, I. K.; Vasiunina, E. A.; Karamysheva, T. V.; Danilenko, A. M.; Nikiforov, A. A. *Genetika* **1997**, *33*, 405.
23. Wainwright, M.; Falih, A. M. *Microbiology* **1997**, *143*, 2097.
24. Moussa, F.; Chrétien, P.; Pressac, M.; Trivin, F.; Szwarc, H.; Céolin, R. *Fullerenes Science and Technology* **1997**, *5*, 503.
25. Moussa, F.; Roux, S.; Pressac, M.; Genin, E.; Hadchouel, M.; Trivin, F.; Rassat, A.; Céolin, R.; Szwarc, H. *New J. Chem.* **1998**, *32*, 989.
26. Chiron, J. P.; Lamandé, J.; Moussa, F.; Trivin, F.; Céolin, R. *Ann. Pharm. Fr.* **2000**, *58*, 170.
27. Mori, T.; Takada, H.; Ito, S.; Matsubayashi, K.; Miwa, N.; Sawaguchi, T. *Toxicology* 2006, *225*, 48.
28. Ungurunasu, C.; Airinei, A. *J. Med. Chem.* **2000,** *43*, 3186.
29. Satoh, M.; Matsuo, K.; Takanashi, Y.; Takayanagi, I. *Gen. Pharmac.* **1995**, *26*, 1533.
30. Tsuchiya, T.; Oguri, I.; Yamakoshi, Y. N.; Miyata, N. *FEBS Lett.,* **1996**, *393*, 139.
31. Oberdorster, E. *Environ. Health Perspect.* **2004**, *112*, 1058.
32. Sayes, C. M.; Fortner, J. D.; Guo, W.; Lyon, D.; Boyd, A. M.; Ausman, K. D.; Tao, Y. J.; Sitharaman, B.; Wilson, L. J.; Hughes, J. B.; West, J. L.; Colvin, V. L. *Nano Lett.* **2004**, *4*, 1881.
33. Feder, B. J. *New York Times* **2004,** 29 March. Available: http://www.wisdomportal.com/NYTimes-Mar2004.html.
34. Rittner, M. Confusion in the mass media; *Nanoparticles News* April **2004**.

35. Sayes, C. M.; Gobin, A. M.; Ausman, K. D.; Mendez, J.; West, J. L.; Colvin, V. L. *Biomaterials* **2005**, *26*, 7587.
36. Isakovic, A.; Markovic, Z.; Todorovic-Markovic, B.; Nikolic, N.; Vranjes-Djuric, S.; Mirkovic, M.; Dramicanin, M.; Harhaji, L.; Raicevic, N.; Nikolic, Z.; Trajkovic, V. *Toxicol. Sci.* **2006**, *91*, 173.
37. Oberdorster, E.; Zhu, S.; Blickley, M.; McClellan,-Green, P.; Haasch, M. L. *Carbon* **2006**, *44*, 1112.
38. Lovern, S. B.; Klaper, R. *Environ. Toxicol. Chem.* **2006**, *25*, 1132.
39. Rajagopalan, P.; Wudl, F.; Schinazi, R. F.; Boudinot F. D. *Antimicrob. Agents Chemother.* **1996**, *40*, 2262.
40. Schuster, D. I.; Wilson, S. R.; Schinagi, R. F. *Bioorg. Med. Chem. Lett.* **1996**, *6*, 1253.
41. Gharbi, N; Pressac, M.; Tomberli, V.; Fabre, P.; Ceolin, R.; Szwarc, H.; Moussa, F. *Proc. Electrochem. Soc.* **2000**, *9*, 240.
42. Dugan, L. L.; Lovett, E. G.; Quick, K. L.; Hardt, J. I. United States Patent US 2003/0162837 A1.
43. Rancan, F.; Rosan, S.; Boehm, F.; Cantrell, A.; Brellreich, M.; Schoenberger, H.; Hirsch, A.; Moussa, F. *J. Photochem. Photobiol. B* **2002**, *67*, 157.
44. Bosi, S.; Feruglio, L.; Da Ros, T.; Spalluto, G.; Gregoretti, B.; Terdoslavich, M.; Decorti, G.; Passamnti, S.; Moro, S.; Prato, M. *J. Med. Chem.* **2004**, *47*, 6711.
45. Yamawaki, H.; Iwai, N. *Am. J. Physiol. Cell. Physiol.* **2006**, *290*, C1495.
46. Colvin, V.; Sayes, C. M.; Ausman, K. D.; Fortner, J.; Lyons, D. [Abstract]. In: Proceedings of the 227th ACS National Meeting, Anaheimn, CA, 28 March–1 April 2004. IEC 18. Washington, DC: American Chemical Society. **2004** Available: http://oasys2.confex.com/acs/227nm/techprogram/ P721792.HTM.
47. Andrievsky, G.; Klochkov V.; Derevyanchenko L. *Fullerenes, Nanotubes, Carbon Nanostruct.* **2005**, *13*, 1.
48. Avdeev, M. V.; Khokhryakov, A. A.; Tropin, T. V.; Andrievsky, G. V.; Klochkov, V. K.; Derevyanchenko, L. I.; Rosta, L.; Garamus, V. M.; Priezzhev, V. B.; Korobov, M. V.; Aksenov, V. L. *Langmuir* **2004**, *20*, 4363.
49. Brant, J.; Lecoanet, H.; Hotze, M.; Wiesner, M. *Environ. Sci. Technol.* **2005**, *39*, 6343.
50. Zha, Q. Q.; Wei, X. W.; Sun, J. *et al. Proc. 7th Biennial International Workshop on Fullerenes and Atomic Clusters*, St. Petersburg, Russia, June 27–July 1, **2005**; Taylor & Francis: Abingdon, UK, **2006**.
51. Isakovic, A.; Markovic, Z.; Nikolic, N.; Todorovic-Markovic, B.; Vranjes-Djuric, S.; Harhaji, L.; Raicevi, N.; Romcevic, N.; Vasiljevic-Radovic, D.; Dramicanin, M.; Traikovic, V. *Biomaterials* **2006**, *27*, 5049.
52. Deguchi, S.; Mukai, S.; Tsudome, M.; Horikoshi, K. *Adv. Mat.* **2006**, *18*, 729.
53. Jia, G.; Wang, H.; Yan, L.; Wang, X.; Pei, R. J.; Yan, T.; Zhao, Y. L.; Guo, X. B. *Environ. Sci. Technol.* **2005**, *39*, 1378.
54. Fiorito, S.; Serafino, A.; Andreola, F.; Bernier, P. *Carbon* **2006**, *44*, 1100.
55. Brant, J. A.; Labille, J.; Bottero, J. Y.; Wiesner, M. R. *Langmuir* **2006**, *22*, 3878.
56. Sayes, C. M.; Marchione, A. A.; Reed, K. L.; Warheit, D. B. *Nano Lett.* **2007**, *7*, 2399.
57. Johnston, H. J.; Hutchison, G. R.; Christensen, F. M.; Aschberger, K.; Stone, V. *Toxicol. Sci.* **2010**, *114*, 162.
58. Henry, T. B.; Menn, F. M.; Fleming, J. T.; Wilgus, J.; Compton, R. N.; Sayler, G. S. *Environ. Health Perspect.* **2007**, *115*, 1059.

59. Zhang, B.; Cho, M.; Fortner, J. D.; Lee, J.; Huang, C. H.; Hughes, J. B.; Kim, J. H. *Environ. Sci. Technol.* **2009**, *43*, 108.
60. Spohn, P.; Hirsch, C.; Hasler, F.; Bruinink, A.; Krug, H. F.; Wick, P. *Environ. Pollut.* **2009,** *157*, 1134.
61. Kovochich, M.; Espinasse, B.; Auffan, M.; Hotze, E. M.; Wessel, L.; Xia, T.; Nel, A. E.; Wiesner, M. R. *Environ. Sci. Technol.* **2009**, *43*, 6378.
62. Xia, X. R.; Monteiro-Riviere, N. A.; Riviere, J. E. *Toxicol. Lett.* **2010**, *197*, 128.
63. Hadduck, A. N.; Jindagolla, V.; Contreras, A. E.; Li, Q.; Bakalinsky, A. T. *Appl. Environ. Microbiol.* **2010**, *76*, 8239.
64. Han, B.; Karim, M. N. *Scanning* **2008**, *30*, 213.
65. Zogovic, N. S.; Nikolic, N. S.; Vranjes-Djuric, S. D.; Harhaji, L. M.; Vucicevic, L. M.; Janjetovic, K. D.; Misirkic, M. S.; Todorovic-Markovic, B. M.; Markovic, Z. M.; Milonjic, S. K.; Trajkovic, V. S. *Biomaterials* **2009**, *30*, 6940.
66. Dugan, L. L.; Gabrielsen, J. K.; Yu, S. P. *Neurobiology of Disease* **1996**, *3*, 129.
67. Dugan, L. L.; Lovett, E. G.; Quick, J.; Lotharius, J.; Lin, T. T.; O'Malley, K. L. *Parkinsonism and Related Disorders* **2001**, *7*, 243.
68. Dugan, L. L.; Turetsky, D. M.; Du, C.; Lobner, D.; Wheeler, M.; Almli, C. R.; Shen, C. K.F.; Luh, T. Y.; Choi, D. W.; Lin, T. S. *PNAS* **1997**, *94*, 9434.
69. Lin, Y. L.; Lei, H. Y.; Wen, Y. Y.; Luh, T. Y.; Chou, C. K.; Liu, H. S. *Virology* **2000**, *275*, 258.
70. Straface, E.; Natalini, B.; Monti, D.; Franceschi, C.; Schettini, G.; Bisaglia, M.; Fumelli, C.; Pincelli, C.; Pellicciari, R.; Malorni, W. *FEBS Lett.* **1999**, *454*, 335.
71. Monti, D.; Moretti, L.; Salvioli, S.; Straface, E.; Malomi, W.; Pellicciari, R.; Scettini, G.; Bisaglia, M.; Pincelli, C.; Fumelli, C.; Bonate, M.; Franceschi, C. *Biochem. Biophys. Res. Commun.* **2000**, *277*, 711.
72. Lin, A. M.; Chyi, B. Y.; Wang, S. D.; Yu, H. H.; Kanakamma, P. P.; Luh, T. Y.; Chou, C. K.; Ho, L. T. *J. Neurochem.* **1999**, *72*, 1634.
73. Tsao, N.; Luh, T. Y.; Chou, C. K.; Wu, J. J.; Lin, Y. S.; Lei, K. Y. *Antimicrob. Agents Chemother.* **2001**, *45*, 1788.
74. Tsao, N.; Luh, T. Y.: Chou, C. K.; Chang, T. Y.; Wu, J. J.; Liu, C. C.; Lei, H. Y. *J. Antimicrob. Chemother.* **2002**, *49*, 641.
75. Sijbesma, R.; Srdanov, G.; Wudl. F.; Castoro, J. A.; Wilkins, C.; Friedman, S. H.; Decamp, D. L.; Kenyon, G. L. *J. Am. Chem. Soc.* **1993**, 115, 6510.
76. Schinazi, R. F.; McMillan, A.; Juodawlkis, A. S.; Pharr, J.; Sijbesma, R.; Srdanov, G.; Hummelen, J.-C.; Boudinot, F. D.; Hill, C. L.; Wudl, F. *Proc. Electrochem. Soc.* **1994**, *94*, 689.
77. Yamakoshi, Y.; Yagami, T.; Sueyoshi, S.; Miyata, N. *J. Org. Chem.* **1996**, *61*, 7236.
78. Schinazi, R. F.; Sijbesma, R.; Srdanov, G.; Hill, C. L.; Wudl, F. *Antimicrob. Agents Chemother.* **1993**, *37*,1707.
79. Huang, H. M.; Ou, H. C.; Hsieh, S. J.; Chiang, L. Y. *Life Sci.* **2000**, *66* ,1525.
80. Bisaglia, M.; Natalini, B.; Pellicciari, R.; Straface, E.; Malomi, W.; Monti, D.; Franceschi, C.; Schettini, G. *J. Neurochem.* **2000**, *74*, 1197.
81. Rancan, F.; Helmreich, M.; Molich, A.; Jux, N.; Hirsch, A.; Roder, B.; Witt, C.; Bohm, F. *J. Photochem. Photobiol. B* **2005**, *80*, 1.
82. Chueh, S. C.; Lai, M. K.; Chen, S. C.; Chiang, L. Y.; Chen, W. C. *Transplant. Proc.* **1997**, *29*, 1313.

83. Klaper, R; Crago, J.; Barr, J.; Arndt, D.; Setyowati, K.; Chen, *J. Environ. Pollut.* **2009**, *157*, 1152.
84. Gao, J.; Wang, Y.; Folta, K. M.; Krishna, V.; Bai, W.; Indeglia, P.; Georgieva, A.; Nakamura, H.; Koopman, B.; Moudgil, B. *PLoS One* **2011**, *6*, 1.
85. Quick, K. L.; Ali, S. S.; Arch, R.; Xiong, C.; Wozniak, D.; Dugan, L. L. *Neurobiol. Aging* **2009**, *29*, 117.
86. Gao, J.; Wang, H. L.; Shreve, A.; Iyer, R. *Toxicol. Appl. Pharmacol.* **2010**, *244*, 130.
87. Henry, T. B.; Petersen, E. J.; Compton, R. N. *Curr. Opin. Biotechnol.* **2011**, *22*, 533.
88. Park, J. W.; Henry, T. B.; Ard, S.; Menn, F. M.; Compton, R. N.; Sayler, G. S. *Nanotoxicology* **2011**, *5*, 406.
89. Baun, A.; Sorensen, S. N.; Rasmussen, R. F.; Hartmann, N. B.; Koch, C. B. *Aquat. Toxicol.* **2008**, *86*, 379.
90. Pan, B.; Lin, D.; Mashayekhi, H.; Xing, B. *Environ. Sci. Technol.* **2008**, *42*, 5480.
91. Ma, X. M.; Wang, C. Systems *Environ. Eng. Sci.* **2010**, *27*, 989.
92. Hou, W. C.; Jafvert, C. T. *Environ. Sci. Technol.* **2009**, *43*, 362.
93. Lee, J.; Cho, M.; Fortner, J. D.; Hughes, J. B.; Kim, J. H. *Environ. Sci. Technol.* **2009**, *43*, 4878.
94. Hou, W. C.; Jafvert, C. T. *Environ. Sci. Technol.* **2009**, *43*, 5257.
95. Hwang, Y. S.; Li, Q. L. *Environ. Sci. Technol.* **2010**, *44*, 3008.
96. Gelca, R.; Surowiec, K.; Anderson, T. A.; Cox, S. B. *J. Nanosci. Nanotechnol.* **2011**, *11*, 1225.
97. Mukherji, S. T.; Leisen, J.; Hughes, J. B. *Chemosphere* **2011**, *84*, 390.
98. Li, D.; Fortner, J. D.; Johnson, D. R.; Chen, C.; Li, Q. L.; Alvarez, P. J. J. *Environ. Sci. Technol.* **2010**, *44*, 9170.
99. Available at http://www.drugs.com/fda-approval-process.html.
100. Szwarc, H.; Moussa, F. *J. Nanosci. Lett.* **2011**, *1*, 61.
101. Bianco, A.; Kostarelos, K.; Prato, M. *Curr. Opin. Chem. Biol.* **2005**, *9*, 674.
102. Dresselhaus, M.; Dresselhaus, G.; Charlier, J.; Hernandez, E. *Philos. Trans. R. Soc. London, A* **2004**, *362*, 2065.
103. Sinha, N; Yeow, J. T. W. *IEEE Trans. Nano Biosci.* **2005**, *4*, 180.
104. Ziegler, K. J.; Gu, Z.; Peng, H.; Flor, E. L.; Hauge, R. H.; Smalley, R. E. *J. Am. Chem. Soc.* **2005**, *127*, 1541.
105. Service, R. *Science* **1998**, *281*, 941.
106. Kolosnjaj, J.; Szwarc, H.; Moussa, F. *Adv. Exp. Med. Biol.* **2007**, *620*, 181.
107. Casey, A.; Herzog, E.; Davoren, M.; Lyng, F.; Byrne, H.; Chambers, G. *Carbon* **2007**, *45*, 1425.
108. Kroll, A.; Pillukat, M. H.; Hahn, D.; Schnekenburger, J. *Eur. J. Pharm. Biopharm.* **2009**, *72*, 370.
109. Huczko, A.; Lange, H. *Fullerene Sci. Technol.* **2001**, *9*, 247.
110. Ema, M.; Matsuda, A.; Kobayashi, N.; Naya, M.; Nakanishi, J. *Regul. Toxicol. Pharmacol.* **2011,** *61*, 276.
111. Maynard, A.; Baron, P.; Foley, M.; Shvedova, A.; Kisin, E.; Castranova, V. *J. Toxicol. Environ. Health Part A* **2004**, *67*, 87.
112. Lam, C. W.; James, J. T.; McCluskey, R.; Hunter, R. L. *Toxicol. Sci.* **2004**, *77*, 126.
113. Warheit, D. B.; Laurence, B.; Reed, K. L.; Roach, D.; Reynolds, G.; Webb, T. *Toxicol. Sci.* **2004**, *77*, 117.

114. Muller, J.; Huaux, F.; Moreau, N.; Misson, P.; Heilier, J. F.; Delos, M.; Arras, M.; Fonseca, A.; Nagy, J. B.; Lison, D. *Toxicol. Appl. Pharmacol.* **2005**, *207*, 221.
115. Shvedova, A. A.; Kisin, E. R.; Mercer, R.; Murray, A. R.; Johnson, V. J.; Potapovich, A. I.; Tyurina, Y. Y.; Gorelik, O.; Arepalli, S.; Schwegler-Berry, D.; Hubbs, A. F.; Antonini, J.; Evans, D. E.; Ku, B. K.; Ramsey, D.; Maynard, A.; Kagan, V. E.; Castranova, V.; Baron, P. *Am. J. Physiol. Lung Cell. Mol. Physiol.* **2005**, *289*, L698.
116. Muller, J.; Huaux, F.; Fonseca, A.; Nagy, J. B.; Moreau, N.; Delos, M.; Raymondo-Pinero, E.; Beguin, F.; Kirsch-Volders, M.; Fenoglio, I.; Fubini, B.; Lison, D. *Chem. Res. Toxicol.* **2008**, *21*, 1698.
117. Mutlu, G. M.; Budinger, G. R. S.; Green, A. A.; Urich, D.; Soberanes, S.; Chiarella, S. E.; Alheid, G. F.; McCrimmon, D. R.; Szleifer, I.; Hersam, M. C. *Nano Lett.* **2010**, *10*, 1664.
118. Mercer, R. R.; Scabilloni, J.; Wang, L.; Kisin, E.; Murray, A. R.; Schwegler-Berry, D.; Shvedova, A. A.; Castranova, V. *Am. J. Physiol. Lung Cell. Mol. Physiol.* **2008**, *294*, L87.
119. Kobayashi, N.; Naya, M.; Ema, M.; Endoh, S.; Maru, J.; Mizuno, K.; Nakanishi, J. *Toxicology* **2010**, *276*, 143.
120. Morimoto, Y.; Hirohashi, M.; Ogami, A.; Oyabu, T.; Myojo, T.; Todoroki, M.; Yamamoto, M.; Hashiba, M.; Mizuguchi, Y.; Lee, B. W.; Kuroda, E.; Shimada, M.; Wang, W. N.; Yamamoto, K.; Fujita, K.; Endoh, S.; Uchida, K.; Kobayashi, N.; Mizuko, K.; Inada, M.; Tao, H.; Nakazato, T.; Nakanishi, J.; Tanaka, I. *Nanotoxicology* **2011**, doi:10.3109/17435390.2011.594912.
121. Kane, A. B.; Hurt, R. H. *Nature Nanotechnol.* **2008**, *3*, 378.
122. Donaldson, K.; Poland, C. A. *Nature Nanotechnol.* **2009**, *4*, 708.
123. Donaldson, K.; Murphy, F. A.; Duffin, R.; Poland, C. A. *Particle Fibre Toxicol.* **2010**, *7*, Article Number 5.
124. Lai-Fook, S. J. *Physiolog. Rev.* **2004**, *84*, 385.
125. Balkwill, F.; Mantovani, A. *The Lancet* **2001**, *357*, 539.
126. Ryman-Rasmussen, J. P.; Cesta, M. F.; Brody, A. R.; Shipley-Phillips, J. K.; Everitt, J. I.; Tewksbury, E. W.; Moss, O. R.; Wong, B. A.; Dodd, D. E.; Andersen, M. E. *Nature Nanotechnol.* **2009**, *4*, 747.
127. Porter, D. W.; Hubbs, A. F.; Mercer, R. R.; Wu, N.; Wolfarth, M. G.; Sriram, K.; Leonard, S.; Battelli, L.; Schwegler-Berry, D.; Friend, S. *Toxicology* **2010**, *269*, 136.
128. Mercer, R. R.; Hubbs, A. F.; Scabilloni, J. F.; Wang, L.; Battelli, L. A.; Schwegler-Berry, D.; Castranova, V.; Porter, D. W. *Particle Fibre Toxicol.* **2010**, *7*, 28.
129. Murphy, F. A.; Poland, C. A.; Duffin, R.; Al-Jamal, K. T.; Ali-Boucetta, H.; Nunes, A.; Byrne, F.; Prina-Mello, A.; Volkov, Y.; Li, S.; Mather, S. J.; Bianco, A.; Prato, M.; Macnee, W.; Wallace, W. A.; Kostarelos, K.; Donaldson, K. *Am. J. Pathol.* **2011**, *178*, 2587.
130. Sato, Y.; Yokoyama, A.; Shibata, K.; Akimoto, Y.; Ogino, S.; Nodasaka, Y.; Kohgo, T.; Tamura, K.; Akasaka, T.; Uo, M.; Motomiya, K.; Jeyadevan, B.; Ishiguro, M.; Hatakeyama, R.; Watari, F.; Tohji, K. *Mol. Biosyst.* **2005**, *1*, 176.
131. Koyama, S.; Endo, M.; Kim, Y. A.; Hayashi, T.; Yanagisawa, T.; Osaka, K.; Koyama, H.; Haniu, H.; Kuroiwa, N. *Carbon* **2006**, *44*, 1079.
132. Abu-Hijleh, M. F.; Habbal, O. A.; Moqattash, S. T. *Journal of Anatomy* **1995**, *18*, 453.
133. Hartman, K.; Kolosnjaj, J.; Gharbi, N.; Boudjemaa, S; Wilson, L. J.; Moussa, F. *211th Meeting of The Electrochemical Society*, Chicago, USA, **2007,** May 6–10

134. Takagi, A.; Hirose, A.; Nishimura, T.; Fukumori, N.; Ogata, A.; Ohashi, N.; Kitajima S.; Kanno, J. *J. Toxicolog. Sci.* **2008**, *33*, 105.
135. Ichihara, G.; Castranova, V.; Tanioka, A.; Miyazawa, K. *J. Toxicolog. Sci.* **2008**, *33*, 381.
136. Takagi, A.; Hirose, A.; Nishimura, T.; Fukumori, N.; Ogata, A.; Ohashi, N.; Kitajima S.; Kanno, J. *J. Toxicolog. Sci.* **2008**, *33*, 382.
137. Muller, J.; Delos, M.; Panin, N.; Rabolli, V., Huaux, F.; Lison, D. *Toxicolog. Sci.* **2009**, *110*, 442.
138. Bignon, J.; Brochard, P.; Brown, R.; Davis, J.; Vu, V.; Gibbs, G.; Greim, M.; Oberdörster, G.; Sebastien, P. *Annals Occup. Hygiene* **1995**, *39*, 89.
139. Sakamoto, Y.; Nakae, D.; Fukumori, N.; Tayama, K.; Maekawa, A.; Imai, K.; Hirose, A.; Nishimura, T.; Ohashi, N.; Ogata, A. *J. Toxicolog. Sci.* **2009**, *34*, 65.
140. Moore, A. J.; Parker, R. J.; Wiggins, J. *Orphanet. J. Rare Dis.* **2008**, *3*, 34.
141. Poland, C. A.; Duffin, R.; Kinloch, I.; Maynard, A.; Wallace, W. A. H.; Seaton, A.; Stone, V.; Brown, S.; MacNee, W.; Donaldson, K. *Nature Nanotechnol.* **2008**, *3*, 423.
142. Kolosnjaj-Tabi, J.; Hartman, K. B.; Boudjemaa, S.; Ananta, J. S.; Morgant, G.; Szwarc, H.; Wilson, L. J.; Moussa, F. *ACS Nano* **2010**, *4*, 1481.
143. Schipper, M. L.; Nakayama-Ratchford, N.; Davis, C. R.; Kam, N. W. S.; Chu, P.; Liu, Z.; Sun, X.; Dai, H.; Gambhir, S. S. *Nature Nanotechnol.* **2008**, *3*, 216.
144. Liu, Z.; Davis, C.; Cai, W.; He, L.; Chen, X.; Dai, H. *Proc. Nat. Acad. Sci. USA* **2008**, *105*, 1410.
145. Yang, S. T.; Wang, X.; Jia, G.; Gu, Y.; Wang, T.; Nie, H.; Ge, C.; Wang, H.; Liu, Y. *Toxicol. Lett.* **2008**, *181*, 182.
146. Pietroiusti, A.; Massimiani, M.; Fenoglio, I.; Colonna, M.; Valentini, F.; Palleschi, G.; Camaioni, A.; Magrini, A.; Siracusa, G.; Bergamaschi, A.; Sgambato, A.; Campagnolo, L. *ACS Nano* **2011**, *5*, 4624.
147. Lacerda, L.; Ali-Boucetta, H.; Herrero, M. A.; Pastorin, G.; Bianco, A.; Prato, M.; Kostarelos, K. *Nanomedicine* **2008**, *3*, 149.
148. Ji, Z.; Zhang, D.; Li, L.; Shen, X.; Deng, X.; Dong, L.; Wu, M.; Liu, Y. *Nanotechnology* **2009**, *20*, 445101.
149. Lim, J. H.; Kim, S. H.; Shin, I. S.; Park, N. H.; Moon, C.; Kang, S. S.; Kim, S.H.; Park SC; Kim JC. *Birth Defects Res., Part B* **2011**, *92*, 69.
150. Folkmann, J. K.; Risom, L.; Jacobsen, N. R.; Wallin, H.; Loft, S.; Muller, P. *Environ. Health Perspect.* **2009**, *117*, 703.

Published in final edited form as:
Carbon N Y. 2007 August ; 45(9): 1891–1898.

In vivo evaluation of carbon fullerene toxicity using embryonic zebrafish

Crystal Y. Usenko, **Stacey L. Harper**, and **Robert L. Tanguay***
Department of Environmental and Molecular Toxicology and the Marine and Freshwater Biomedical Sciences Center; Oregon State University, Corvallis, OR, 97331.

Abstract

There is a pressing need to develop rapid whole animal-based testing assays to assess the potential toxicity of engineered nanomaterials. To meet this challenge, the embryonic zebrafish model was employed to determine the toxicity of fullerenes. Embryonic zebrafish were exposed to graded concentrations of fullerenes [C_{60}, C_{70}, and $C_{60}(OH)_{24}$] during early embryogenesis and the resulting morphological and cellular responses were defined. Exposure to 200 μg/L C_{60} and C_{70} induced a significant increased in malformations, pericardial edema, and mortality; while the response to $C_{60}(OH)_{24}$ exposure was less pronounced at concentrations an order of magnitude higher. Exposure to C_{60} induced both necrotic and apoptotic cellular death throughout the embryo. While $C_{60}(OH)_{24}$ induced an increase in embryonic cellular death, it did not induce apoptosis. Our findings concur with results obtained in other models indicating that $C_{60}(OH)_{24}$ is significantly less toxic than C_{60}. These studies also suggest that that the embryonic zebrafish model is well-suited for the rapid assessment of nanomaterial toxicity.

1. Introduction

Unique physicochemical properties of nanomaterials make them attractive for a wide range of novel applications in the electronics, healthcare, cosmetics, technologies and engineering industries [1–6]. The rapid discovery and development of new nanomaterials will undoubtedly increase the potential for human and environmental exposures [7]. Lack of toxicological data on nano-sized materials makes it difficult to determine if there is a risk associated with nanomaterial exposure. Timely evaluation of nanomaterial toxicity will provide this critical data, improve public trust of the nanotechnology industry, assist regulators in determining environmental and health risks of commercial nanomaterials, and provide industry with information to direct the development of safer nanomaterials and products [8–10]. Thus, there is an immediate need to develop rapid, relevant and efficient testing strategies to assess emerging materials of concern.

Numerous biological models have been used for toxicological assessments. *In vitro* techniques, such as cell culture, are often preferred because they are rapid, efficient and cost effective. While these studies are useful, direct translation to a human health risk is often difficult to infer. *In vivo* (whole animal) studies, on the other hand, can provide improved prediction of the biological response in intact systems. Since *in vivo* studies often employ rodent models;

*Corresponding Author: Robert L. Tanguay, Ph.D., Department of Environmental and Molecular Toxicology, Environmental Health Sciences Center, Marine and Freshwater Biomedical Sciences Center, Oregon State University, Corvallis, OR, 97331-7301, 541-737-6514 (voice), 541-737-7966 (fax), robert.tanguay@oregonstate.edu.

assessments are generally expensive, time-consuming and require extensive facilities for housing experimental animals. Cost, labor, time and infrastructure requirements can be significantly reduced by replacing the traditional rodent model with the embryonic zebrafish model. Embryonic zebrafish are a well-established model for studying basic developmental biological processes (reviewed in 11) and for toxicological assessments [12–14]. Zebrafish are vertebrates that share many cellular, anatomical and physiological characteristics with other vertebrates. Their small size, rapid development and short life cycle make zebrafish logistically attractive for rapidly evaluating integrated system effects [15,16].

Research presented herein examines the utility of embryonic zebrafish as a model for rapid assessment of nanomaterial toxicity. For proof-of-concept, three carbon fullerenes varying in size and surface functionalization [C_{60}, C_{70}, and $C_{60}(OH)_{24}$] were tested in the system and the results were compared to available nanotoxicity data obtained using different methods, test systems and routes of exposure. Carbon fullerenes were chosen because much nanotechnology attention, particularly nanotoxicological evaluations, has focused on carbon-based nanomaterials. C_{60}, otherwise known as “bucky balls” or “Buckminster fullerenes”, have been proposed for use in fuel cells, groundwater remediation, cosmetics and drug delivery. C_{70}, a common by-product of C_{60} synthesis, is likely to be found in products containing C_{60} unless extensive purification steps are taken. The lack of solubility of C_{60} in water has limited its research in biological systems [17]. However, surface functionalization with hydroxyl groups produces $C_{60}(OH)_{24}$, which is readily soluble in water. Similarly to C_{60}, hydroxylated C_{60} have been proposed for use in groundwater remediation and drug delivery [2,17,18]. Numerous reports suggest that differences in size and surface functionalization among the three fullerenes tested are reflected in their relative toxic potential [19–21].

2. Methods

2.1 Preparation of Solutions

Fullerenes C_{60} and C_{70} were obtained from Sigma Aldrich, WI (98+% and 99% purity respectively) and hydroxylated C_{60} was obtained from MER Corporation, AZ (99.98% purity). The purity of the materials used in these studies was not tested and assumed to be as stated by the manufacturer (2% and 1% higher order fullerene impurities in C_{60} and $C_{70,}$ respectively; 0.02% water and sodium impurities in $C_{60}(OH)_{24}$). Due to the insolubility of C_{60} and C_{70} in water, each was sonicated to form a uniform suspension in 100% dimethyl sulfoxide (DMSO). Stock solution of 50 ppm (C_{60} and C_{70}) and 500 ppm [$C_{60}(OH)_{24}$] were based on the maximum achievable concentration of nanomaterials to dissolve in DMSO after sonication. The highest exposure concentration was made by adding 1% of the DMSO-fullerene solution to fish water. Previous evaluations in our laboratory have demonstrated no adverse biological effect of DMSO at this concentration; however, use of a solvent will likely increase the uptake of material into the animal. It is important to point out that our studies were specifically designed to evaluate interactions between the nanomaterial and the biological system, not to mimic, for example, an environmental exposure scenario. Dilutions were made at 100 ppb increments with concentrations ranging between 100 and 500 ppb for C_{60} and C_{70} and 500 to 5000 ppb for $C_{60}(OH)_{24}$. C_{60} and C_{70} solutions were sonicated for 1.5 hours to ensure a uniform concentration and size distribution. Only 5 minutes of sonication was necessary to uniformly distribute $C_{60}(OH)_{24}$ in solution. Particle size distributions obtained using photon correlation spectroscopy on an N4 Plus submicron particle sizer (Beckman Coulter, Fullerton, CA) are indicated in Figure 1.

2.2 Exposure Protocol

Embryonic zebrafish were obtained from an AB strain of zebrafish (*Danio rerio*) reared in the Sinnhuber Aquatic Research Laboratory (SARL) at Oregon State University. Adults were kept

at standard laboratory conditions of 28°C on a 14h light/10h dark photoperiod in fish water (FW) consisting of reverse osmosis water supplemented with a commercially available salt solution (0.6% Instant Ocean®). Zebrafish were group spawned and embryos were collected and staged as described by Kimmel et al [22]. To increase bioavailability, the chorion, an acellular envelope surrounding the embryo, was removed via enzymatic reaction with pronase prior to exposure. Briefly, embryos at 24 hours post fertilization (hpf) were placed in 25 ml of FW with 50 μl of 50 mg/ml pronase for 10 minutes. Embryos were then rinsed with pure FW for 10 minutes prior to the initiation of nanomaterial exposure. Dechorionated embryos were immediately transferred to individual wells of a 96-well plate with 100 μl of prepared nanomaterial solution. Control animals were exposed to vehicle (1% DMSO) only. Non-treated animals (embryos grown in pure FW with the chorion intact) were retained to ensure embryo quality was good. The static nanomaterial exposure continued in sealed plates until 96 hpf, and the exposure solutions were changed every 24 hours. At 96 hpf, the embryos were rinsed and raised in pure FW. Each individual embryo was scored for morphohological malformations and developmental delays daily for five days. The cumulative mortality rates were graphed and analyzed to estimate the lethal concentration to cause 50% embryonic mortality (LC_{50}).

2.3 Cellular Death Assays

To determine if *in vivo* fullerene exposures induced inappropriate cellular death, two independent cellular death assays were exploited. Cell death was detected in live embryos using acridine orange staining, a nucleic acid selective metachromatic dye that interacts with DNA and RNA by intercalation or electrostatic attractions. Acridine orange stains cells with disturbed plasma membrane permeability so it preferentially stains necrotic or very late apoptotic cells. Dechorionated embryos were exposed to carbon fullerenes at 24 hpf and were analyzed for cellular death at 36 hpf. The 36 hpf time point of assessment was selected because at this developmental stage, there were no overt morphological signs of toxicity. Embryos were rinsed with FW and then incubated in 100 μl of 5μg/ml acridine orange for one hour in the dark at 28 °C. Embryos were rinsed again with FW, mounted in low melt agarose (1% w/v, Promega, Madison, WI) and imaged using an Axiovert 200M Zeiss microscope (Carl Zeiss International, Germany) with a 546 nm filter and AxioVision software (Carl Zeiss International, Germany). For each captured image, the initial focal plane was the otolith. A 50 member z-series was collected and merged into one plane corresponding to approximately 300 micron thick section of the embryo. Whole-embryo fluorescense was measured and quantified using ImagePro Plus software (Media Cybernetics, Inc., Silver Spring, MD).

To more specifically quantify cellular death due to apopotosis, the terminal deoxynucleotidyl transferase (TdT)-mediated dUTP nick end labeling (TUNEL) assay was performed on whole mounted 36 hpf embryos exposed beginning at 24 hpf. The TUNEL assay fluorescently labels the blunt ends of double-stranded DNA breaks which are indicative of programmed cell death (apoptosis). Embryos were fixed overnight in 4% paraformaldehyde and stored in phosphate buffered saline (PBS) + 0.01% sodium azide at 4°C until analysis. Embryos were incubated in proteinase K (1 mg/ml) for 30 minutes at 37°C to permeabolize the tissue. The permeabolized embryos were rinsed in PBS and incubated in 25 μl of 1X TTase buffer (Roche Diagnostics Corp., Indianapolis, IN), 25 mM $CoCl_2$, and dH_2O (sterile H_2O) for 15 minutes at 37°C. Embryos were then transferred to a reaction solution (10 μl 5X TTase buffer, 4 μl 25 mM $CoCl_2$, 0.2 μl FL-dUTP, 0.25 μl TTase enzyme and 35.6 μl dH_2O) on ice, in the dark, for 60 minutes and incubated an additional 60 minutes in the dark at 37°C. Embryos were washed 3 times in PBS, mounted in 50% glycerol and analyzed on the fluorescent microscope (488 nm) as described for the acridine orange assay.

2.4 Statistics

All statistics were compiled using SigmaStat and plotted using Sigma Plot (SPSS Inc, Chicago, IL). Fischer's exact test was used to determine significant difference between control and treated groups ($p<0.05$). All exposure groups consisted of 24 individually exposed embryos (N=24) unless otherwise noted with 80% confidence of significant difference. LC_{50} was calculated using probit and sigmoidal regression analyses. Significant difference from control for cell death assays was determined using one-way ANOVA ($p<0.05$).

3. Results

3.1 In Vivo Toxic Potential of Carbon Fullerenes

The advantage of evaluating the consequence of nanomaterial exposure during development is that perturbations of the developmental program can lead to a number of easily detected responses. Again, the goal of these studies was to determine if the zebrafish embryonic responses could be used to determine, and eventually predict, the structural properties of nanomaterials that produce toxicity. In our system, an adverse biological response to nanomaterial exposure can result in delayed development, morphological malformations (i.e. body axis, eye, snout, jaw, otic vesicle, notochord, heart, brain, somite, fins) and/or behavioral abnormalities (i.e. hyperactivity, hypoactivity, paralysis). Embryos exposed to graded concentration of C_{60}, C_{70}, and $C_{60}(OH)_{24}$ were scored daily for these effects. Concentrations above 200 ppb C_{60} and C_{70} resulted in 100% mortality during the first 48 hours (Figure 2 a,b). $C_{60}(OH)_{24}$ exposure did not result in significant mortality until the exposure concentration was above 4000 ppb (Figure 2c). The estimated LC_{50} for C_{60}/C_{70}- and $C_{60}(OH)_{24}$-exposures were approximately 200 ppb and 4000 ppb, respectively. Sublethal morphological and developmental effects are presented in Figure 2 as cumulative values for the 5 day scoring period, not accounting for mortality that may have occurred before or after scoring the effects. Representative pictures of the malformations resulting from exposure are shown in Figure 2 (d,i). Embryonic exposure to 200 ppb of C_{60} and C_{70} resulted in delayed development (approximately 12–20 hours according to staging of embryogenesis) and a specific caudal fin malformation (Figure 2 d,e). Exposure to C_{60} also resulted in significant pericardial edema and yolk sac edema at 200 ppb (Figure 2 h,i). Neither C_{60} nor C_{70} induced sublethal responses at concentrations higher than 200 ppb due to the high mortality observed at these concentrations within the first 24 hours of exposure. Concentrations less than 2500 ppb of $C_{60}(OH)_{24}$ did not elicit a significant response; whereas, concentrations over 2500 ppb induced pericardial edema, yolk sac edema and pectoral fin malformations (Figures 2 f,g). Exposure to 5000 ppb $C_{60}(OH)_{24}$ resulted in an overall swelling of embryos and delayed development (approximately 15–20 hours).

3.2 Fullerene-induced Cellular Death

Cellular death assays were performed to determine if exposure to fullerenes would lead to an increase in cellular death in specific cells or tissues, prior to the overt signs of toxicity reported in Figure 2. C_{60}-exposed embryos exhibited a concentration-dependent increase in overall cellular death, significant at 100 ppb and higher (Figure 3). Cell death was detected throughout the head region (Figures 3 a–d) and down the notochord to the region of the caudal fin malformations (Figures 3 e–h). Conversely, embryos exposed to $C_{60}(OH)_{24}$ exhibited significant overall cell death only in the head region and only at a concentration of 5000 ppb (data not shown). For C_{60} exposures, acridine orange staining for cellular death was a more sensitive endpoint than any morphological malformations.

Acridine orange binds all cells undergoing cellular death, both necrosis and apoptosis, and the TUNEL assay is more specific for detecting cells undergoing programmed cellular death. Similar to the results of the acridine orange staining for overall cell death, there was a

concentration-dependent increase in apoptotic cellular death detected in the head (Figures 4 a–d) and trunk region (Figures 4 e–h) of C_{60}-exposed embryos. The total fluorescence of TUNEL positive ($TUNEL^+$) cells was approximately half of the total fluorescence measured using acridine orange staining suggesting that at least a portion of overall C_{60}-induced cell death was attributed to induction of apoptotic pathways (compare Figures 3i,4i). In embryos exposed to $C_{60}(OH)_{24}$ there was no significant difference in apoptosis compared to control embryos, even at 5000 ppb $C_{60}(OH)_{24}$ (data not shown).

4. Discussion

The toxicological effects of carbon fullerenes were assessed *in vivo* using the zebrafish embryo as a model organism. Research presented herein clearly demonstrates the usefulness of this model as an effective platform to rapidly assess novel nanomaterial toxicity. Several attributes make embryonic zebrafish tractable for such studies. The embryos develop rapidly with most body organs formed within 48 hours; thus, thorough toxicological evaluations can be completed within just a few days. Due to the transparent nature of the embryos, numerous effects can be assessed non-invasively over the course of the experiment. Cellular death assays, the most sensitive endpoint defined in these studies, were completed within two days. Females produce hundreds of eggs weekly so large sample sizes are easily achieved for statistically powerful dose-response studies. This abundant supply of embryos also makes it possible to simultaneously assess the toxicity of a large number of materials in a short period of time.

There are additional advantages to using zebrafish as part of a comprehensive approach to nanomaterial risk assessment. Although beyond the scope of this paper, many routes of exposure (i.e. ingestion, injection and dermal) could also be assessed individually or in combination. Since zebrafish are amenable to genetic manipulations, biological targets and modes of action can be determined. Because embryos are transparent, tissue dose and distribution could potentially be determined using fluorescently labeled nanomaterials and laser scanning confocal microscopy. In addition, zebrafish attain sexual maturity by 90 days post-fertilization (dpf) making chronic studies feasible. Because zebrafish adults grow to an average size of 3–4 cm and are easy to maintain at high densities, the infrastructure and maintenance costs required for housing the large numbers of animals required for screening are relatively low. Such features are favorable for adapting this model system to high-throughput assays for nanomaterial toxicity evaluations.

The potential toxicity of fullerenes was evaluated during early vertebrate development for two important reasons. First, fundamental processes of development are remarkably conserved across species. Second, vertebrates at the earliest life stages are often more responsive to chemical insult (NRC, 2000). The probable molecular explanation for increased embryonic susceptibility is that during this period, the full repertoire of molecular signaling is necessary and active. It has been postulated that overall there are only 17 general molecular signaling pathways in vertebrates and that each of these is active during early development. Importantly, each of these pathways is essential for other cells in tissues later in life (NRC, 2000). Since development is highly coordinated requiring cell-to-cell communications, if nanomaterials perturb these interactions, then development would be expected to be disrupted.

Much of data, thus far, on the effects of fullerene exposure had been gained from *in vitro* methods (with few exceptions: Mori et al. 2006; Oberdorster 2004; Oberdorster et al. 2005; Tsuchiya et al. 1996b; Zhu et al. 2006) using C_{60} or a derivative of C_{60}, such as hydroxylated C_{60}. There is almost no information regarding the toxicity of C_{70}. *In vitro* data may be of limited use in predicting *in vivo* responses especially since those results may be dependent on the cell culture system chosen for the experiment. For example, the cytotoxicity of C_{60} to human dermal fibroblasts, human liver carcinoma cells (HepG2) and neuronal human astrocytes was found

to be dependent on cell type [23]. However, Isakovic and others found the toxicity of C_{60} and $C_{60}(OH)_n$ to be neither species nor cell specific, nor selective for primary or transformed cell lines [24]. Independent of evaluation method/system, studies on C_{60} and C_{60} derivatives consistently report on differences in physicochemical properties and biological effects [17, 25].

In our studies, embryo exposure to fullerenes elicited increased mortality, sublethal malformations and increased cellular death. Studies in an embryonic mammalian model (mouse) also report severe morphological malformations and increased mortality when exposed to C_{60} *in utero* [26]. All carbon fullerenes tested in our system produced deleterious effects to the developing fin regions indicative of signaling perturbation during early development. C_{60} and C_{70} elicited similar responses, indicating the small difference in size does not significantly affect the toxic potential of these materials. Functionalization of the C_{60} material with hydroxyl groups; however, decreased the toxic potential in our system. These results are similar to studies conducted in other systems [23,27–29]. In cell culture studies of C_{60} and $C_{60}(OH)_{24}$, Sayes (2004) reported that underivatized fullerenes were at least three orders of magnitude more toxic than their hydroxylated counterpart. In addition, the cytotoxic action of underivatized C_{60} was much faster and more effective than its hydroxylated derivative [24]. Results obtained from our studies are consistent with the predominant belief that hydroxylated-C_{60} is less toxic than underivatized C_{60} and that the toxicity of C_{60} can be diminished through manipulation of surface functionalization [30].

In addition to gross pathologies, the mechanism of cellular death induction is an important consideration because of its correlation with overall tissue damage. Necrosis tends to cause extensive tissue damage resulting in an inflammatory response *in vivo*; while apoptosis does not cause tissue damage since macrophages effectively remove apoptotic signaling cells. Prior cell culture studies have suggested that pristine and hydroxylated-C_{60} have distinct mechanisms for the induction of cellular death [24]. The cellular death assays in this study also demonstrated a difference in mechanism of cell death induction between C_{60} and $C_{60}(OH)_{24}$. Although C_{60} elicited a concentration-dependent response in both total cell death and apoptosis, $C_{60}(OH)_{24}$ did not induce an apoptotic response. We suspect that $C_{60}(OH)_{24}$ interacts with water and permeabilizes membranes upon uptake. If this is the mechanism by which the animals swelled in response to $C_{60}(OH)_{24}$ exposure, then apoptosis would not be expected to occur. Alternatively, the swelling observed in $C_{60}(OH)_{24}$ exposed embryos could be due to significant uptake of $C_{60}(OH)_{24}$ into the animal followed by a simple osmotic response. These findings are not consistent with cell culture studies that found hydroxylated-C_{60} to induce cell death with characteristics of apoptosis and C_{60} to induce cell death independent of apoptotic cell signaling [24]. These pathway level effects may be more cell or tissue specific, since fullerene-induced cell death (both necrosis and apoptosis) has been demonstrated in various cell culture lines with different effects dependent on the type of material, surface functionalization and cell culture system [19,24,31,32]. These discrepancies show a need for further evaluations into the mechanisms through which fullerenes initiate cellular death resulting in toxic effects.

The cellular death measured in this study could result from oxidative stress, the most often proposed mechanism of action for fullerene toxicity, or due to direct interaction of the fullerene with cells through an unknown mechanism. Oxidative stress can lead to a variety of downstream effects including lipid peroxidation, DNA and protein adduction and cellular death. Since there are limited tests that directly measure reactive oxygen species (ROS), researchers rely on detection of lipid peroxidation products and cell death as markers of oxidative stress. With few exceptions, underivatized C_{60} are reportedly toxic due to pro-oxidant behavior that results in cytotoxicity [24]. *In vitro*, C_{60} synergized the effects of oxidative stress-inducing agents and elicited cytotoxic action through ROS-mediated cell membrane lipid

peroxidation [23,24]. *In vivo*, C_{60} induced oxidative stress and lipid peroxidation in the brain of juvenile largemouth bass [28]. However, a recent article by Gharbi and others has questioned whether derivations of C_{60} really are less toxic than their pristine counterparts [33]. Their study reported that C_{60} acted as a powerful antioxidant *in vivo* in rats with no acute or subacute toxicities [33]. Methods currently being developed to fluorescently detect ROS *in vivo*, will be applied to the embryonic zebrafish model in order to localize the stress in these transparent animals.

5. Summary and Conclusions

The effects of carbon fullerenes were assessed *in vivo* using the zebrafish embryo as a model organism for nanotoxicology evaluations. Research presented herein clearly demonstrates the usefulness of this model as an effective tool for rapidly assessing nanomaterial toxicity and investigating the details of exposure-related effects. The time involved for animal maintenance, experimental preparation and completion of these studies has been vastly improved over traditional *in vivo* studies. Our dynamic whole animal assay can be used to reveal the toxic potential of novel nanomaterials at the genetic, cellular and physiological level. Since these processes are highly conserved between zebrafish and humans, especially early in development, information gained by exploiting the unique advantages of one vertebrate model system can be immediately applied to predict effects in other systems. Furthermore, information gained using this model system can be used as rapid feedback for engineers designing novel nanomaterials, such that they can take into consideration potential toxicity to favor the development of materials with minimal toxicity.

Acknowledgements

We would like to thank Jane La Du for her technical assistance. These studies were partially supported by the Oregon State University Research Office, The Safer Nanomaterials and Nanomanufacturing division of the Oregon Nanoscience and Microtechnologies Institute and NIEHS grants ES03850 and ES07060.

References

1. Lecoanet HF, Bottero JY, Wiesner MR. Laboratory assessment of the mobility of nanomaterials in porous media. Environmental Science & Technology 2004;38(19):5164–5169. [PubMed: 15506213]
2. Lecoanet HF, Wiesner MR. Velocity effects on fullerene and oxide nanoparticle deposition in porous media. Environmental Science & Technology 2004;38(16):4377–4382. [PubMed: 15382867]
3. Lecoanet H, Wiesner MR. Assessment of the mobility of nanomaterials in groundwater acouifers. Abstracts of Papers of the American Chemical Society 2004;227:U1275–U1275.
4. Okamoto Y. Ab initio investigation of hydrogenation of C-60. Journal of Physical Chemistry A 2001;105(32):7634–7637.
5. Sun O, Wang Q, Jena P, Kawazoe Y. Clustering of Ti on a C-60 surface and its effect on hydrogen storage. Journal of the American Chemical Society 2005;127(42):14582–14583. [PubMed: 16231905]
6. Forrest DR. Molecular Nanotechnology. IEEE 2001:11–20.
7. Thomas K, Sayre P. Research strategies for safety evaluation of nanomaterials, Part I: evaluating the human health implications of exposure to nanoscale materials. Toxicol Sci 2005;87(2):316–21. [PubMed: 16049265]
8. Guzman KAD, Taylor MR, Banfield JF. Environmental risks of nanotechnology: National nanotechnology initiative funding, 2000–2004. Environmental Science & Technology 2006;40(5): 1401–1407. [PubMed: 16568748]
9. Hurt RH, Monthioux M, Kane A. Toxicology of carbon nanomaterials: status, trends, and perspectives on the special issue. Carbon 2006;44:1028–1033.
10. Hoet P, Bruske-Hohlfeld I, Salata O. Nanoparticles- known and unknown health risks. Journal of Nanobiotechnology 2004;2:12–37. [PubMed: 15588280]

11. Wixon J. Featured organism: Danio rerio, the zebrafish. Yeast 2000;17(3):225–31. [PubMed: 11025533]
12. Hill AJ, Teraoka H, Heideman W, Peterson RE. Zebrafish as a model vertebrate for investigating chemical toxicity. Toxicol Sci 2005;86(1):6–19. [PubMed: 15703261]
13. Ton C, Lin Y, Willett C. Zebrafish as a model for developmental neurotoxicity testing. Birth Defects Res A Clin Mol Teratol 2006;76(7):553–67. [PubMed: 16933308]
14. Tilton F, La Du JK, Vue M, Alzarban N, Tanguay RL. Dithiocarbamates have a common toxic effect on zebrafish body axis formation. Toxicol Appl Pharmacol 2006;216(1):55–68. [PubMed: 16797628]
15. Rubinstein AL. Zebrafish: from disease modeling to drug discovery. Curr Opin Drug Discov Devel 2003;6(2):218–23.
16. Dodd A, Curtis PM, Williams LC, Love DR. Zebrafish: bridging the gap between development and disease. Hum Mol Genet 2000;9(16):2443–9. [PubMed: 11005800]
17. Nakamura E, Isobe H. Functionalized fullerenes in water. The first 10 years of their chemistry, biology, and nanoscience. Accounts of Chemical Research 2003;36(11):807–815. [PubMed: 14622027]
18. Anderson R, Barron AR. Reaction of hydroxyfullerene with metal salts: a route to remediation and immobilization. Journal of American Chemical Society 2005;127:10458–10459.
19. Sayes CM, Fortner JD, Guo W, Lyon D, Boyd AM, Ausman KD, et al. The differential cytotoxicity of water-soluble fullerenes. Nano Lett 2004;4(10):1881–1887.
20. Sayes CM, Liang F, Hudson JL, Mendez J, Guo W, Beach JM, et al. Functionalization density dependence of single-walled carbon nanotubes cytotoxicity in vitro. Toxicol Lett 2006;161(2):135–42. [PubMed: 16229976]
21. Lockman P, Koziara J, Mumper R, Allen D. Nanoparticle surface charges alter blood-brain barrier integrity and permeability. Journal of Drug Target 2004;12:635–641.
22. Kimmel C, Ballard W, Kimmel S, Ullmann B, Schilling T. Stages of embryonic development of the zebrafish. Developmental Dynamics 1995;203:253–310. [PubMed: 8589427]
23. Sayes CM, Gobin AM, Ausman KD, Mendez J, West JL, Colvin VL. Nano-C60 cytotoxicity is due to lipid peroxidation. Biomaterials 2005;26(36):7587–95. [PubMed: 16005959]
24. Isakovic A, Markovic Z, Todorovic-Markovic B, Nikolic N, Vranjes-Djuric S, Mirkovic M, et al. Distinct cytotoxic mechanisms of pristine versus hydroxylated fullerene. Toxicological Sciences 2006;91(1):173–183. [PubMed: 16476688]
25. Bosi S, Da Ros T, Spalluto G, Prato M. Fullerene derivatives: an attractive tool for biological applications. European Journal of Medical Chemistry 2003;38:913–923.
26. Tsuchiya T, Oguri I, Yamakoshi Y, Miyata N. Novel harmful effects of [60]fullerene on mouse embryos *in vitro* and *in vivo*. FEBS Letters 1996;393:139–145. [PubMed: 8804443]
27. Lovern SB, Klaper R. *Daphnia magna* mortality when exposed to titanium dioxide and fullerene (C_{60}) nanoparticles. Environmental Toxicology & Chemistry 2006;25(4):1132–1137. [PubMed: 16629153]
28. Oberdorster E. Manufactured nanomaterials (fullerenes, C_{60}) induce oxidative stress in the brain of juvenile largemouth bass. Environmental Health Prospectives 2004;112:1058–1062.
29. Zhu S, Oberdorster E, Haasch ML. Toxicity of an engineered nanoparticle (fullerene, C60) in two aquatic species, *Daphnia* and fathead minnow. Marine Environmental Research. 2006in press
30. Jensen AW, Wilson SR, Schuster DI. Biological applications of fullerenes. Bioorganic & Medicinal Chemistry 1996;4(6):767–779. [PubMed: 8818226]
31. Dugan LL, Gabrielesen JK, Yu SP, Lin TS, Choi DW. Buckminsterfullerenol free radical scavengers reduce excitotoxic and apoptotic death of cultured cortical neurons. Neurobiology of Disease 1996;3:129–135. [PubMed: 9173920]
32. Edinger AL, Thompson CB. Death by design: apoptosis, necrosis and autophagy. Current Opinion in Cell Biology 2004;16:663–669. [PubMed: 15530778]
33. Gharbi N, Pressac M, Hadchouel M, Szwarc H, Wilson SR, Moussa F. [60]fullerene is a powerful antioxidant in vivo with no acute or subacute toxicity. Nano Lett 2005;5(12):2578–85. [PubMed: 16351219]

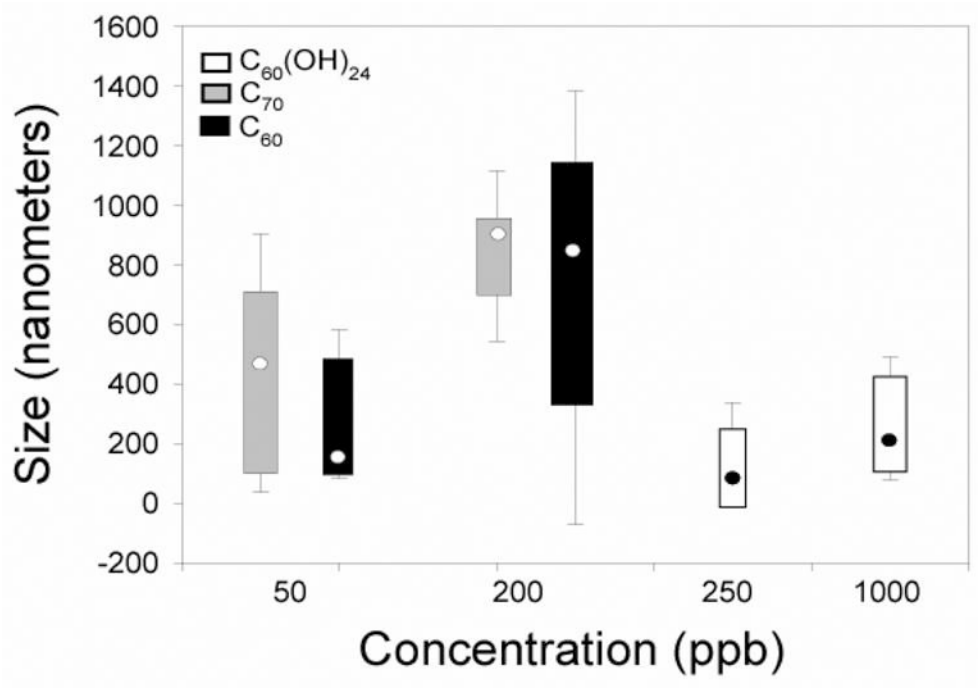

Figure 1.

Photon correlation spectroscopy of C_{60} (black) and C_{70} (gray) at 50 and 200 ppb, and $C_{60}(OH)_{24}$ (white) at 250 and 1000 ppb. Mode size of particles (highest number of observations) for each concentration is indicated by (•). Boxes represent particle size distribution with upper and lower standard deviation determined by size distribution processor analysis.

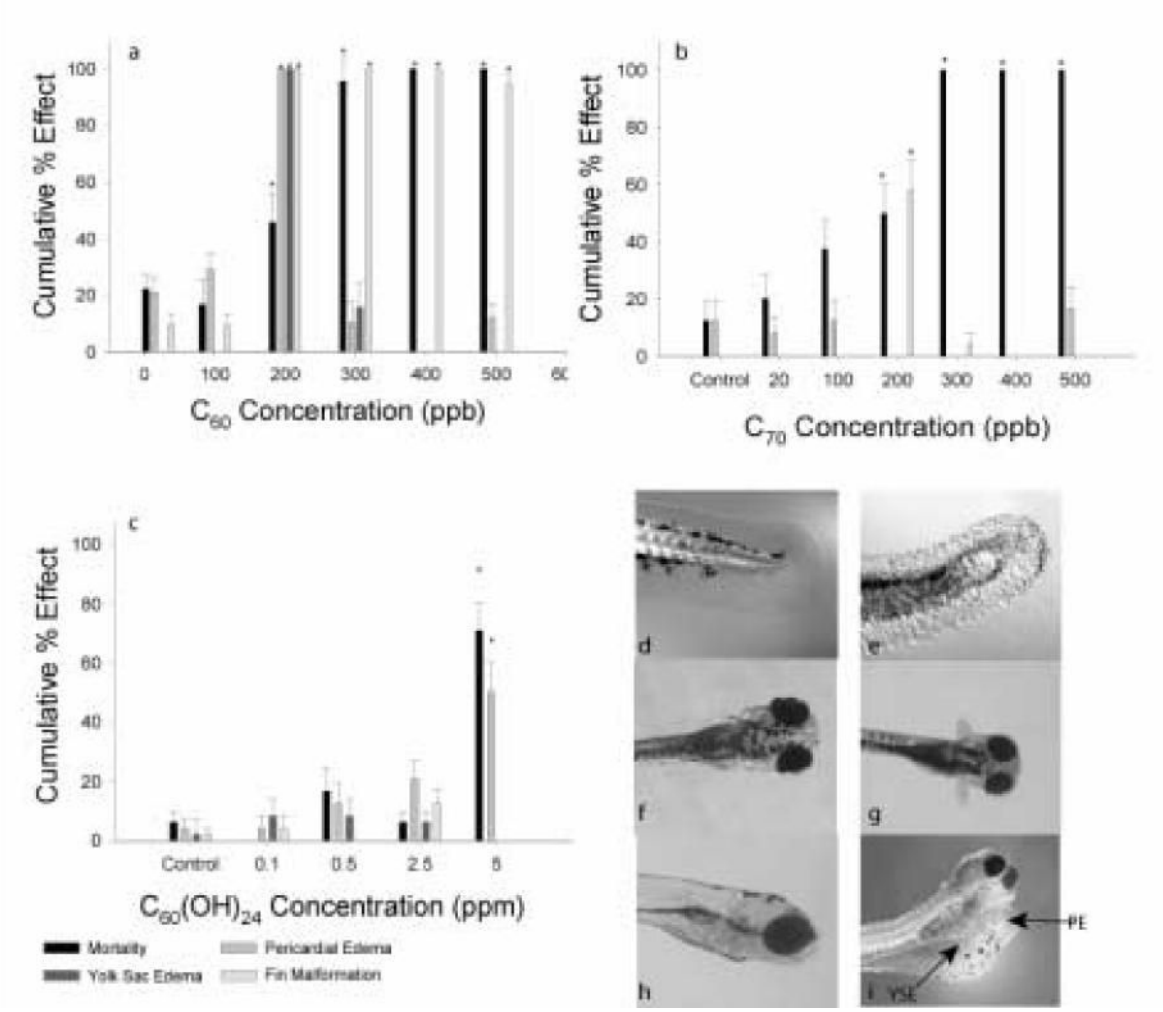

Figure 2.

Concentration-responses observed for embryonic zebrafish exposed to (a) C_{60}, (b) C_{70}, and (c) $C_{60}(OH)_{24}$ from 24 hpf to 96 hpf; evaluated daily until 6 dpf. Values represent the % showing the effect by day 6 (Cumulative % Effect): mortality, pericardial edema, yolk sac edema, and fin malformations. Representative images of the caudal fins for (d) control and (e) 200 ppb C_{60}-exposed animals are given. Representative images of the pectoral fin for (f) control and (g) 3500 ppb $C_{60}(OH)_{24}$-exposed animals. Representative images of (h) 1% DMSO control head at 6 dpf and (i) 200 ppb C_{60}-exposed head at 6 dpf; arrows designate pericardial edema (PE) and yolk sac edema (YSE). Significance was determined using Fisher's Exact test (*$p<0.05$) compared to 1% DMSO control (N=24).

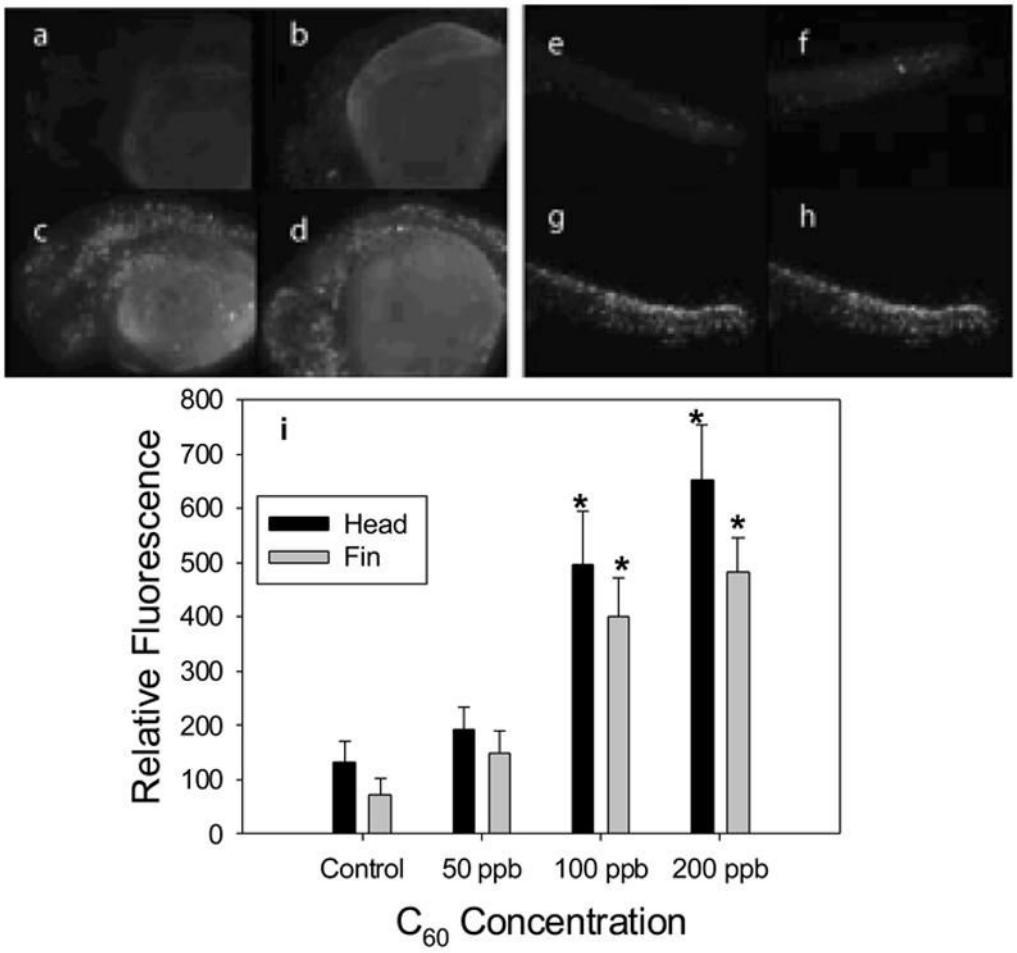

Figure 3. C_{60}-exposure leads to increased cellular death in the live zebrafish embryo

Cellular death was determined using acridine orange staining of C_{60}-exposed embryos at 36 hpf, after a 12 hour C_{60} exposure. Fluorescence emitted from cells undergoing cellular death indicated by white signal on a black background, shown for the head region for (a) 1% DMSO control, (b) 50 ppb C_{60}-exposed (c) 100 ppb C_{60}-exposed (d) 200 ppb C_{60}-exposed; and the caudal fin for (e) 1% DMSO control, (f) 50 ppb C_{60}-exposed, (g) 100 ppb C_{60}-exposed, and (h) 200 ppb C_{60}-exposed embryos. (i) Concentration-response curves for cell death measured as relative fluorescence in the head (•) and trunk regions (°) of the embryos. Cellular death was significantly different than controls at 100 and 200 ppb determined using one-way ANOVA (*$p<0.05$), N=12

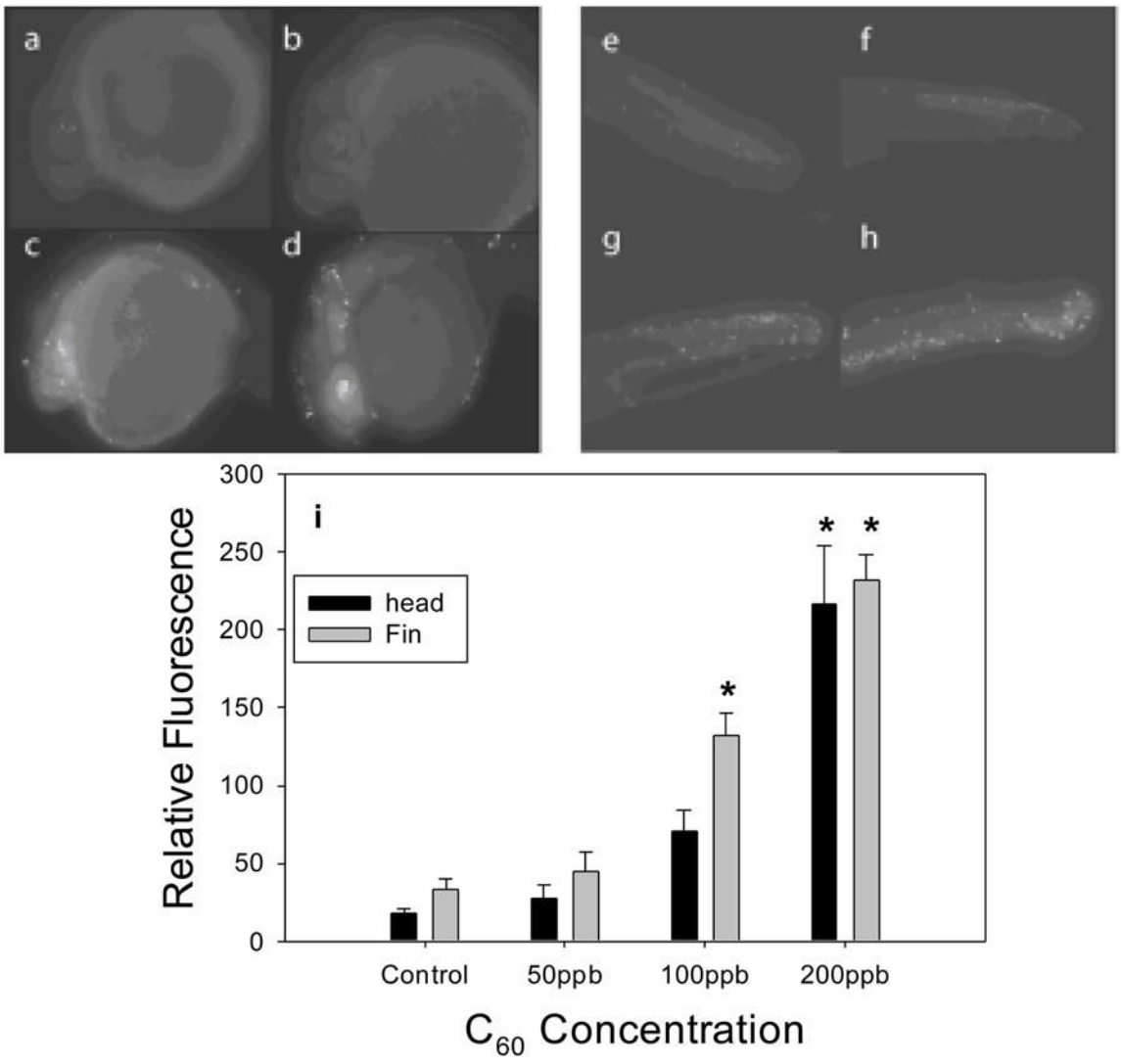

Figure 4.

Apoptotic cell death was measured in embryos at 36 hpf, after 12 hours of exposure. White spots indicating a TUNEL$^+$ response (apoptotic signaling) shown for the head region (a) 1% DMSO control, (b) 50 ppb C_{60}-exposed (c) 100 ppb C_{60}-exposed (d) 200 ppb C_{60}-exposed and the caudal fin region (e) 1% DMSO control, (f) 50 ppb C_{60}-exposed, (g) 100 ppb C_{60}-exposed, and (h) 200 ppb C_{60}-exposed embryos. (i) Concentration-response curves for cell death measured as relative fluorescence in the head (black) and trunk (grey) regions of the embryos. Apoptotic cellular death was significantly different than controls at 100 and 200 ppb determined using one-way ANOVA (*$p<0.05$), N=12.